Assessment of the effects of anthropogenic activities on forest resources using remote sensing and GIS: A case study of the Atewa Range Forest Reserve in Ghana

リモートセンシングと GIS を用いた森林資源に対する人為的活動の影響の評価：ガーナ・アテワ森林保護区を例に

ADAMS Lukman Boakye

The dissertation submitted for the partial fulfillment of Doctor of Philosophy (Ph.D.), September 2025

Division of Environmental Science Development

Graduate School of Environmental Science

Hokkaido University, Japan

Assessment of the effects of anthropogenic activities on forest resources using remote sensing and GIS: A case study of the Atewa Range Forest Reserve in Ghana

リモートセンシングと GIS を用いた森林資源に対する人為的活動の影響の評価：ガーナ・アテワ森林保護区を例に

By

ADAMS Lukman Boakye

Graduate School of Environmental Science
Hokkaido University, Japan

Supervisor
Yuichi S. Hayakawa (Ph.D.)
Associate Professor
Faculty of Environmental Earth Science
Hokkaido University, Japan

September 2025

Abstract

The Atewa Range Forest Reserve (ARFR), located in southeastern Ghana, is recognized as a key biodiversity hotspot and an essential part of the country's ecological and hydrological systems. Despite its ecological importance, the ARFR is under increasing threat from human activities, notably farming, small-scale logging, and alluvial gold mining. These pressures have significantly impacted the forest's biodiversity and ecosystem services. This research combines multiple remote sensing and GIS approaches to monitor and assess the effects of these disturbances on the forest's structure, function, and carbon storage capacity over time. To assess the spatial and temporal dynamics of mining activities and land use changes in the Atewa landscape (Chapter 2), high-resolution PlanetScope satellite imagery (2018–2023) was analyzed using Geographic Object-Based Image Analysis (GEOBIA), which is ideal for reducing misclassifications resulting from the characteristic high spectral variability of high-resolution satellite images. Post-classification change detection was conducted to identify transitions in land use and land cover (LULC), particularly areas that were converted to alluvial mining sites. Additionally, post-mining vegetation recovery was evaluated to assess how long it took for the degraded sites to recover from vegetation loss. Buffer analysis was then applied to determine the proximity of mining sites to river channels and forest boundaries. This was crucial in assessing how mining activities affected the river channels in the area, as well as the effects on the edge of the ARFR. Results showed an annual increase in mining activities at a rate of 12.3% between 2018 and 2023. Notably, the ARFR recorded a decreasing trend in mining activity within its bounds, with a rate of change of -21.4%, indicating irregular mining patterns in the reserve compared to the broader landscape. Critically, a significant portion of mining, at least 49.7% annually, occurred within 100 meters of river channels,

highlighting severe risks to aquatic ecosystems. Additionally, 0.7% of mining activities occurred within the 100 m buffer around the ARFR, emphasizing encroaching threats.

While Chapter 2 focused on large-scale disturbance activities in the Atewa landscape, the third chapter sought to fill the knowledge gap in small-scale canopy disturbance dynamics, which often preceded permanent forest loss. Sentinel-2 satellite imagery was utilized to map small-scale canopy gaps using Linear Spectral Mixture Analysis (LSMA) and GIS. Annual change detection within 100 m × 100 m grids tracked canopy disturbances and assessed their spatial correlation with topographical and geospatial variables. Disturbances within the grids were identified through the annual changes that occurred in the soil fraction image derived from the LSMA. Findings revealed consistent deforestation trends and increasing canopy gaps over time, except in 2024, which showed a decrease in gap coverage, a possible indication of forest regeneration. Canopy gaps exhibited rapid transitions from low to high disturbance annually and were predominantly located near forest edges and river channels. Disturbance levels showed a non-linear relationship with elevation and slope (increase followed by decrease), and most disturbances occurred on west-facing slopes, suggesting the possibility of strong anthropogenic drivers such as selective logging and small-scale resource extraction. These findings underscore the need for targeted monitoring strategies focusing on low-scale, progressive degradation activities.

In addition to monitoring disturbances, the study addressed the estimation of above-ground biomass (AGB) and carbon accumulation (CAc) in the ARFR (Chapter 4), an essential component for climate change mitigation. Due to the lack of comprehensive National Forest Inventory (NFI) data in Ghana, remotely sensed Sentinel-2 data were coupled with field-measured AGB to generate accurate biomass estimates. Ten vegetation indices and biophysical variables were tested as predictors in linear and non-linear models to predict AGB. Among these, the Normalized

Difference Vegetation Index (NDVI) emerged as the single most effective predictor. The selected logarithmic model yielded an R^2 value of 0.56 and a Root Mean Square Error (RMSE) of 40.37 Mg/ha, indicating good model performance. The final AGB and carbon accumulation (CAc) maps recorded mean values of 115.12 Mg/ha and 88.79 Mg/ha, respectively. Comparisons between measured and predicted AGB produced an RMSE of 45.70 Mg/ha and an R^2 value of 0.52, validating the reliability of the NDVI in estimating forest biomass.

Collectively, this research demonstrates the potential of integrating high-resolution satellite data, object-based image analysis, spectral unmixing techniques, and topographic variables in monitoring environmental changes in tropical forest reserves. It provides robust evidence of the growing anthropogenic pressures on the ARFR, notably from mining and small-scale forest degradation, and highlights the forest's role in carbon sequestration. The findings advocate enhanced surveillance, enforcement of buffer zone regulations, and strategic reforestation to protect the integrity of the ARFR and its surrounding ecosystems.

Keywords: Remote sensing, GIS, Geographic object-based image analysis (GEOBIA), Spectral Mixture Analysis (SMA), Above-ground biomass (AGB), Carbon accumulation (CAc), forest reserve, alluvial mining, Atewa Range Forest Reserve (ARFR).

Table of contents

Abstract .... **II**

Table of contents .... **V**

List of figures .... **VIII**

List of tables .... **IX**

Chapter 1 .... **1**

General introduction **1**

1.1 Background of study 1

1.2 Study Objectives 9

1.3 Study approach and thesis structure 10

Chapter 2 .... **13**

Mapping alluvial mine dynamics in the Atewa landscape in Ghana using Geographic Object-based Image Analysis (GEOBIA) and GIS **13**

2.1 Introduction 13

2.2 Materials and Methods 17

2.2.1 Study area 17

2.2.2 Satellite image and ground truthing 18

2.2.3 Data analysis 20

2.2.4 Geographic Object-Based Image Analysis (GEOBIA) 20

2.2.5 Post-classification correction 23

2.2.6 Accuracy assessment 23

2.2.7 Post-classification change detection 24

2.2.8 Buffer analysis 26

2.3 Results 27

2.3.1 Land use land cover classification results 27

2.3.2 Change detection 29

2.3.3 Annual loss/gain in alluvial mines 30

2.3.4 Forest reserve and water channel buffer analysis 30

2.4 Discussion 34

2.4.1 Land use land cover classification results 34

2.4.2 Alluvial mine dynamics 37

2.4.3 Mine proximity to forest reserve and river channels 42

2.5 Limitations of the study 44

2.6 Conclusions 45

Chapter 3 .... **46**

Inferring canopy disturbance sources in the Atewa Range Forest Reserve in Ghana through their relationship with topographic and geospatial features **46**

3.1 Introduction 46

3.2 Materials and Methods 49

3.2.1 Study area 49

3.2.2 Sentinel-2 satellite data pre-processing 50

3.2.3 Creation of forest masks 51

3.2.4 Mapping canopy disturbances 51

3.2.5 Accuracy assessments 54

3.2.6 Relationships between canopy disturbances and topographic and geospatial features 54

3.3 Results 56

3.3.1 Disturbance and recovery patterns 56

3.3.2 Relationship between disturbance and topographic and geospatial features 61

3.4 Discussion 62

3.4.1. Disturbance and recovery dynamics 62

3.4.2 Inferring canopy disturbance sources 64

3.5 Study limitations 68

3.6 Conclusions 69

Chapter 4 .... **70**

Estimating above-ground biomass of the Atewa Range Forest Reserve in Ghana using Sentinel-2 imagery **70**

4.1 Introduction 70

4.2 Materials and methods 73

4.2.1 Study area 73

4.2.2 Field data collection 74

4.2.3 Satellite data pre-processing 76

4.2.4 Vegetation indices and Biophysical variable extraction 76

4.2.5 Statistical models and model evaluation 77

4.3 Results 79

4.3.1 Field-measured AGB of the ARFR 79

4.3.2. Model development and evaluation 79

4.3.3. Spatial distribution of estimated above-ground biomass and carbon accumulation in the ARFR 82

4.4 Discussion 85

4.4.1. Model validation and contributing factors ... 85
4.4.2. Distribution of low above-ground biomass areas ... 86
4.5. Potential sources of errors in the AGB estimation ... 88
4.6. Conclusions ... 90
Chapter 5 ... 91
General discussion ... 91
5.1 Anthropogenic activities in the Atewa landscape and the Atewa Range Forest Reserve (ARFR) ... 91
5.2 The implications of disturbances in the ARFR on biodiversity ... 96
5.3 The implications of disturbances of the ARFR on climate change mitigation ... 98
5.4 Study limitations and ways forward ... 99
Chapter 6 ... 101
6.1 Conclusions ... 101
Acknowledgements ... 103
References ... 105
List of abbreviations ... 131

List of figures

Fig. 1.1	The Atewa landscape showing the location of the Atewa Range Forest Reserve	9
Fig. 1.2	Study approach flow chart	11
Fig. 2.1	Map of the study area showing the distribution of training and test samples in 2023 (Polygons represent high-resolution satellite image training/test samples; corresponding points represent ground-truthed training/test points)	18
Fig. 2.2	Flowchart of methodology	25
Fig. 2.3	(a) Multiresolution segmentation; (b) Classified vector polygons	26
Fig. 2.4	LULC maps from 2018 to 2023	32
Fig. 2.5	**(a)** Four-year average of classes converted into Alluvial mine in the Atewa landscape; **(b)** Annual conversion of other classes into Alluvial mine in the ARFR; Area of annual post-mine vegetation recovery in **(c)** Atewa landscape, **(d)** ARFR; Percentage of mined area that has undergone revegetation in **(e)** Atewa landscape, **(f)** ARFR; AM = Alluvial mine; B = Bare land; Bu = Built-up; CC = Closed-canopy vegetation; HC = Herbaceous cover	36
Fig. 2.6	Alluvial mine loss/gain maps from 2018 to 2023	40
Fig. 2.7	Distribution of mines, where yellow polygons represent mines within a multiple-ring buffer around **(a)** a portion of the ARFR; **(b)** river channels	41
Fig. 2.8	**(a)** A mine close to the Atewa Range Forest Reserve; **(b)** Increased turbidity of a river body as a result of mining activities	44
Fig. 3.1	Map of the Atewa landscape showing the Atewa Range Forest Reserve	50
Fig. 3.2	**Fig. 3.2.** Flowchart showing the methods applied in mapping disturbance and the relationship with topographic and geospatial features	56
Fig. 3.3	A portion of the ARFR showing **(a)** false colour composite of Sentinel-2 image; **(b)** soil fraction image; **(c)** canopy gap coverage classification	58
Fig. 3.4	**(a)** Trends of deforestation, canopy gaps, and NDVI **(b)** Trends of disturbance and recovery	59
Fig. 3.5	Disturbance/recovery maps from 2020 to 2024	60
Fig. 3.6	Annual change trajectory area	61
Fig. 3.7	**(a-d)** Relationship between disturbances and topographic and geospatial features, **(e-g)** Distribution of disturbances in relation to aspect	64
Fig. 3.8	Tree logging sites in the ARFR	68
Fig. 4.1	(A) Distribution of protected areas in Ghana (B) Study area elevation and field sample plots	74
Fig. 4.2	Steps applied in model development	78
Fig. 4.3	Relationship between predicted and measured AGB	83
Fig. 4.4	**(A)** Map of predicted AGB **(B)** CAc map	83
Fig. 4.5	Density distribution of pixels with AGB values less than 50 Mg/ha	84
Fig. 5.1	Summary of the effects of human-induced disturbances on the Atewa landscape and ARFR	98

List of tables

Table 2.1	Acquisition dates of PlanetScope monthly mosaicked images used in the study	22
Table 2.2	LULC classes used in the study and their descriptions	23
Table 2.3	Pixel count of training and test samples used for classification and validation	25
Table 2.4	Summary of classification accuracies from 2018 to 2023	28
Table 2.5	LULC area (Ha) from 2018 to 2023 in the Atewa landscape	33
Table 2.6	LULC area (Ha) from 2018 to 2023 in the Atewa Range Forest Reserve	33
Table 2.7	Alluvial mine loss/gain statistics	43
Table 2.8	Mined area proximity to ARFR and river channels	43
Table 3.1	Change trajectories that were used to identify disturbances and recoveries	53
Table 3.2	Summary of accuracy assessments for soil fraction images derived from SMA	58
Table 4.1	Sample plots with measured parameters and corresponding measured AGB	75
Table 4.2	Vegetation indices and biophysical variables used as predictor variables. Biophysical variables were calculated using neural networks in the SNAP software (Kamenova and Dimitrov, 2021)	78
Table 4.3	Tree species information from sample plots	81
Table 4.4	r and R^2 values of correlation and regression analysis between AGB and predictor variables	82
Table 4.5	AGB model statistics	84

Chapter 1

General introduction

1.1 Background of study

Forests play a crucial role in the continuous existence of biodiversity. A wide array of ecosystem services and functions is provided by forest resources which cater for some of the basic necessities of life such as food and water, raw materials, climate regulation, pest regulation, improved air quality, carbon sequestration, hydrological cycle protection, improved soil fertility, habitat provisioning, and the protection of biodiversity among many others (Tian et al., 2015; Campos, et. al., 2005; Brockerhoff et al., 2017). Forests cover about 4.06 billion hectares (ha) of the earth surface, accounting for about 31 percent of the Earth's total land area. The tropical regions of the world have the most forested areas, accounting for about 45 percent of the total forested lands of the Earth. Between 1990 and 2020, the world is reported to have lost about 178 million ha of forests owing mostly to anthropogenic activities such as illegal logging, population growth, and urbanization (FAO, 2020; Mitchell, Rosenqvist, and Mora, 2017; DeFries, et al., 2010). Even though there has been a consistent decline in the rate of forest loss in the last three decades, Africa has recorded the highest rate of deforestation, even in 2020. This loss of forest cover could be attributed to anthropogenic activities such as timber extraction, shifting cultivation, bush burning, grazing activities of livestock, and harvesting trees for firewood, among others (Adedire, 2002). Between 2010 and 2020, Asia recorded the highest recovery from forest loss, followed by Oceania, then Europe (FAO, 2020).

According to Penman et al. (2003), forest degradation involves any direct anthropogenic-induced and continuous decline in carbon density in forests over time. The loss of forest cover comes with severe environmental consequences which may be felt in the short, medium- or long-term. In the absence of the burning of fossil fuels, forest degradation and deforestation contribute the most to the greenhouse effect (Simula and Mansur, 2011). Climate models predict a more than 2°C increase in global temperature should the current emission rates continue (Leon et al*.,* 2022). As carbon density reduces due to forest degradation, the overall sequestration of carbon by plants reduces, increasing the volume of CO_2, which is a major contributor to the greenhouse effect (Masuda et al., 2019). That is, forest cover plays a crucial role in combating climate change, and its continued degradation means an increase in global temperature. Habitat loss has, over the years, remained a pronounced consequence of deforestation and forest degradation. As forests are indiscriminately cleared, habitats may be destroyed, altered, and/or fragmented, which may eventually lead to species extinction (Mullu, 2016). According to Haddad et al. (2015), when habitats are fragmented, biodiversity is subjected to 13-75% reduction with an accompanying dwindle in ecosystem functions owing to a decrease in biomass and alteration in nutrient cycles. Destruction of forest resources has a direct impact on the hydrological cycle and water resources. Intensified agriculture coupled with other human activities that result in deforestation may lead to increased runoff frequency, reduced baseflows, erosion, and sedimentation of streams and rivers as well as pesticide contamination (Mati et al., 2008; Hlásny et al., 2015; García Chevesich et al., 2017). In some developing countries where there is inadequate technology for domestic use, the continuous removal of forest cover could affect water supply, especially for potable use.

Mining, as important as it may be towards the acquisition of minerals for the general well-being of humans, has been known to be a contributor to forest degradation and deforestation. According to Hosonuma, et al., (2012), 7 percent of forests lost is as a result of mining activities. The various stages of mining are characterized by activities that require the clearing of vegetation, such as the construction of mine camps, roads, the actual extraction process, rail infrastructure for the transportation of minerals, among other economic activities at the mines. Bradley (2020) made reference to works by The World Bank and PROFOR (2020), which report 1,500 active mines and 1,800 idle mines in forests contributing to at least one-third of global forest degradation.

Mining, like other anthropogenic activities, also contributes to habitat loss and the loss of biodiversity. Unplanned mining activities have resulted in various consequences on the environment, where forests are lost, biodiversity is lost, water resources are polluted, and landscapes are destroyed (Mahalik and Satapathy, 2016; Mayani-Parás et al., 2019). Ghana, formerly known in the colonial days as the Gold Coast, was so called due to its large economic quantities of gold. Ghana, since 2018, has been the leading producer of gold in Africa, and the third largest producer of Aluminium on the continent. For a long time, mining of not just gold but other minerals such as diamond, bauxite, aluminium, and manganese in the country has immensely contributed towards the economic growth of the country (Akabzaa, 2001; Coakley, 2003; Amponsah-Tawiah and Dartey-Baah; Okyere et al., 2021). According to Appiah et al. (2013), Ghana's mining industry in 2011 contributed to 41% of total exports, 17.5% of corporate tax, 27.6% of government revenue, and 6% of the country's GDP. In 2019, the mining sector was reported to have contributed to 50% of all Foreign Direct Investments, and constituted more than 30% of export revenues (The Ghana Chamber of Mines, 2019). The mining industry of Ghana is categorized into the small-, medium-, and large-scale, and has been a source of direct and indirect employment to many citizens. It is estimated that over 27,000 people have been directly employed in the large-scale mining sector, as well as more than 1,000,000 people in the small-scale sector (Minerals Commission, 2015).

Mining in Ghana has, over the years, come with its environmental consequences (Okyere et al., 2021). Despite the attempts of the government and other Non-governmental bodies to ensure a minimal effect of mining activities on the environment, the country still experiences the impacts of mining activities on its forest resources, water resources, and land resources (Tenkorang, 2021). The environmental effects of mining activities are mostly a result of the operations of unregistered miners in the informal small-scale sector. Over the years, mining activities have cost the country a good portion of its forest resources. According to the Ministry of Lands and Natural Resources (2012), a deforestation rate of about 135,000 ha annually has led to the reduction of the country's forest cover from 8.2 million hectares at the start of the 20th century to an estimated 1.6 million hectares. Thus, Mining in forest reserves has been an issue of environmental concern in the country for a long time (Hilson and Nyame, 2006). Important forest reserves such as the Atewa Range Forest Reserve (ARFR) and the Offi shelterbelt forest reserve have been under the threat of depletion owing to mining activities (Boadi et al., 2016).

In Ghana, stringent regulations exist for the large-scale mining companies, which ensure that they operate in an environmentally friendly manner. An example of these policies is the reclamation security bond agreement, which was introduced by the Environmental Protection Agency (EPA), where money from large-scale mining institutions is deposited at a reputable bank to be used solely for the required reclamation, only if the mining company refuses to undertake reclamation. The situation is, however, different for the small-scale mining sector, which is usually referred to as the informal sector (Bansa et al., 2017). The informal sector comprises authorized groups of individuals who engage in mining on a relatively smaller scale as compared to the large-scale mining companies, and unauthorized groups of people or bodies who engage in mining activities illegally using crude and rudimentary tools. The poorly unregulated nature of the informal mining sector in Ghana usually results in dire environmental consequences, more topical of them being the degradation of water and forest resources in recent times.

In recent years, the rise in illegal mining activities in the country has led to an increase in pollution in many water bodies. The use of water in the mining process by both small- and large-scale companies leads to increased sedimentation, as well as the discharge of harmful chemicals such as mercury and cyanide into water bodies (Attiogbe and Nkansah, 2017). Some major water bodies such as the Pra, Tano, Offin, Ankobra, and Birim, which serve many communities, have been heavily polluted as a result of mining activities (Duncan et al., 2018). A report by the Ghana Water Resource Commission (2021) indicated that all these major rivers had turbidity values greater than 150 NTU in most areas. Thus, water resources in Ghana are in critical condition and warns of water availability threats in the near future if the situation remains unchanged. The government of Ghana has put in place some measures to curb the menace of mining and logging on the forest and land resources. However, some unregistered bodies remain in the hearts of these forests, away from surveillance, and continue to mine while causing damage to the environment.

The ARFR (Fig. 1.1) stands as one of Ghana's most ecologically significant landscapes, providing critical habitat for more than 100 globally threatened species. Notably, it supports a remarkable diversity of avifauna, with approximately 227 bird species recorded within its bounds. Beyond its ecological value, the forest plays a vital hydrological role, serving as the headwaters for three major rivers, Birim, Densu, and Ayensu, which sustain numerous downstream communities, including Ghana's capital, Accra (McCullough et al., 2007; Akomaning et al., 2021). Geologically, the ARFR is situated within the Kibi-Winneba belt of the Birimian rock formation, characterized by gold-mineralized rocks and extensive alluvial soils. This has attracted both legal and illegal mining operations, significantly altering the forest's landscape. Additionally, the forest harbors an estimated 960 million metric tons of bauxite, fueling recent national debates around the potential for commercial exploitation and the environmental trade-offs involved. The presence of valuable timber and mineral resources has led to a surge in anthropogenic pressures, with mining and logging emerging as dominant threats to the forest's integrity. The cumulative impact of these disturbances is alarming. Despite growing awareness, the rate of forest degradation has remained persistent in recent years, with direct consequences for water security and biodiversity conservation. The deterioration of river systems originating in the ARFR now threatens the livelihoods and well-being of both local populations and over one million residents of Accra who depend on these water sources (IUCN, 2016).

Remote sensing has been useful in the mapping and monitoring of mining activities in Ghana in recent years. It has provided insights into the spatial characteristics and dynamics of these mining activities (Forkuor et al., 2020; Gallwey et al., 2020; Kumi-Boateng and Stemn, 2020). A number of research studies have been conducted using remote sensing techniques in the Atewa landscape to map changes in the forest structure over the years as well (Kusimi, 2015; Amponsah et al., 2023). Results from these studies highlight how the ARFR has transitioned from predominantly closed-canopy to open-canopy as a result of human activities such as farming and mining. Also, a study by Nyamekye et al. (2021) focused on mapping mining activities in the study area using remote sensing techniques, where the results showed evidence of continued mining activities even during the 2017 ban on mining activities by the government of Ghana. Despite the contributions provided by these works towards curbing the menace caused by mining activities in the country, they mostly focused on mapping areas that were mined and degraded, and lacked the integration of the affected forest and water resources.

This study employs remote sensing and GIS techniques, utilizing satellite imagery with spatial resolutions of 10 m or finer, to develop an integrated approach for monitoring anthropogenic activities across the Atewa landscape and the ARFR. The analysis also considers the impacts of these human activities on forest and water resources. These are addressed in Chapter 2, where high-resolution PlanetScope satellite images are used to map the annual dynamics of alluvial mining in the landscape and inside the ARFR (2018 – 2023) while assessing the conversion of the various land covers to and from mined sites. It also assesses the proximity of mines to the ARFR and water channels in the study area. In Chapter 3, Sentinel-2 satellite images are used to map small-scale canopy disturbances in the ARFR. This study applies Linear Spectral Mixture Analysis (LSMA) and GIS in identifying small-scale disturbances, such as non-mechanized logging and other possible natural disturbances that are known to precede deforestation. The study uses the relationship of the mapped disturbances and topographic and geospatial features to infer the likely sources of the disturbances, as they do not exhibit spatially explicit proxies that could facilitate source identification. This study explored the capability of the Sentinel-2 satellite imagery in mapping canopy disturbances at the pixel and subpixel levels, while filling the gap of little or no research on the canopy disturbances in the ARFR. Lastly, with little or no information on the above-ground biomass (AGB) and carbon accumulation (CAc) estimates of the ARFR, Sentinel-2 derived vegetation and biophysical indices were used in a logarithmic regression to estimate the AGB and CAc in the ARFR in Chapter 4. This is a crucial aspect of the study as it highlights the significance of the forest reserve in carbon sequestration while emphasizing the effects of human activities on the reserve's ability to sequester carbon. The individual chapters of the study will holistically address conservation issues in the biodiversity hotspot, Atewa landscape in Ghana, by mapping and monitoring changes in land use and land cover (LULC) resulting from human activities such as mining, farming, and logging, which have deteriorating effects on the forest and aquatic ecosystems. It will also bring to light the importance of the forest reserve in contributing to carbon capture and ultimately to climate change in the national and international regimes. Following the background of the study, the research seeks to address the following research questions:

1. How do human activities, especially mining in the Atewa landscape, affect the forest and water resources in the area annually?
2. How can the characteristic small-scale canopy disturbances in the Atewa Range Forest Reserve (ARFR) that do not exhibit spatially explicit source identification proxies be mapped while determining the possible disturbance agents?
3. What is the estimated above-ground biomass (AGB) and carbon accumulation (CAc) of the ARFR that contributes to combating local and global climate change?

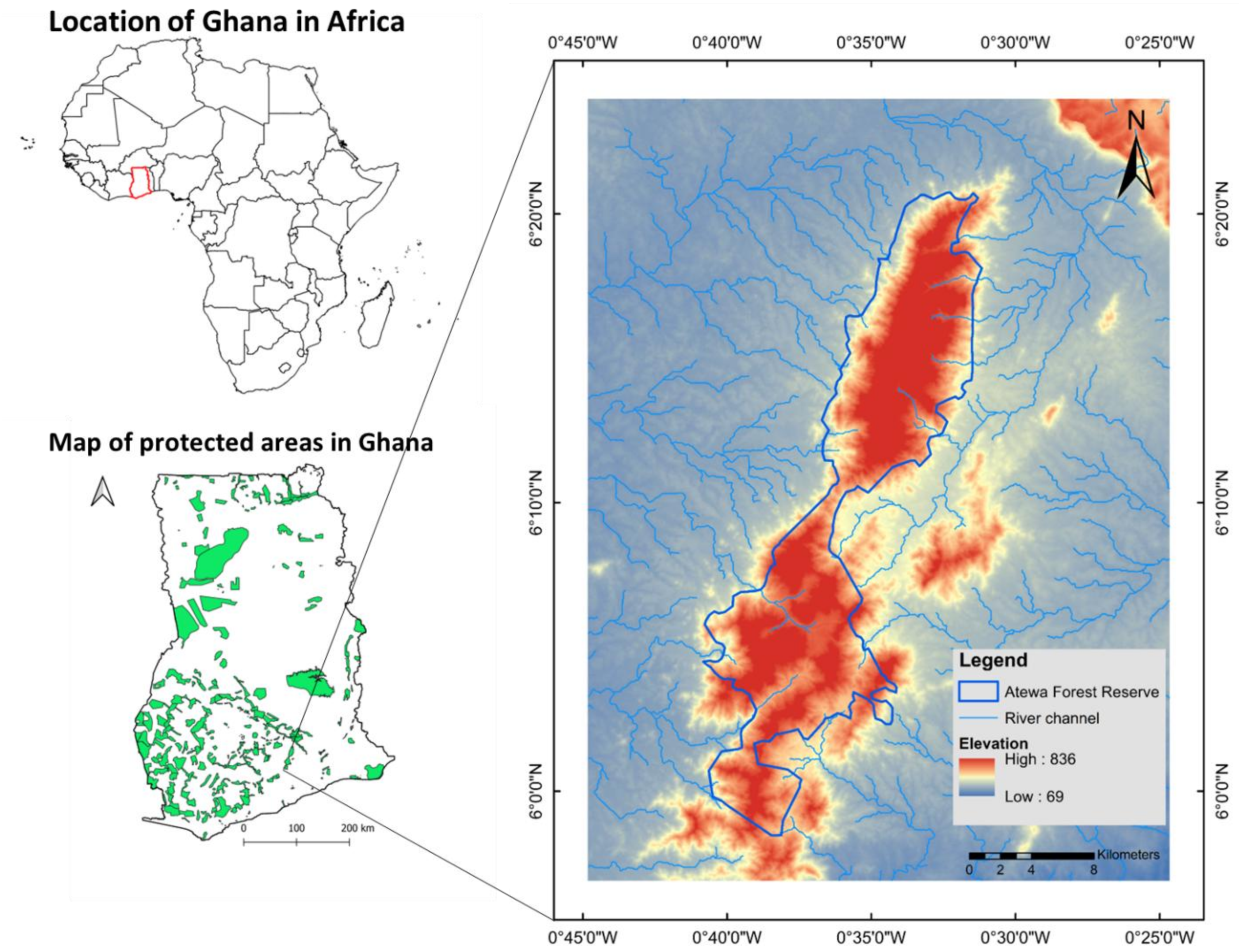

Fig. 1.1. The Atewa landscape showing the location of the Atewa Range Forest Reserve

1.2 Study Objectives

Given the limitations of manual ground-based monitoring in forested areas of Ghana, this research seeks to employ automated approaches using remote sensing and GIS to map and monitor human activities such as mining, farming, and logging, among others, across the Atewa landscape and in the Atewa Range Forest Reserve (ARFR) while highlighting the effects these activities on the ARFR's capability in combating climate change. The specific objectives of the study are:

1. To map alluvial mine dynamics in the Atewa landscape while assessing the proximity of mines to forest and water resources.
2. To map canopy disturbances in the ARFR and infer the possible source (natural or human-induced).
3. To estimate the above-ground biomass (AGB) and carbon accumulation (CAc) of the ARFR.
4. To assess the implications of forest disturbances on biodiversity and climate change.

1.3 Study approach and thesis structure

This thesis presents an integrated remote sensing framework combining Geographic Object-Based Image Analysis (GEOBIA), Spectral Mixture Analysis (SMA), GIS, and aboveground biomass (AGB) estimation to characterize and monitor anthropogenic disturbances within the Atewa Range Forest Reserve (ARFR). Geographic Object-Based Image Analysis facilitates the segmentation of very high-resolution satellite imagery into spectrally and spatially homogeneous image objects, allowing for object-level classification that incorporates not only spectral signatures but also shape, texture, and contextual relationships. Spectral Mixture Analysis is applied to decompose mixed pixels into fractional abundances of endmembers, specifically soil, green vegetation, and shade, enhancing sub-pixel level discrimination in complex, fragmented forest-soil mosaics. Aboveground biomass mapping is conducted using empirical models that integrate vegetation and biophysical indices. This combined approach enables a spatially explicit assessment of forest structure, degradation gradients, and land-use transitions, offering a robust methodological framework for quantifying human-induced changes in forest ecosystems. Figure 1.2 shows a summary of the study approach adopted in this research.

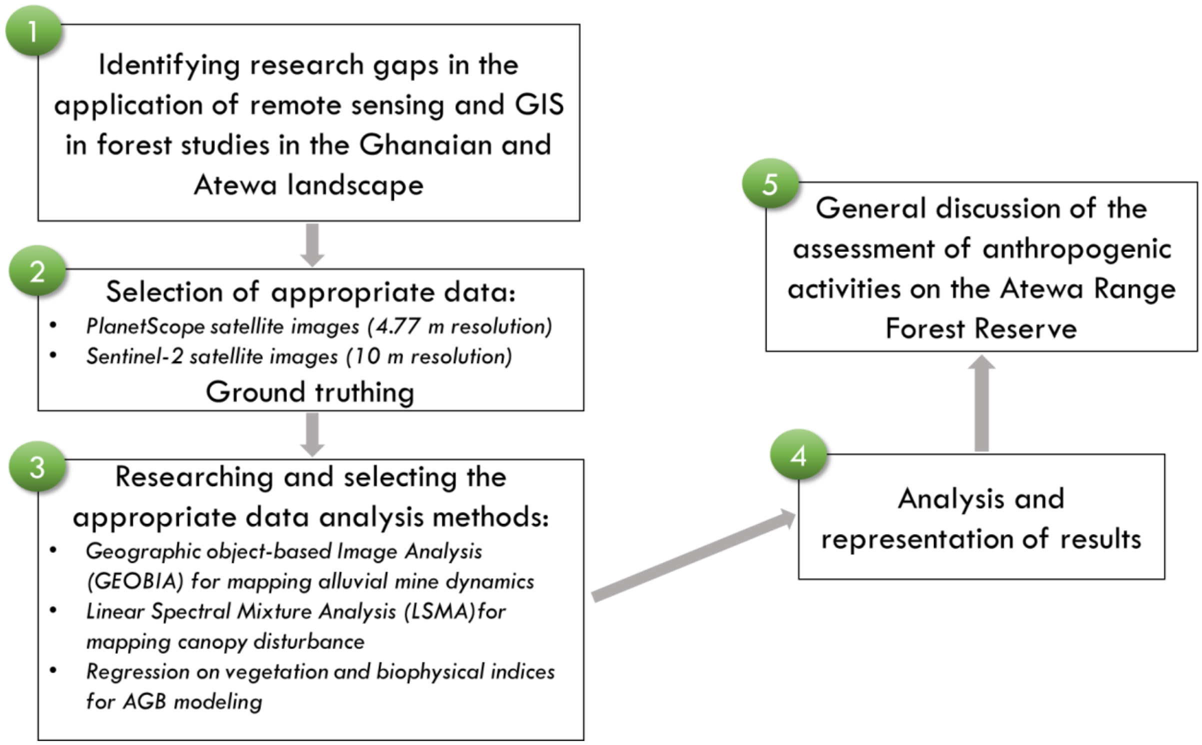

Fig. 1.2. Study approach flow chart

The structuring of the thesis follows the sequence:

Chapter 2: Mapping alluvial mine dynamics in the Atewa landscape using Geographic Object-based Image Analysis (GEOBIA) to understand the annual loss/gain dynamics of alluvial mines, proximity of mines to the Atewa Range Forest Reserve (ARFR) and river channels, and the transitioning of land use to and from alluvial mines.

Chapter 3: Inferring canopy disturbance sources in the ARFR through their relationship with topographic and geospatial features to understand the degradation dynamics that usually precede deforestation.

Chapter 4: Estimating above-ground biomass of the ARFR in Ghana using Sentinel-2 imagery to establish the importance of the forest reserve in carbon sequestration and mitigating climate change.

Chapter 5: General discussion of the assessment of anthropogenic activities on the ARFR and its implications for biodiversity and climate change.

Chapter 6: Holistic conclusions inferred from chapter outcomes.

Chapter 2

Mapping alluvial mine dynamics in the Atewa landscape in Ghana using Geographic Object-based Image Analysis (GEOBIA) and GIS

2.1 Introduction

Mining is a significant driver of environmental degradation, particularly impacting forest ecosystems and water resources (Kahhat et al., 2019). It is an extractive activity that involves the removal of valuable minerals, metals, and other geological materials from the Earth's crust for economic purposes (Hartman, 2002). Among the various forms of mining, alluvial mining, also known as river mining, focuses on extracting precious minerals from unconsolidated sediments in riverbeds or floodplains (Hilson, 2002a; Dethier et al., 2023). Due to its reliance on simple and rudimentary tools and techniques, alluvial mining has become a viable livelihood for many small-scale artisanal miners globally (Hilson, 2002b; Schwartz et al., 2021). However, this practice has exacerbated environmental harm, particularly through the destruction of forests and the pollution of water bodies, posing significant ecological challenges (Roach et al., 2013; Asner and Tupayachi, 2017). In Ghana, mining, particularly for gold, has been a major economic driver but has also caused substantial environmental damage. The mining sector of Ghana has remained a significant contributor to exports, government revenue, and employment over the years (Okyere et al., 2021). However, despite efforts to mitigate its impact, mining has led to severe deforestation and water pollution, especially from illegal mining operations (Attiogbe and Nkansah, 2017; Tenkorang, 2021). Ghana has lost about 100,000 hectares of forest mainly as a result of illegal mining activities between 2010 and 2020 (IUCN, 2024). Mining in forest reserves has been an issue of environmental concern in the country for a long time (Hilson and Nyame, 2006) as important forest reserves such as the Atewa Range Forest Reserve (ARFR), and the Offin Shelterbelt Forest

Reserve have been under the threat of depletion owing to mining activities (Boadi et al., 2016). Also, some major water bodies such as the Pra, Tano, Offin, Ankobra, and Birim which serve many communities have been heavily polluted as a result of mining activities (Duncan et al., 2018). A report by the Ghana Water Resource Commission, (2021) indicated that all these major rivers had turbidity values greater than 150 Nephelometric Turbidity units (NTU), which is an indication of high values of suspended density (Azis et al., 2015) from mining activities. Thus, water resources in Ghana are in critical condition and warns of water availability threats shortly if the situation remains unchanged.

The ARFR is one of the most important forest resources in Ghana as it is the habitat for over 100 globally threatened species. Among the numerous species of wildlife in the forest, about 227 species of birds are found in the forest reserve as well. The forest serves as a source to the Birim, Densu, and Ayensu rivers which are major rivers with many tributaries, serving many communities including the capital city of Ghana, Accra (McCullough et al., 2007; Akomaning et al, 2021). The geological location of the forest reserve has led to the establishment of some registered mining companies around the forest reserve with a good number of illegal miners reported to have been operating in the reserve as well. The ARFR again bears about 960 million metric tons of bauxite deposits which in recent times has sparked the debate concerning its exploitability (Purwins, 2022). The availability of timber and minerals in this highly diversified forest reserve has attracted a lot of anthropogenic activities. Unregulated activities of miners endanger the ecosystem and hence, the biodiversity of the forest reserve. It is estimated that about 14 km^2 of the buffer zone surrounding the forest reserve has been mined and alluvial gold recovery methods that make use of high-pressure water have increased the rate of sedimentation in rivers and have affected water quality downstream. The rate of degradation of the ARFR has remained steady in recent times with activities of miners and loggers affecting the quality of rivers that serve people in surrounding communities and over 1 million people in Accra (IUCN, 2016). However, government interventions, which have mostly been ground-based monitoring of illegal mining activities have been limited by area coverage and time factor considering the urgency of the situation.

The use of remote sensing has over the years been extremely useful in the automated mapping and monitoring of degradation caused by mining activities. Various studies have shown that remote sensing applications in the monitoring of alluvial mines are cost-effective as well as time-saving (Bruno et al., 2020; Barenblitt et al., 2021; Nyamekye et al., 2021; Moomen et al., 2022). Most studies that employ the use of remote sensing in the monitoring of mining activities do so using pixel-based methods. However, due to issues of high spectral variability, there is usually a reduction in classification accuracies where high-resolution satellite images are used (Simionato et al., 2021). The use of Geographic Object-Based Image Analysis (GEOBIA) in land use land cover (LULC) classification, especially in high-resolution satellite imagery has significantly improved classification accuracies. Segments of objects that are created by the grouping of homogenous pixels, and the subsequent classification based on object features such as shape, texture, context, and ancillary data such as Digital Elevation Model (DEM) do away with misclassification that is likely to occur in pixel-based classifications (Tonyaloglu et al., 2021; Lestari et al., 2023). The applicability of GEOBIA in LULC classification extends to terrains with varying characteristics while improving classification accuracy. In a comparative study by Whiteside et al. (2011) in the non-mining savannas of Australia, object-based classification yielded statistically significantly higher accuracy than a pixel-based classification in an ASTER satellite image. When Grebby et al. (2016) used GEOBIA in a lithological mapping study on a 4-meter resolution Airborne Thematic Mapper (ATM) multispectral imagery, it again outperformed the pixel-based method in terms of accuracy. Simionato et. al. (2021) also applied GEOBIA in identifying artisanal mining sites in the Amazon rainforest and achieved global accuracies of up to 88.18%. In a study by Nyamekye et al. (2021) in the Atewa landscape, even though the pixel-based classified images produced high accuracies, they were outperformed by the object-based classification.

While the 2017 ban on mining activities by the government of Ghana might not have been effective overall (Nyamekye et al., 2021), it succeeded in depriving many mining community members of their livelihoods which eventually led to its repeal (Kumah and Nyarko, 2018; Orleans-Boham et al., 2020). The post-ban periods, starting from 2018, have been characterized by reports of increased water turbidity and mining activities in forest reserves as miners rushed back into business (Duncan et al., 2018; Ghana Water Resource Commission, 2021). This has necessitated the need for monitoring and mapping activities of miners, especially in forest reserves and river bodies. Previous studies on mapping artisanal alluvial mines in Ghana have predominantly relied on satellite imagery with resolutions ranging from 10 to 30 meters (m) (Kusimi, 2015; Forkuor et al., 2020; Gallwey et al., 2020; Kumi-Boateng and Stemn, 2020; Nyamekye et al., 2021) with little focus on the annual proximity patterns of mines to forests and river channels. While these studies focused on the changes in mined areas in the periods of study, they did not analyze the transition dynamics of other LULC classes to alluvial mines or provide information on post-mine vegetation recovery. This study utilizes high-resolution PlanetScope imagery at 4.77 m, combined with GEOBIA, to accurately map alluvial mine dynamics, reducing intra-class misclassifications and enhancing overall accuracy. The study also assesses the annual proximity patterns of mines to the ARFR and water resources in the study area while providing the dynamics of class transitions to alluvial mines and post-mine vegetation recovery. While mapping changes caused by mining activities over longer time intervals with emphasis on time nodes that signify important changes is crucial, it risks missing important details on changes between such longer time intervals. An understanding of the annual dynamics of mining activities and their proximity to important resources like river bodies and the ARFR is thus necessary for understanding the possible factors that compound into substantial changes over time. The specific objectives of the study were: (1) to determine how the post-ban alluvial mining activities affect the LULC pattern of the study area annually, (2) to assess annual alluvial mine dynamics and (3) to assess the annual proximity patterns of mines to the ARFR and river channels in the study area. Results from this study will contribute to the effective management of the ARFR and provide insights into the dynamics of alluvial mines in the Atewa landscape, especially after the mandatory halt in the activity.

2.2 Materials and Methods

2.2.1 Study area

The study was conducted in the Atewa Range Forest Reserve (ARFR) and its surroundings referred to as the Atewa landscape in this study (Fig. 2.1). The study area falls between latitudes 5° 56’ to 6° 23’ North and longitudes 0° 24’ to 0° 40’ West while covering parts of eleven districts in the Eastern region of Ghana. The landscape covers three important river basins: the Birim, Densu, and Ayensu basins whose heads originate from within the ARFR. The forest reserve which lies between latitudes 5° 58’ to 6° 20’ North and longitudes 0°31’ to 0°41 West represents the predominant highland area of the study area. It lies on the Atewa range of mountains with heights reaching 842 meters (m) above sea level (McCullough et al., 2007). It covers about 26,300 ha with a north-south orientation (Kusimi, 2015; IUCN, 2023).

The Eastern region of Ghana experiences average temperatures between 22-33°C and is characterized by semi-deciduous rainforests to the south and a transitional savanna zone to the north. The major rainy season falls between March and July while the minor is from September to November. The dry season, characterized by cold and dry weather, starts in November and ends in February (MOFA, 2024). The ARFR has an average temperature range between 24 and 29°C with an average annual rainfall between 1,200 and 1,600 mm. The two rainy seasons record the highest rainfall from May to July, then from September to November (McCullough et. al., 2007; Kusimi, 2015).

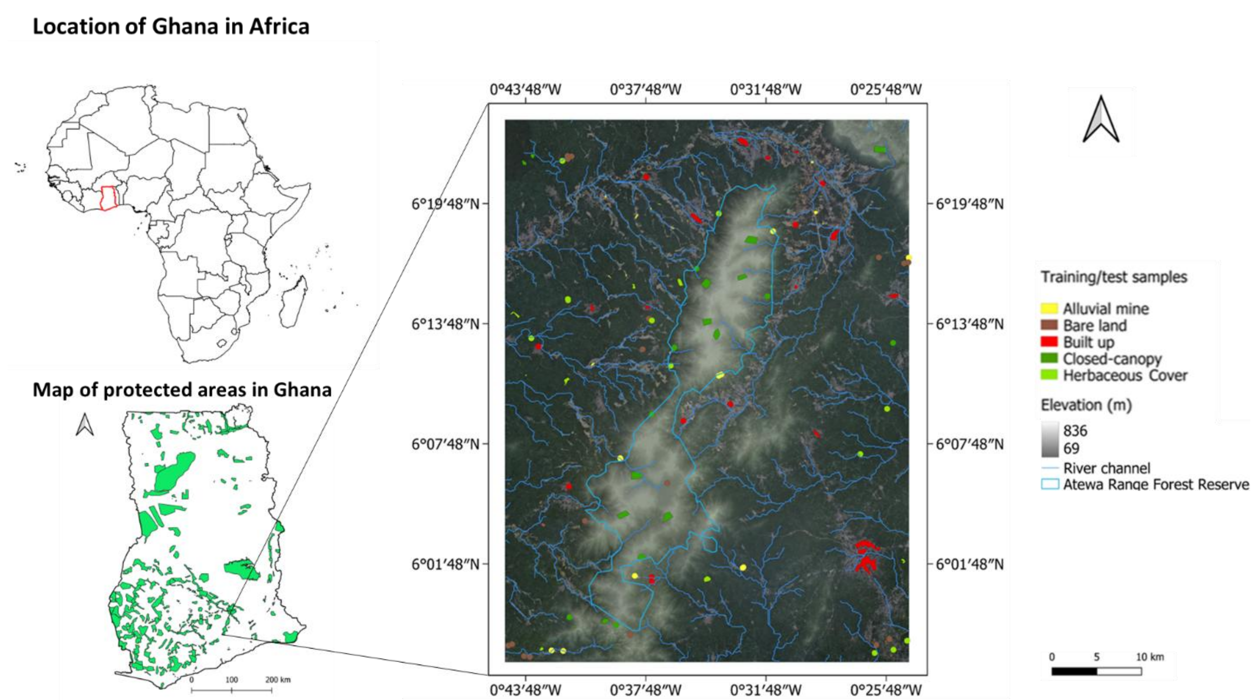

Fig. 2.1. Map of the study area showing the distribution of training and test samples in 2023 (Polygons represent high-resolution satellite image training/test samples; corresponding points represent ground-truthed training/test points)

2.2.2 Satellite image and ground truthing

True color (Red, Green, and Blue - RGB) monthly mosaicked PlanetScope satellite imagery with 4.77 m resolution for the periods 2018, 2020, 2021, 2022, and 2023 were downloaded via the Planet Explorer website, https://www.planet.com/explorer/ (Planet, 2023) for the study. To increase the chances of acquiring cloud-free data, satellite images were acquired between November and March which is mostly the dry season of the study area. The year 2019 was skipped as there was no cloud-free satellite image for the study area. Table 2.1 shows the dates of acquisition of the satellite images used. Despite the differences in the acquisition dates, the acquisition of all images in the dry season implies a high likelihood of exposure to similar seasonal environmental conditions to ensure consistency. A minimum of twelve (12) image tiles were downloaded for each year. The downloaded tiles were then mosaicked into a single image and clipped to the study area shape file.

Ground truthing was undertaken in 2023 for some selected safe and unrestricted parts of the study area where training and test data for the LULC types were collected using a handheld Global Navigation Satellite System (GNSS) receiver (Garmin GPSMAP). The training and test data were supplemented by high-resolution Google Earth Pro images, especially for inaccessible areas. In the absence of ground truth data for 2018 to 2022, training and test samples were derived from high-resolution Google Earth Pro images with guidance from existing LULC data. Each year, the data was split into 60% for training and 40% for testing. The split ratio decision was based on providing enough data to enable the classification algorithm to learn the varying characteristics of each class accurately while providing adequate data for a robust accuracy assessment. A stratified sampling technique was employed for training and testing to ensure that underrepresented classes, such as bare land and alluvial mines, were proportionally represented in the dataset. This approach helps maintain class balance and improves model performance by preventing bias toward dominant land cover types.

2.2.3 Data analysis

The main stages of the data analysis process of the method used in the study are displayed in Fig. 2.2.

2.2.4 Geographic Object-Based Image Analysis (GEOBIA)

2.2.4.1 Segmentation

The multiresolution segmentation algorithm in the eCognition software was used where different objects were segmented based on the parameters, scale, shape, and compactness (Baatz, 2000). These are dimensionless parameters that are used to fine-tune the segmentation process, allowing for the desired level of detail and object definition. The scale parameter, a positive integer, determines the size of objects while the shape parameter is based on pixel spectral values and shape homogeneity of segments. Compactness affects how the segmentation captures compact objects (Simionato et al., 2021). All 3 bands of each image were used for the segmentation with an assigned weight value of 1. The selection of segmentation parameter values is crucial to the subsequent classification accuracy (Kucharczyk et al., 2020). The optimal segmentation parameter values were selected based on trial and error through visual inspections where scale = 60, Shape = 0.05, and compactness = 0.8. The scale value of 60 was used because lower values led to over-segmentation which could affect the classification accuracies for built-up areas and alluvial mines due to their spectral, and textural similarities. Thus, distinguishing alluvial mine sites from other land use classes such as non-mine bare land and built-up areas was a crucial consideration in the segmentation process.

2.2.4.2 Classification

Five dominant LULC classes were identified for the study. These are Alluvial Mine, Bare Land, Built-up, Closed-canopy vegetation, and Herbaceous cover. Table 2.2 shows the LULC classes considered and their descriptions. The Nearest Neighbor classification algorithm in eCognition was used for the supervised classification. The Nearest Neighbor classifies objects based on their proximity to the closest training data while assigning an object the class of the majority of its neighbors (Whiteside et al., 2011).

First, object attribute features under spectral, textural, and custom features were selected. The spectral attributes comprised the mean values of all three bands while the Gray Level Co-occurrence Matrix (GLCM) contrast, entropy, and correlation were considered for the textural attributes. The GLCM contrast textural attribute consistently produced values that were significantly different for built-up areas and alluvial mine sites and was considered an important object feature in the differentiation of the two classes. On the other hand, GLCM entropy and correlation produced values that were similar for alluvial mine sites and built-up areas, and as such were discarded to save computational workload. The custom attribute used was the Green-Red Vegetation Index (GRVI) which was used to accurately detect and differentiate the different vegetation classes. In the absence of near-infrared (NIR) bands, the Normalized Difference Vegetation Index (NDVI) was not applicable, hence the application of GRVI. Equation (1) shows the formula used to compute GRVI.

$$\text{GRVI} = \frac{\rho green - \rho red}{\rho green + \rho red} \qquad \text{Equation (1)}$$

Where ρgreen and ρred are the respective reflectance of green and red in the visible light spectrum.

Green vegetation, soil, and water may have GRVI values that are positive, negative, and near zero. At the threshold GRVI = 0 however, green vegetation becomes distinguishable from non-green vegetation (Motohka et al., 2010). In this study, different values for the vegetation classes were produced by the GRVI in different years. This facilitated the differentiation of vegetation from other classes. For instance, in 2023, values ranged between 0.38 and 0.44 for the herbaceous cover class while recording > 0.44 for the closed-canopy vegetation class. GRVI values for the other classes were < 0.38.

The sample selection was guided by the training data through visual interpretation. This resulted in a minimum of 22 samples per class and at least 110 for all classes. The pixel count of the training and test samples are shown in Table 2.3. The resulting classified vector polygons were exported for further analysis. Images of a segmented satellite image and the corresponding classified vector polygons are shown in Fig. 2.3.

Table 2.1

Acquisition dates of PlanetScope monthly mosaicked images used in the study

Year	PlanetScope imagery acquisition date
2018	March 2018
2020	January 2020
2021	March 2021
2022	December 2022
2023	December 2023

Table 2.2

LULC classes used in the study and their descriptions

LULC Classes	Description
Alluvial Mine	Areas used for mining activities. Usually characterized by highly turbid water and dugouts of wet laterite
Bare Land	Tilled lands usually for agricultural purposes, non-vegetated surfaces of human settlements (non-mine lands)
Built-up	Human settlements in the form of buildings, villages, towns, and cities
Closed canopy	Forests, thickets, oil palm, and cocoa plantations, fully grown agric. fields (vegetation that is not easily accessible)
Herbaceous cover	Shrub, herb, grasses, and young-stage agric. fields (vegetation that is easily accessible)

2.2.5 Post-classification correction

Post-classification correction is important in increasing classification accuracies by reducing misclassification resulting from similarities in spectral reflectance (Manandhar et al., 2009; Ibrahim et al., 2020). Because many alluvial mines within the study area exist close to settlements (Nyamekye et al., 2021), and because the alluvial mine and built-up classes share similar spectral and textural characteristics, there was the issue of misclassification between the two classes. To minimize classification errors, OpenStreetMap data and vectorized river channels of the study area were utilized to differentiate settlements from alluvial mines. Field observations indicated that alluvial mines predominantly occur along river channels, making the presence of large settlement areas near these waterways unlikely in the classified images. Based on this knowledge, built-up areas located within a 20 m buffer of river channels were reassigned as alluvial mines, using OpenStreetMap as a reference for validation.

2.2.6 Accuracy assessment

Accuracy assessment is a crucial stage in the classification process as it determines the level of agreement between classified maps and reference data (Tonyaloğlu et al., 2021). A pixel-based accuracy assessment was chosen over the polygon-based approach to minimize potential bias and ensure a more objective evaluation of the classification results (Radoux and Bogaert, 2017). The confusion matrix was used in the evaluation of the accuracy of the classification. From the confusion matrix, the Overall Accuracy (OA), Producer's Accuracy (PA), User's Accuracy (UA), and Kappa coefficient were determined.

2.2.7 Post-classification change detection

Post-classification change detection was key in determining the annual changes that occurred in the study area among the LULC classes. It was employed in determining and quantifying the LULC transitions as well as their gains and losses (Radwan et al., 2021). Change detection was undertaken on an annual basis by pairing images from a particular year with that of the preceding year. For instance, using classified images from the base year (2018) and that of the preceding year (2020), and so on. To undertake change detection, the vector polygons comprising the various LULC classes were first dissolved in ArcGIS to make the acquisition of area statistics for each class easy. The vectorized classified image was then converted into a raster file for change detection analysis. The formulas used for calculating the rate of change of the classes and the alluvial mine loss/gain percentages are presented in Equations (2) and (3) respectively.

$$\text{Rate of change} = \frac{1}{(t_2 - t_1)} ln(\frac{A_2}{A_1}) \quad \text{Equation (2)}$$

$$\text{Loss/gain \%} = (\frac{Change\ in\ area\ of\ final\ year}{Area\ of\ initial\ year}) \times 100 \quad \text{Equation (3)}$$

where, A_1 = Area of initial year, A_2 = Area of final year, t_1 = Initial year, and t_2 = Final year.

Table 2.3

Pixel count of training and test samples used for classification and validation

	2018		2020		2021		2022		2023	
Class	Training sample	Test sample	Training sample	Test sample	Training sample	Test sample	Training sample	Test sample	Training sample	Test sample
Alluvial Mine	89,415	73,254	92,601	81,221	87,557	79,334	90,168	72,372	89,112	77,211
Bare Land	99,462	64,308	97,351	66,011	95,577	65,501	95,941	60,988	96,312	60,223
Built up	197,847	105,232	199, 031	100,101	187,912	98,887	196,981	102,399	200,100	102,144
Closed canopy	222,740	148,493	225,665	140,236	230,010	151,278	226,110	150,477	229,458	155,364
Herb. cover	268,079	175,386	283,121	235,202	281,145	269,898	275,441	241,143	277,233	198,992

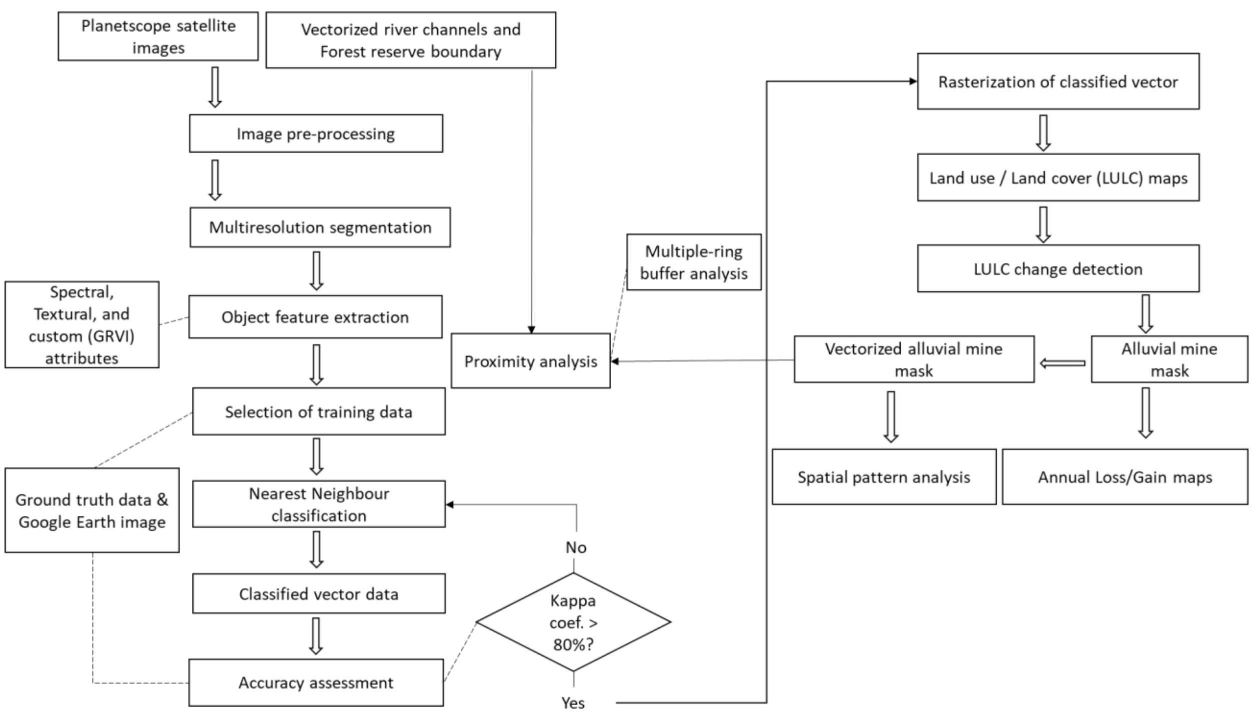

Fig. 2.2. Flowchart of methodology

2.2.8 Buffer analysis

To assess the proximity of alluvial mines to the forest reserve, experimental multiple-ring buffers of distances 100 m, 200 m, 500 m, and 1 kilometer (km) were created around the boundary of the forest reserve. The 100 m buffer was considered the most important of all the forest reserve buffers because any mining activity within the 100 m buffer is likely to have a direct or indirect effect on the forest. The rest were used to track the changes in mined areas as one moves closer to the forest edge. Multiple-ring buffer analysis was again employed to assess the proximity of alluvial mines to river channels. Buffer distances used for river channels were 100, 200, and 300 m. The base 100 m buffer was based on the Riparian Buffer Policy for Managing Freshwater Bodies in Ghana (Ministry of Water Resources, Works and Housing, 2013) which states that no human activities be undertaken within 100 m off water marks. The 200 and 300-meter buffers were used to assess the changes in mined areas as one moves closer to river channels. The area of alluvial mines within the buffers was determined and used for the proximity analysis.

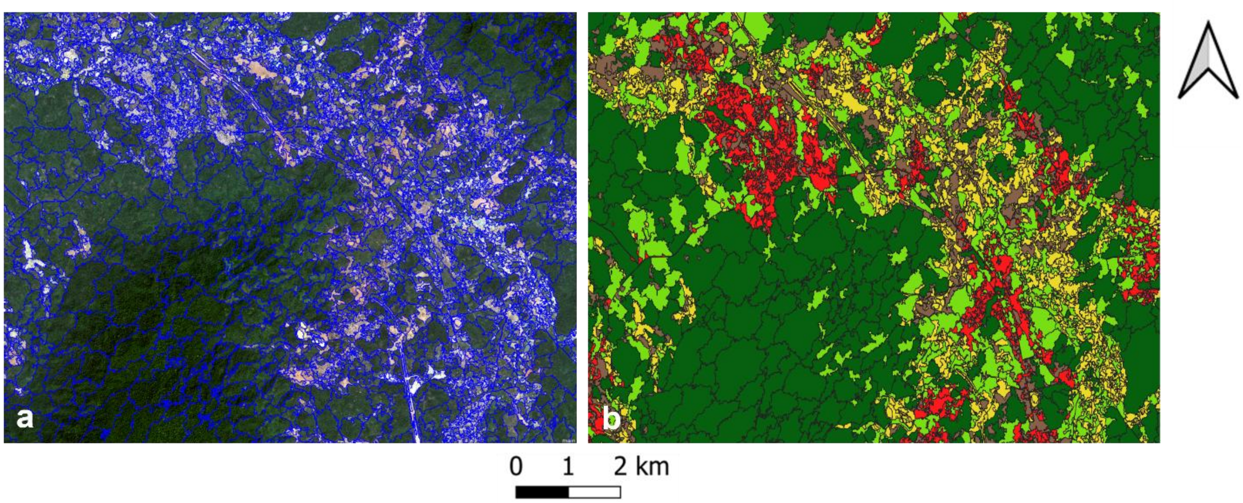

Fig. 2.3. (a) Multiresolution segmentation; (b) Classified vector polygons

2.3 Results

2.3.1 Land use land cover classification results

Accuracy assessments of the various LULC maps are displayed in Table 2.4. The Kappa coefficient value was used in assessing the accuracy of the classified maps. It ranges from -1 to 1 where values approaching 1 imply high accuracy and vice versa (Pandey et al., 2023). The Kappa coefficient for the classified maps ranged from 0.82 in 2021 to 0.89 in 2018 which signifies an almost perfect agreement (Bogoliubova and Tymków, 2014).

From the annual average values in Table 2.5, the alluvial mine class remained the least dominant class in most years, except in 2022, and showed a continuous increase (Nyamekye et al., 2021), peaking at 8,005.2 ha in 2021. Between 2018 and 2023, it recorded a total change rate of 12.3%. This was followed by the bare land class which showed a consistent decline except in 2024. The bare land class changed by -21.1% between 2018 and 2023. The built-up class followed a steady annual growth trend, with an overall change rate of 1.4%, expanding from 8,399.1 ha in 2018 to 9,011.0 ha in 2023. The herbaceous cover class exhibited a consistent decline across all years, except in 2021, with an overall change rate of -16.2%. It reached its largest extent in 2018 at 71,445.1 ha and its lowest in 2023 at 31,706.6 ha. The study area was dominated by the closed-canopy vegetation class, which occupied the majority of the area throughout the periods of consideration. The closed-canopy vegetation class recorded the highest area of 135,871.5 ha in 2023 representing 71.8% of the total landscape area while recording a low of 91,743.4 ha in 2018 making up 48.5%. Between 2018 and 2023, it exhibited a change rate of 7.9%.

In the Atewa Range Forest Reserve (ARFR), the alluvial mine class showed an irregular trend of increase and decrease across the periods with a high of 20.3 ha in 2018 and a low of 1.7 ha in 2020. Its recorded rate of change between 2018 and 2023 was -21.4% (Table 2.6). The bare land class recorded its highest coverage of 70.9 ha in 2021 and an annual average of 32.5 ha. It also exhibited an irregular trend of increase and decrease while changing at a rate of -54.4%. The built-up class was the least dominant in the forest reserve. It showed a decreasing trend except in 2021 and recorded a change rate of -49.2%. The herbaceous cover showed consistency in annual decrease except in 2023 as seen from its rate of change (-4.6%) while averaging 10% of the reserve's total area annually. The Closed-canopy vegetation class was consistently the major class with an average coverage representing 90% of the entire reserve across the five years. It recorded a positive rate of change of 0.6% even though its increase was not annually consistent. By visual inspection, bare land and herbaceous cover were mostly observed along the fringes of the reserve (Fig. 2.4).

Table 2.4

Summary of classification accuracies from 2018 to 2023

	2018		2020		2021		2022		2023	
	PA (%)	UA (%)	PA (%)	UA (%)	PA (%)	UA (%)	PA (%)	UA (%)	PA (%)	UA (%)
Herb. cover	94.21	86.33	93.66	89.45	78.91	93.11	92.15	94.44	93.84	91.5
Closed canopy	96.76	92.82	97.22	91.34	98.97	83.1	97.05	87.65	97.66	90.87
Bare Land	76.46	81.01	58.78	77.02	82.35	74.61	61.27	89.22	69.47	68.23
Alluvial Mine	80.89	93.85	85.28	94.04	77.1	77.58	65.33	90.01	63.2	95.68
Built-up	89.66	85.91	91.24	63.71	71.8	97.55	88.91	72.71	92.06	74.65
OA (%)	91.68		89.28		86.00		89.44		88.38	
Kappa	0.89		0.86		0.82		0.86		0.85	

2.3.2 Change detection

Post-classification change detection was useful in determining the dynamics of alluvial mining activities. The dynamics considered in this study were (i) the transition of other LULC to alluvial mines and (ii) post-mine vegetation recovery.

The herbaceous cover was mostly converted into alluvial mine, making up an annual average of 45.2% of all classes that were converted to alluvial mines. The Closed-canopy vegetation class followed with an annual average of 38.7% while bare land recorded 15.4%. The built-up class was the least converted into alluvial mines (Fig. 2.5a).

Post-mine vegetation recovery was mostly represented by a transition from alluvial mines to herbaceous cover and could not confirm prior mine restoration. Alluvial mines were consistently converted into herbaceous cover in the Atewa landscape, representing over 99% of the vegetation classes in the post-mine vegetation recovery (Fig. 2.5c). The highest post-mine vegetation recovery occurred between 2021 and 2022, representing 40% of the mined area while 2020-2021 recorded the least recovery. Between 2018 and 2023, 42.1% of the mined area had been recovered in terms of vegetation regrowth in the Atewa landscape.

In the forest reserve, the vegetation classes were mostly converted into alluvial mines with bare land being the next contributor (Fig. 2.5b). The highest conversion of the combined vegetation classes into alluvial mines occurred between 2020 and 2021 with 8.2 ha. The conversion of bare land into alluvial mines began between 2020 and 2021 with 4.2 ha while showing a decrease from 2022 - 2023 after peaking between 2021 and 2022 with 5.2 ha. Post-mine vegetation recovery in the forest reserve was dominated by the herbaceous cover class and was highest between 2021 and 2022, representing 87.7% of the mined area. Between 2020 and 2021, there was the lowest record of post-mine vegetation recovery of 1.2%, while 46.0% of mines recovered with vegetation between 2018 and 2023. Figures 2.5e and 2.5f show the percentage of mined area that showed revegetation.

2.3.3 Annual loss/gain in alluvial mines

Alluvial mine loss/gain maps displayed in Fig. 2.6 show areas that gained, lost, or remained alluvial mines along the various river channels in the study area. In 2023, the area of alluvial mines in the landscape showed a 147% increase compared to 2018, while a 50.2% decrease was also recorded relative to the same year. This corresponded to a 48.7 and 96.9% increase and decrease, respectively, in the forest reserve (Table 2.7). The highest gain in alluvial mine activities in the landscape was recorded between 2020 and 2021 with the landscape recording a 105% increase while the ARFR recorded a 7-fold increase of over 600%. In 2022, the landscape recorded the highest loss of mines, which represented 47.5% of mines in 2021. The largest mined area lost within the forest reserve occurred between 2018 and 2020 by 98.2%. Outside the forest reserve, at least 52% of mines from the previous year remained unchanged in each new year while 49.8% of mines in 2018 remained unchanged in 2023. The area of unchanged mines within the ARFR ranged between 0 and 67.1% of the previous years' mines while 3.1% of the mines in 2018 persisted in 2023.

2.3.4 Forest reserve and water channel buffer analysis

To determine the proximity of mines to the forest reserve, a multiple-ring buffer of 100 m, 200 m, 500 m, and 1 km was created around the boundary of the forest reserve (Fig. 2.7a). The number of mines within each buffer, represented by the number of polygons and their corresponding area was calculated to determine the mines' proximity to the forest reserve. From Table 2.8, it is observed that at least 7.7% of the total area mined annually was within the 1 km buffer zone. The 100 m buffer zone recorded a low of 34.3 ha of mines in 2020 and a high of 119.8 ha in 2021. These represented 0.7 and 1.4% of the total mined area in 2020 and 2021, respectively.

Multiple-ring buffers of 100, 200, and 300 m were created around river channels to determine their proximity to mining activities (Fig. 2.7b). Most of the mining activities across the years fell within the 300 m buffer of the river channels with a high of 6,296.0 ha in 2021 and a low of 3,263.1 ha in 2018. These represented 75.9 and 78.8% of the total area mined each respective year. Within the 100 m buffer zone, 2018 recorded the lowest mining activity with 2,556.0 ha which represented 61.8% of the total mined area. The largest mined area within the 100 m buffer was recorded in 2021 with 5,010.7 ha, representing 60.4% of the total mined area. At least 49.7% of the total mined area was within the 100 m buffer around the river channels.

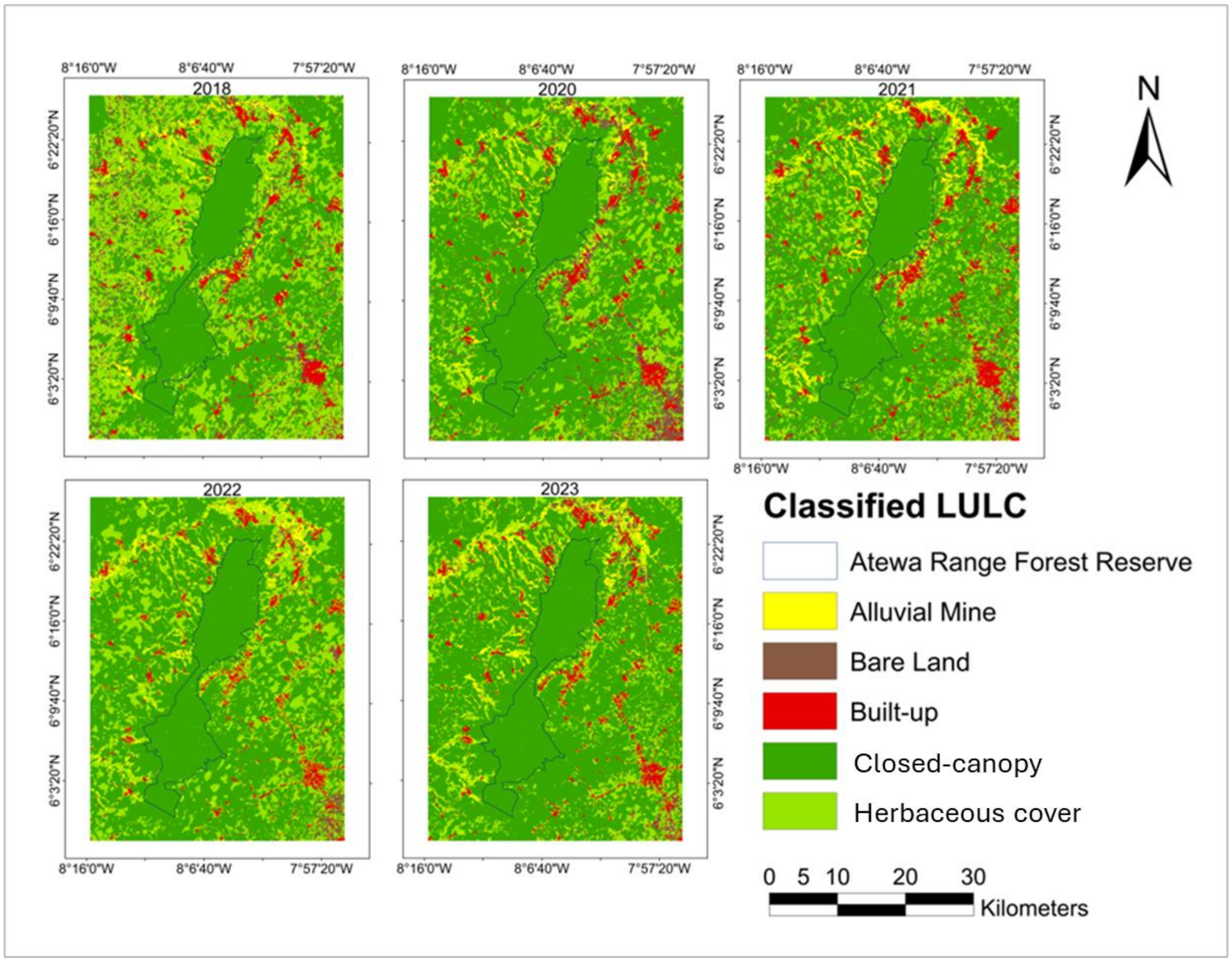

Fig. 2.4. LULC maps from 2018 to 2023

Table 2.5

LULC area (Ha) from 2018 to 2023 in the Atewa landscape

	Alluvial mine (ha)	%	Bare land (ha)	%	Built up	%	Closed canopy	%	Herb. cover	%
2018	4,271.7	2.3%	13,340.5	7.1%	8,399.1	4.4%	91,743.4	48.5%	71,445.1	37.8%
2020	4,563.4	2.4%	10,483.7	5.5%	8,644.1	4.6%	125,248.7	66.2%	40,259.9	21.3%
2021	8,005.2	4.2%	9,242.9	4.9%	8,698.4	4.6%	122,426.4	64.7%	40,826.9	21.6%
2022	6,424.6	3.4%	3,435.0	1.8%	9,001.5	4.8%	126,100.9	66.7%	44,237.8	23.4%
2023	7,907.1	4.2%	4,646.8	2.5%	9,011.0	4.8%	135,871.5	71.8%	31,763.4	16.78%
Ann. Av.	6,234.4	3.3%	8,229.8	4.4%	8,750.8	4.6%	120,278.2	63.6%	45,706.6	24.2%
ROC	12.3%		-21.1%		1.4%		7.9%		-16.2%	

Ann. Av. = Annual average; ROC = Rate of change (Negative values represent a decrease while positive values represent an increase)

Table 2.6

LULC area (Ha) from 2018 to 2023 in the Atewa Range Forest Reserve

	Alluvial mine (ha)	%	Bare land (ha)	%	Built up areas	%	Closed canopy	%	Herb. cover	%
2018	20.3	0.0	54.9	0.0	0.4	0.0	21,454.8	90.0	2,608.8	10.0
2020	1.7	0.0	31.4	0.0	0.3	0.0	22,390.1	90.0	1,715.6	10.0
2021	12.7	0.0	70.9	0.0	0.4	0.0	23,090.3	100.0	964.9	0.0
2022	12.1	0.0	1.7	0.0	0.0	0.0	23,156.6	100.0	968.7	0.0
2023	7.0	0.0	3.6	0.0	0.0	0.0	22,055.6	90.0	2,073.1	10.0
Ann. Av.	10.8	0.0	32.5	0.0	0.2	0.0	22,429.5	90.0	1,666.2	10.0
ROC	-21.4%		-54.4%		-49.2%		0.6%		-4.6%	

Ann. Av. = Annual average; ROC = Rate of change (Negative values represent a decrease while positive values represent an increase)

2.4 Discussion

2.4.1 Land use land cover classification results

The Increasing trends in alluvial mining activities in the study area as seen from the positive rate of change (Table 2.5), can be attributed to the presence of the Birim and the Ayensu, rivers. Taking their sources from within the forest reserve, these rivers are known to hold economic quantities of alluvial gold deposits and have attracted large numbers of Artisanal and Small-scale miners (ASM) in the area over the years. This has led to pollution in these river bodies as sedimentation increases turbidity and heavy metal concentrations (Afum and Owusu, 2016). The Densu River, which serves over one million people in Accra, is affected by sedimentation resulting from these mining activities and has led to a constant threat to water supply (IUCN, 2016; Fianko and Boadua, 2021). The general decline in the herbaceous cover and the bare land classes over the years can be attributed to the steady regrowth and growth of vegetation and farmlands respectively in the study area. Except for the forest resource which sees little changes annually, the other vegetation types under the closed-canopy vegetation and herbaceous cover classes such as shrubs, herbs, grasses, and food crops undergo noticeable changes as they recover after removal (Fig. 2.4). This could explain the dynamic annual distribution of vegetation in the study area (Kusimi, 2015). The consistent but slowly increasing rate of the built-up class implies an increasing urbanization among settlements (Li and Chen, 2023).

The irregular trend of increase and decrease of alluvial mining in the Atewa Range Forest Reserve (ARFR, Table 2.6) could be explained by the highly illegal nature of the mining activity within the forest which takes place as and when monitoring is relaxed. Most of the alluvial mines within the boundary of the forest reserve are extensions of mines that exist right outside the reserve's boundary. Even though mining activities show a decreasing rate of change (-21.4%), its increasing and decreasing trend is cause for concern. The ARFR is made up primarily of semi-deciduous vegetation and that explains the dominance of the closed-canopy vegetation class in the reserve. From the LULC analysis, it is seen that the fringes of the forest reserve continuously experience farming activities from close by communities (Kusimi, 2015). This is evident from the presence of the herbaceous cover and bare land classes found along the reserve's boundaries.

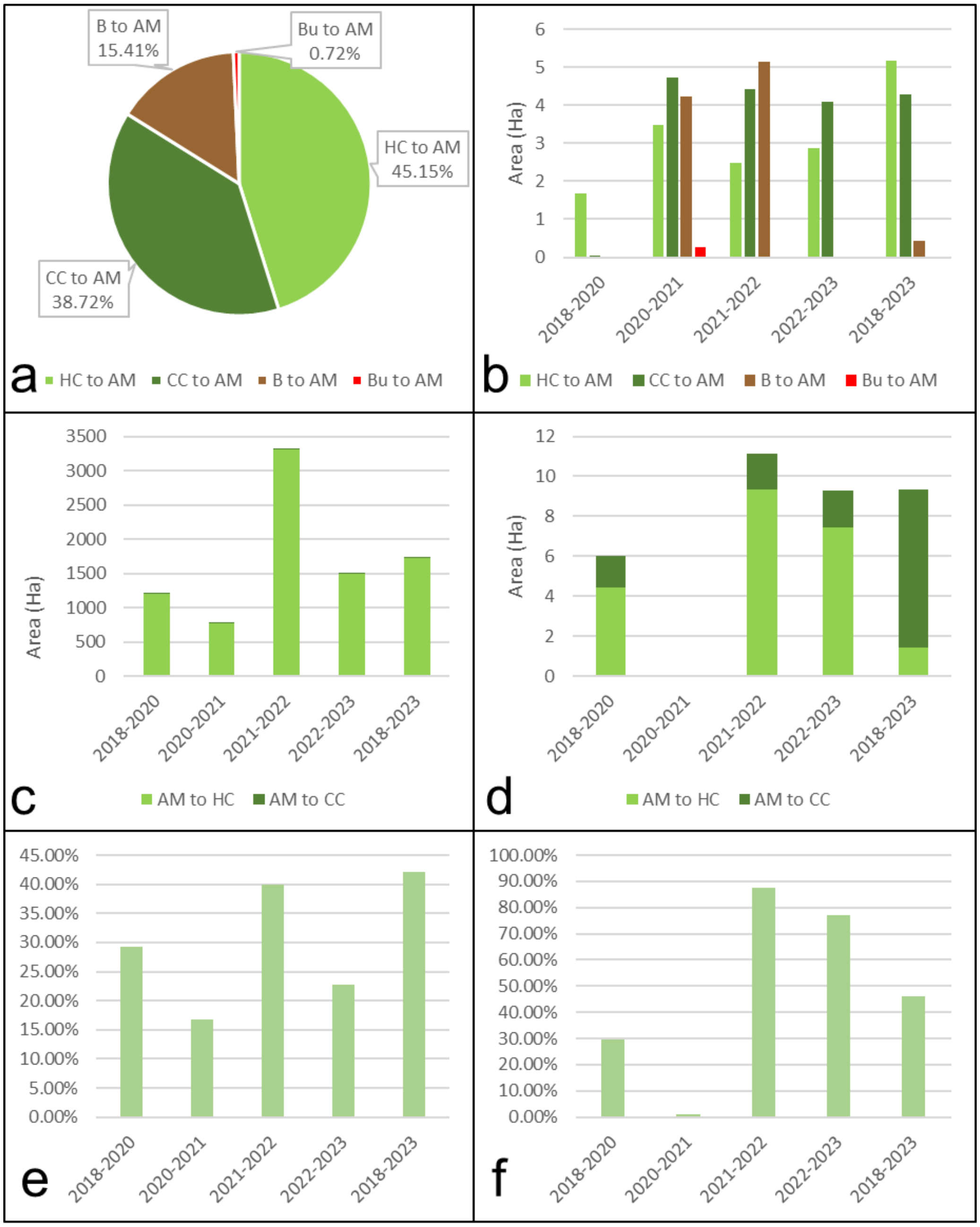

Fig. 2.5. (a) Four-year average of classes converted into Alluvial mine in the Atewa landscape; **(b)** Annual conversion of other classes into Alluvial mine in the ARFR; Area of annual post-mine vegetation recovery in **(c)** Atewa landscape, **(d)** ARFR; Percentage of mined area that has undergone revegetation in **(e)** Atewa landscape, **(f)** ARFR; AM = Alluvial mine; B = Bare land; Bu = Built-up; CC = Closed-canopy vegetation; HC = Herbaceous cover

2.4.2 Alluvial mine dynamics

The dynamics of alluvial mining in the study area were assessed on an inter-period basis. This was useful in obtaining the annual changes that occurred among the alluvial mine class and the other classes. In the Atewa landscape, the herbaceous cover class was mostly cleared for mining activities possibly due to the low energy requirements for heavy-duty machinery to remove such vegetation (Fig. 2.5a). In the forest reserve, however, the dominant semi-deciduous vegetation belonging to the closed-canopy vegetation class was mostly removed. Tilled farmlands, classified under bare land, are usually not easily leased or sold out for mining activities even though the pre-mine energy requirements would also be less. This may explain why a greater proportion of herbaceous cover was converted into alluvial mines than bare lands even though mining on bare lands would mean less energy required for vegetation removal.

Less than half of the mined area in the landscape showed revegetation throughout the years. This could be explained by the longer lifespan of mines outside the ARFR where only a few mined areas are decommissioned or abandoned annually. Also, post-mine revegetation is mostly effective after mining activities have halted for a long time.

Herbaceous cover comprising herbs, shrubs, and grasses dominated vegetation that regrew after mining activities in the study area (Peterson and Heemskerk, 2001). Even in the absence of confirmed backfilling, vegetation is known to grow on the dugout overburden. Regrowing vegetation could mitigate adverse environmental effects of mining such as increased surface run-off, thereby reducing erosion and sedimentation. It also confirms that mining activities in the study area mostly represent disturbances rather than deforestation. However, considering the cyclic nature of mining and the possible recurrence at a previous mine site (Veiga et al., 2002) there could be the possibility of deforestation in the study area where vegetation cover will be permanently transformed into other land use. The observed increased vegetation regrowth in both the Atewa landscape and the ARFR between 2018 and 2023 confirms that post-mine vegetation recovery is more effective after extended periods.

Abandoned mines are usually characterized by mine pits that collect water over time. Water collected in the abandoned mine pits becomes eutrophicated because of nutrient loading from surface runoff water (Chlot, 2011). The characteristic green color of the eutrophicated water makes it indistinguishable from the herbaceous cover class. Thus, abandoned mines could be misclassified as post-mine recovered vegetation.

From the loss/gain statistics of alluvial mines, it was observed that the study area experienced a higher annual increase in alluvial mining activities than a decrease. With at least a 39.1% gain in alluvial mines along the river channels in the landscape each year, the threat of water scarcity in communities that depend on these water sources is lurking. In the forest reserve, more alluvial mines were lost annually except between 2020 and 2021 when the peak gain was recorded for the forest reserve and the landscape (Table 2.7). This implies that between 2020 and 2021, post-ban mining activities were the highest in the Atewa landscape as new mines might have been well established since their resumption in 2018. The higher annual loss of mines in the forest reserve could be explained by the rushed nature of mining within the forest reserve considering its illegal nature. As such, the life span of mines in the forest reserve was shorter than those in the landscape as only 3.1% of mines within the forest reserve remained unchanged while 49.8% persisted throughout the 5 years in the landscape. The longer mine life span outside the forest reserve means that very few mines are decommissioned or abandoned annually leading to less than half of the mined area showing revegetation throughout the years. The loss/gain dynamics are useful in determining areas that are restored after degradation without confirmed backfilling.

Even though the annual increase in mining activities may signify a societal benefit of increased livelihoods, its environmental impact may transcend the local and national regimes. Results from the mine dynamics are consistent with findings by Sonter et al. (2017), Siqueira-Gay et al. (2020), Chaddad et al. (2022), and Quash et al. (2024), where mining and its associated infrastructural setup within tropical forests in the Amazon have led to the loss of forest resources. This proves that mining is indeed a crucial contributor to tropical forest loss and should be treated as an issue of global concern.

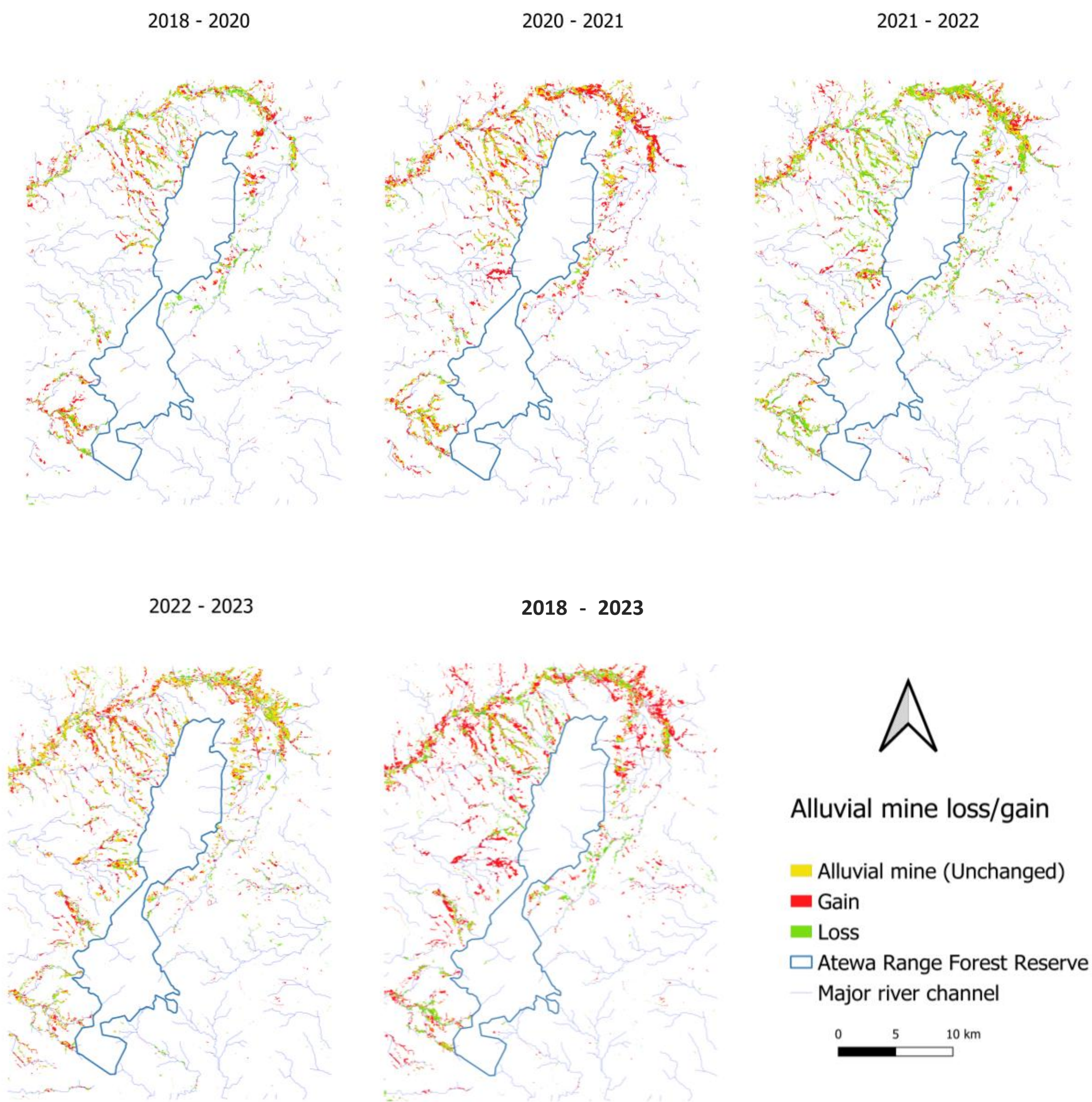

Fig. 2.6. Alluvial mine loss/gain maps from 2018 to 2023

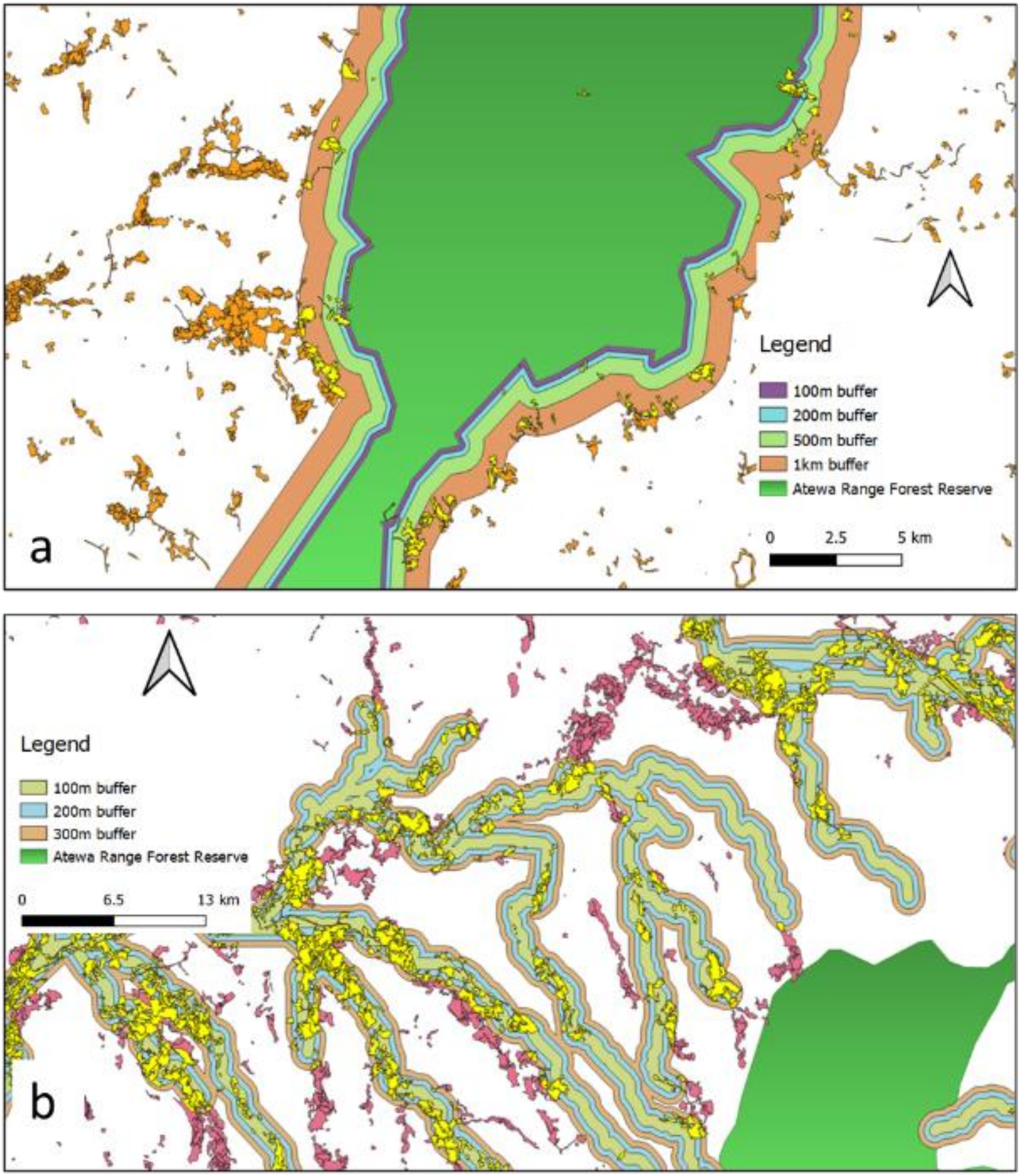

Fig. 2.7. Distribution of mines, where yellow polygons represent mines within a multiple-ring buffer around **(a)** a portion of the ARFR; **(b)** river channels

2.4.3 Mine proximity to forest reserve and river channels

From the multiple-ring buffer analysis, it is observed that the ARFR not only co-exists with active mines but also lies in close proximity to these mines. This is in agreement with findings from Kusimi (2015), Nyamekye et al. (2021), and Amponsah et al. (2022) which report increased encroachment on the forest resource as a result of human activities on its fringes. Aside the loss of forest vegetation from mining activities, other indirect effects of habitat fragmentation, habitat destruction, and biodiversity loss could affect the general forest ecosystem functions (Alvarez-Berríos and Aide, 2015; Bradley 2020; Siqueira-Gay et al., 2020).

Major river bodies in the study area serve as the main source of water for most communities. Results from the river channel buffer analysis indicated a high concentration of mining activities within the 100 m buffer as over 49% of the total mined area was within this buffer zone annually. Thus, the Riparian Buffer Policy for Managing Freshwater Bodies in Ghana (Ministry of Water Resources, Works and Housing, 2013) was not effective throughout the years of consideration. Figure 2.8 shows a mining activity close to the forest reserve and a highly turbid river body resulting from mining activities. Evidence of water pollution resulting from mining activities from this study is buttressed by studies by Meißner (2021) and Ruppen et al. (2023) in which remote sensing and GIS confirmed large-scale water pollution associated with mining activities. Thus, mining poses a threat to the quality of freshwater bodies and aquatic ecosystems globally.

Table 2.7

Alluvial mine loss/gain statistics

	ARFR						Atewa landscape					
	Gain		Loss		Unchanged		Gain		Loss		Unchanged	
	(ha)	%	(ha)	%	(ha)	%	(ha)	%	(ha)	% .	(ha)	%
2018-2020	1.7	8.6	19.9	98.2	0.0	0.0	2614.8	61.2	1887.1	44.2	2,384.6	55.8
2020-2021	10.9	627.0	0.6	34.5	1.2	67.1	4789.5	105.0	1171.2	25.7	3,392.3	74.3
2021-2022	6.6	51.5	7.1	55.8	5.5	43.4	3127.5	39.1	3804.0	47.5	4,201.1	52.5
2022-2023	7.0	57.8	8.4	69.9	3.6	29.5	4008.1	62.4	2034.6	31.7	4,390.0	68.3
2018-2023	9.9	48.7	19.7	96.9	0.6	3.1	6281.3	147.0	2144.0	50.2	2,127.7	49.8

Percentages are based on the previous year's mined area. For instance, in the Atewa landscape from 2018 to 2020, Gain % indicates that by 2020, alluvial mines increased by 61.2% of the 2018 mining area. Loss % reflects a 44.2% reduction in the 2018 mined area, while Unchanged % shows that 55.8% of 2018 mines remained intact in 2020.

Table 2.8

Mined area proximity to ARFR and river channels

	Atewa Forest Reserve Buffer								River channel Buffer						n
	100m		200m		500m		1km		100m		200m		300 m		
	(ha)	%	(ha)	%	(ha)	%	(ha)	%	(ha)	%	(ha)	%	(ha)	%	
2018	47.1	1.1	76.5	1.9	177.3	4.3	398.2	9.6	2556.0	61.8	2915.1	70.5	3263.1	78.8	1,840
2020	34.3	0.7	62.5	1.4	197.6	4.3	401.9	8.7	2699.4	58.5	3177.8	68.8	3484.3	75.5	1,777
2021	119.8	1.4	174.1	2.1	371.4	4.5	791.6	9.5	5010.7	60.4	5723.9	69.0	6296.0	75.9	2,825
2022	93.1	1.4	129.0	2.0	288.6	4.4	536.5	8.1	3435.2	51.9	4143.9	62.7	4668.5	70.6	3,784
2023	83.0	1.1	125.7	1.6	283.5	3.6	608.9	7.7	3931.7	49.7	4733.8	59.9	5368.5	67.9	3,884

n = Number of polygons that correspond to alluvial mines

Fig. 2.8. (a) A mine close to the Atewa Range Forest Reserve; **(b)** Increased turbidity of a river body as a result of mining activities

2.5 Limitations of the study

This study was constrained by persistent cloud cover in the study area, limiting access to consistent cloud-free satellite imagery. To address this, we utilized PlanetScope's three-band (RGB) monthly mosaicked imagery, which was largely cloud-free but had a slightly lower spatial resolution of 4.77 m compared to the standard 3 m. However, no cloud-free image was available for 2019, impacting the consistency of the intended annual analysis. Additionally, the RGB images lacked the NIR and red-edge bands, which are essential for vegetation studies. While the GRVI was employed to classify vegetation types, indices such as NDVI and the Inverted Red-Edge Chlorophyll Index (IRECI) would have likely provided better differentiation between herbaceous cover and closed-canopy vegetation, and between the vegetation and non-vegetation classes. Thus, potentially reducing misclassifications and improving overall classification accuracy.

2.6 Conclusions

The conservation of the Atewa Range Forest Reserve (ARFR) has become a critical issue in Ghana due to rampant mining activities threatening its existence. The application of GEOBIA and GIS on high-resolution PlanetScope imagery proved an effective means of mapping alluvial mining activities in the Atewa landscape. Results show a continuous annual increase in alluvial mining, with most mines originating from vegetation conversion. Mining has been steadily expanding each year, with continuous activities in the sensitive 100 and 200 m buffer zones surrounding the reserve. On average, 10.8 ha of the forest reserve was found to be lost to mining annually. The results also show that at least 49.8% of mines remained active for the five years of the study in the Atewa landscape, necessitating sustainable mining methods to protect water and forest resources. The Riparian Buffer Zone Policy which prohibits human activities within a 100 m buffer of water bodies was found to be ineffective, as over 49% of mining occurred within the 100 m river channel buffer. The study suggests urgent action from the Ministry of Lands and Natural Resources and the Forestry Commission to protect the forest and water resources in the Atewa landscape.

Chapter 3

Inferring canopy disturbance sources in the Atewa Range Forest Reserve in Ghana through their relationship with topographic and geospatial features

3.1 Introduction

Forest degradation in the tropics is a troubling environmental challenge as it is known to pave the way for deforestation (Mollicone et al., 2007; Souza, 2013; Flores et al., 2024). The rate of tropical forest degradation has been reported in recent years to be comparable to that of deforestation (Aguiar et al., 2016; Fischer et al., 2021; Lapola et al., 2023), which in turn has contributed to the increase in carbon emissions from tropical forests (Li et al., 2022). Forest degradation is constrained by the lack of a standard definition in the scientific community, where different definitions have been adopted to suit different conditions. Some definitions have related degradation to forests' structural components, others to the functionality of the forest, and others to the resources provided by the forest (Ghazoul et al., 2015). The Food and Agriculture Organization (FAO, 2002) defines forest degradation as a natural or human-induced process that alters a forest's structure, diminishing its ability to consistently provide goods and services. This degradation weakens forest resilience and disrupts ecosystems (Bourgoin et al., 2024). Deforestation, on the other hand, occurs when forests have been permanently converted to other non-forest land uses (Hansen et al., 2013; FAO, 2020), such as agriculture and urbanization, while significantly impacting biodiversity, carbon storage, and climate regulation (Faria et al., 2023).

To combat the menace of deforestation, it is important first to understand the dynamics of the disturbance that precedes it, be it natural or human induced. Remote sensing has proven capable of monitoring land cover changes over large areas while indicating their possible drivers over time (Shimizu et al., 2019; De Marzo et al., 2022; Slagter et al., 2023). Unlike deforestation and other land cover changes, mapping forest degradation, particularly canopy damage through satellite remote sensing techniques, is not straightforward, as degradation is likely to occur at the subpixel level even in some relatively high-resolution satellite imagery. The visual interpretation technique was among the first to be used for mapping selectively logged areas in the Brazilian Amazon (Watrin and da ROCHA, 1992). However, this method was flawed because of its inability to detect logging in areas where 'scars' did not persist and when logging was at a low intensity. Sousa et al. (2005) also reported on how the automated techniques that were later used also had the challenges of spectral ambiguity between selectively logged areas of various ages and extraction intensities and intact forest. Asner et al. (2002) used canopy gap fraction through Spectral Mixture Analysis (SMA) to map selective logging. This method, however, could not differentiate human-induced disturbances from natural disturbances.

Spectral Mixture Analysis (SMA) is a robust remote sensing technique that decomposes the reflectance signal of a mixed pixel into its constituent components, known as endmembers (Adams et al., 1986; Song, 2005). In optical remote sensing, a single pixel often represents a mixture of multiple surface materials, each contributing to the observed reflectance. The recorded spectral response is, therefore, a composite of the spectral signatures of these materials. Spectral Mixture Analysis is employed to estimate the fractional abundance of each endmember, including subpixel-scale components, within a given pixel. By resolving mixed pixel compositions, SMA enhances classification accuracy and significantly improves image interpretation, mitigating uncertainties associated with spectral mixing in remotely sensed data (Elmore et al., 2000).To successfully map selective logging in tropical forests, researchers have applied SMA on the 30-meter resolution Landsat imagery while using logging proxies such as log landings, skid roads and trails to differentiate them from natural disturbances (Asner et al., 2002; Sousa et al., 2005; Bullock et al., 2020; Pacheco-Angulo et al., 2021). The application of Spectral Mixture Analysis (SMA) in tropical forest disturbance mapping has proven effective, as it exploits the distinct spectral characteristics of various endmembers across multiple wavelength bands to differentiate bare soil, shadow, water, photosynthetic vegetation, and non-photosynthetic vegetation (Shimabukuro et al., 2019). This approach enables the detection and mapping of disturbance extents that may not be discernible at the pixel level, providing a more accurate representation of canopy changes (Mitchell et al., 2017). When applied to relatively high-resolution satellite data, SMA enhances the detection of subtle subpixel-scale changes, improving the precision of disturbance assessments. The reliance on logging-related proxies in mapping disturbances in previous studies, however, implies that, in an area of low disturbances where proxies are not spatially detectable, applying the SMA-proxy method will be ineffective in identifying human-induced disturbances.

The Atewa Range Forest Reserve (ARFR), an upland evergreen forest in the High Forest Zone (HFZ) in Ghana, is crucial in the conservation of biodiversity. It is a biodiversity hotspot that contributes to carbon sequestration, above-ground biomass, and biodiversity conservation. The ARFR is characterized by small-scale, non-mechanized disturbances such as farming, logging, and mining, which typically cause canopy disturbances that are sometimes too subtle to be detected at the pixel level in moderate to low-resolution satellite images. Logging and other disturbances at this scale do not produce spatially explicit proxies that facilitate source identification. Therefore, mapping disturbances in the Atewa landscape has only been possible at time nodes when significant disturbances and/or deforestation are detectable by satellite imagery. Remote sensing-based research in the Atewa landscape on land cover changes over the years points to mining, farming, and logging activities around and within the forest reserve as the main drivers of deforestation (Kusimi, 2015; Nyamekye et al., 2021; Amponsah et al., 2022). Thus, previous research on the land cover changes in the ARFR has mostly focused on deforestation or large-scale degradation or disturbances. In 2020, the government of Ghana commenced infrastructure development for bauxite exploration within the reserve. Although the exploration was ultimately unsuccessful due to strong opposition from conservationists, activities such as road construction and vegetation removal caused significant disturbances.

The freely accessible Sentinel-2 satellite imagery developed by the European Space Agency (ESA) has been an ideal data source for forest monitoring in recent years (Pacheco-Pascagaza et al., 2022; Kalinaki et al., 2023; Liu et al., 2024; Molnár and Király, 2024). With its 10-meter resolution, each pixel likely captures the entirety or a significant portion of a tropical forest's tree crown, enhancing sensitivity to canopy changes. This study aims to explore the capability of the Sentinel-2 satellite image in mapping annual canopy disturbances in tropical forests with small-scale disturbances using SMA and Geographic Information Science (GIS) to provide insights into the dynamics of the disturbances that usually precede deforestation. The canopy disturbances in this study are represented by the gaps created in the canopy when there is a tree loss, either naturally or human induced. Additionally, we seek to identify potential sources of these disturbances by assessing their relationship with the topographic and geospatial features of the study area.

3.2 Materials and Methods

3.2.1 Study area

The ARFR is located on the Atewa range of mountains, a north-south oriented highland with rugged terrain in the Eastern Region of Ghana (Fig 3.1). The 26,300-ha forest reserve lies between latitudes 5° 58' to 6° 20' North and longitudes 0°31' to 0°41 West and records the highest elevation of 842 meters (m) above sea level. The ARFR provides the headwater for the Birim, Densu, and

Ayensu, three major rivers that greatly influence economic activities such as farming and mining. Average temperatures in the area range between 24-29°C with a bimodal rainfall pattern where the major season falls between March and July and the minor season, from September to November. An average of 1,200 to 1,600 mm of rainfall is recorded annually in the area. The dry season typically begins in November and ends in February.

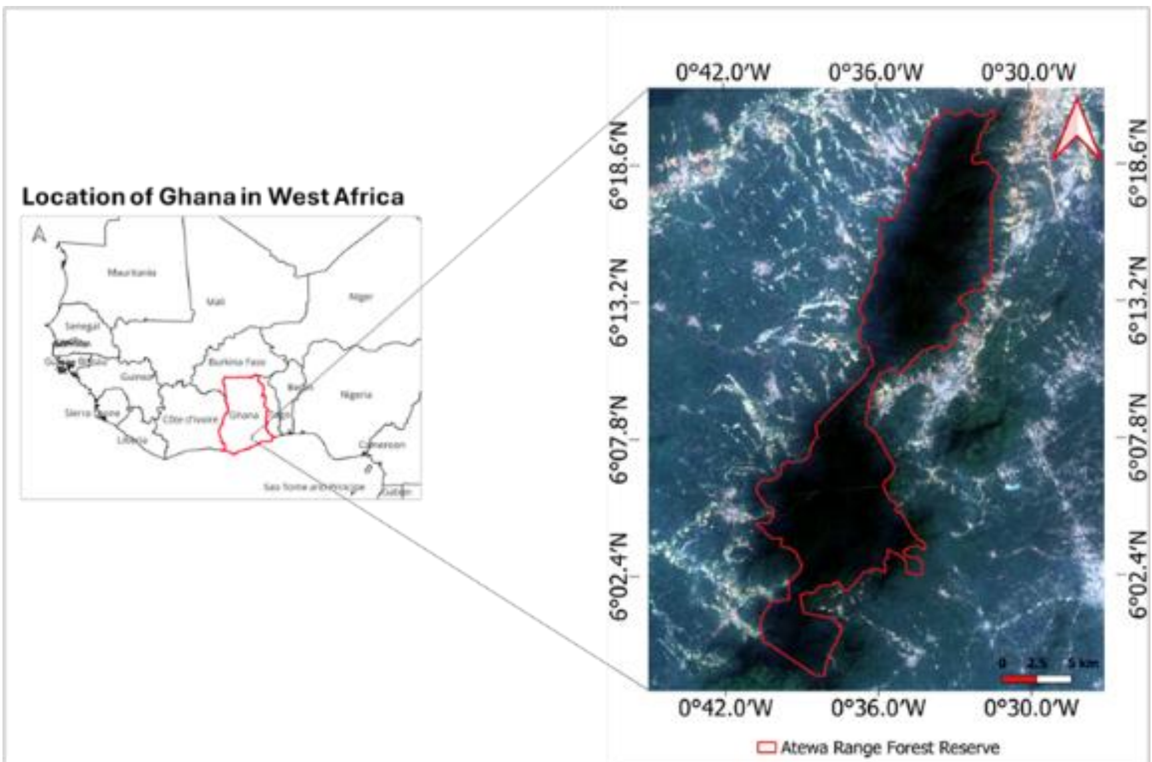

Fig. 3.1. Map of the Atewa landscape showing the Atewa Range Forest Reserve

3.2.2 Sentinel-2 satellite data pre-processing

Cloud-free Sentinel-2 level 1-C satellite images from 2020 to 2024, except for 2021, were obtained from the Copernicus Data Space Ecosystem (https://dataspace.copernicus.eu). The images were radiometrically, atmospherically, and topographically corrected to convert the top-of-atmosphere (TOA) reflectance to bottom-of-atmosphere (BOA) reflectance and to reduce the influence of varying sunlight angles on sloped surfaces using the Sen2Cor software. The bands 2 (blue), 3 (green), 4 (red), 5 (red-edge), 8 (near-infrared - NIR), and 11 (shortwave infrared – SWIR) of the Sentinel-2 images were used in this study. The red-edge and SWIR bands were resampled from 20 m to 10 m to match the resolutions of the visible (blue, green, and red) and NIR bands. All images were then radiometrically normalized to ensure consistency in spectral reflectance across the periods using the ArrNorm plugin in QGIS. Satellite data were collected during the dry season to minimize cloud cover, but the 2021 image was excluded due to the lack of a cloud-free capture. The dry season was a suitable period for satellite data collection because of the persistent cloud cover over the study area in most parts of the year.

3.2.3 Creation of forest masks

Forest masks were created using the object-based classification approach to ensure accurate mapping of canopy disturbances within the forested portions of the ARFR. Using the eCognition software, a forest mask was created for the base year, 2020, which was then updated in the subsequent years with newly deforested sites (Grecchi et al., 2017). The object-based method was applied to leverage its adjustable scale parameter to allow for the inclusion of small clearings in the forest mask as disturbances rather than deforested sites. The non-forest portions of the reserve were mainly shrubs, grasslands, farmlands, mined sites, and permanent road cuts.

3.2.4 Mapping canopy disturbances

Linear Spectral Mixture Analysis (LSMA) was used to decompose each pixel of the Sentinel-2 image into its component endmembers typical of a forested terrain: vegetation, soil, and shade (Adams, 1993; Grecchi et al., 2017). The linear spectral mixing model assumes that the observed reflectance of a mixed pixel is a linear combination of the reflectances of its endmembers, weighted by their fractional abundances (Adams et al., 1986; Equation 1).

$$R_i = f_1R_1+f_2R_2+\ldots+f_nR_n+\epsilon \qquad (1)$$

Where

R_i is the observed reflectance of the pixel in band i,

R_n is the reflectance of endmember n,

f_n is the proportion of endmember n in the pixel,

ϵ is the error in band i

Fraction images comprising the different proportions of each endmember were generated for each year to extract the soil fraction used for mapping canopy disturbances. To identify changes in the soil fraction as an indicator of canopy disturbances, a canopy gap mapping of the baseline year (2020) based on the soil fraction was undertaken and repeated in subsequent years. Canopy gaps were mapped through a binary classification where gaps were assigned a value of 1 and forests, 0. To identify canopy gaps, a threshold of 10% was applied to soil fraction images. The threshold was set based on the combination of (i) soil fractions obtained from ground-truthed non-mechanized logged sites in the ARFR and (ii) the mean soil fraction from degraded sites at the edges of deforested parts of the reserve detected through the Sentinel-2 images. A 100 m × 100 m grid was then applied to the study area to assess the areal coverage of canopy gaps, which were then classified into low, medium, and high gap coverages based on the following threshold:

(i) Gap area < Q2 = Low gap coverage

(ii) Q2 ≤ Gap area ≤ Q3 = Medium gap coverage

(iii) Gap area > Q3 = High gap coverage

Where Q2 and Q3 are the second and third quartiles of the grid cell area.

Classification using the quartile method was ideal as it is less affected by extreme values or skewed distributions, which was the case of the soil fraction mapped in the grid cells. Unlike mapping the areal extent of areas affected by selective logging in the Brazilian Amazon where a 300 m × 300 m grid was applied on Landsat images Grecchi et al (2017), we used a 100 m × 100 m grid in addition to the high resolution Sentinel-2 images in our study to increase sensitivity in gap coverage changes in the absence of proxies such as log landings, skid roads and trails. A change detection analysis on the gap coverage was then undertaken between the years to create 'disturbance', 'recovery', and 'unchanged' classes. The change trajectories applied in the change detection are shown in Table 3.1.

Table 3.1.

Change trajectories that were used to identify disturbances and recoveries

Canopy gap changes	**Class**
High to High	Unchanged
Low to Low	Unchanged
Medium to Medium	Unchanged
High to Low	Recovery
High to Medium	Recovery
Medium to Low	Recovery
Low to High	Disturbance
Low to Medium	Disturbance
Medium to High	Disturbance

3.2.5 Accuracy assessments

An accuracy assessment was first undertaken to validate the 2020 forest mask, based on which forest masks for subsequent years were created. This was to ensure that canopy disturbances were accurately mapped within the forested parts of the reserve with minimum bias from deforested parts. The 2020 Phased Array L-band Synthetic Aperture (PALSAR)-2 global forest/non-forest map from the Japan Aerospace Exploration Agency (JAXA) website (https://www.eorc.jaxa.jp/ALOS/en/palsar_fnf/data/2020/map.htm) was used as a reference image. A Synthetic Aperture Radar (SAR) image was preferred because of its increased sensitivity to vegetation structure, allowing for an accurate mapping of vegetation (Sano et al., 2021). A random sampling technique was used to assess the accuracy of the forest/non-forest map, where 210 sample points were distributed across the forest reserve. This was followed by an accuracy assessment of the soil fraction image from the SMA on which the 10% threshold had been applied. The canopy gap and the subsequent canopy disturbance mapping were based on this soil fraction image. High-resolution images from Google Earth Pro were used as references. Where there was no usable data on Google Earth Pro, images from PlanetScope's basemaps were used. For each year, a minimum of 206 sample points were randomly distributed across the forest reserve to calculate the user's, producer's, and overall accuracies.

3.2.6 Relationships between canopy disturbances and topographic and geospatial features

Because of the lack of spatially explicit logging-related proxies in the study area, the possible sources of canopy disturbances were inferred through their relationship with topographic and geospatial features in the study area. The rugged nature of the area suggests that the various topographic features will contribute to the distribution of canopy disturbance caused either by human activities or natural occurrences. In an area that is dominated by alluvial mining activities, assessing how disturbed areas vary with distance from major river channels was also considered important. Lastly, because the ARFR is bounded at all sides by settlements, it was important to consider how disturbances varied from the edge of the forest to the core. The Digital Elevation Model (DEM) of the study area was obtained from NASA's Shuttle Radar Topography Mission Digital Elevation Model (SRTM) through the United States Geological Survey (USGS) Glovis web application (https://glovis.usgs.gov/app). Elevation, slope, and aspect maps were created from the DEM to represent the topographic features. The geospatial features were the distance from the forest edge to the core and the distance from river channels. The distance from the forest edge to the core was created by creating sections of equal distances from the edge of the forest to 2 km into the forest. The sections used were 0-500, 500-1000, 1000-1500, and 1500-2000 m. The portion beyond the 1500-2000 m section was considered the core of the forest in this study. Again, sections were delineated at 100-meter intervals from the river channels, categorized as 0-100, 100-200, and 200-300 m, to establish the distance zones from river channels. The relationships between topographic and geospatial features and canopy disturbance were evaluated using scatter diagrams. These diagrams plotted the mean values of topographic and geospatial features within each grid against the corresponding percentage of canopy disturbance observed in the same grid. Due to the categorical and cyclical nature of aspect, pie charts were more suitable for representing the distribution of disturbances in relation to aspect compared to scatter plots, which are better suited for continuous variables. Recorded aspect values were categorized into 315-45°, 45-135°, 135-225°, and 225-315° to represent north-facing, east-facing, south-facing, and west-facing disturbances, respectively. Figure 3.2 shows a flowchart of the main processes applied in the methodology.

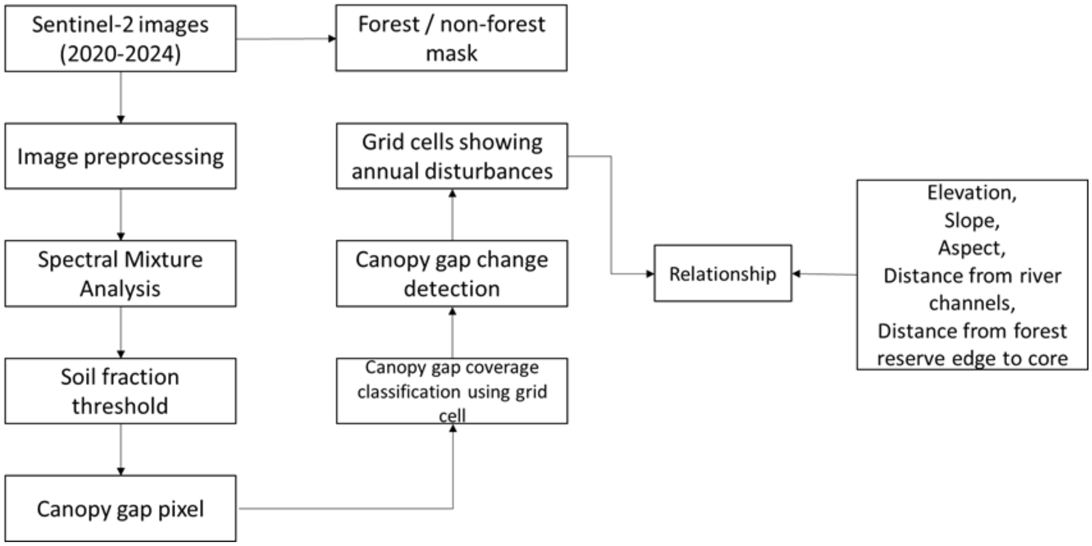

Fig. 3.2. Flowchart showing the methods applied in mapping disturbance and the relationship with topographic and geospatial features

3.3 Results

3.3.1 Disturbance and recovery patterns

Soil fraction images were produced from Spectral Mixture Analysis (SMA) to map the canopy gap openings in the Atewa Range Forest Reserve (ARFR). The annual changes in the canopy gap coverage were then mapped to determine areas of disturbance and recovery. Accuracy assessment for the forest/non-forest of 2020, based on which forest masks for subsequent years were built, produced an overall accuracy of 92.65%. Accuracies of the soil fraction images ranged from 85.71 to 86.41% across the years (Table 3.2). Our assessment revealed that the primary sources of confusion between vegetation and soil fraction were leafless trees in the dry season, which exhibited spectral characteristics similar to bare soil (Streck et al., 2002). Additionally, in pixels containing a mix of low vegetation and relatively high soil cover, the model faced challenges in accurately assigning the correct fraction, resulting in classification errors. However, with a minimum accuracy of 85.71%, the classification was considered reliable.

A map of a portion of the study area and the corresponding soil fraction and canopy gap classification maps are displayed in Fig. 3.3. The canopy gaps showed an increasing trend from 2020 to 2023, with a slight dip in 2024. The trend was similar for deforestation, except that as of 2024, deforestation was still on the rise (see Fig. 3.4(a)). Canopy gap coverage ranged from a low of 117.1 ha in 2020 to a high of 252.9 ha in 2023. This represented 0.49 and 1.07% of the reserve area in the respective years. Similarly, deforestation was lowest in 2020 with 351.4 ha coverage (1.5% of forest reserve area) and highest in 2023 with 500.6 ha (2.11%). Therefore, both deforestation and canopy gap coverage in the ARFR showed an almost similar trend in the study. Comparatively, the canopy gaps covered between a third to a half of the deforested portions of the forest reserve. In 2020 and 2022, the canopy gap area made up 33.31 and 32.38% of the deforested portion, respectively, while making up 50.52 and 44.37% of the deforested portion of the forest in 2023 and 2024, respectively. As observed in Figure 3.4, however, the annual canopy gaps did not significantly affect the trend of NDVI of the forested portions of the reserve across the periods. The average NDVI values were between 0.62 and 0.63, with the highest values being 0.76 for all the years except 2023, where it was 0.75.

Table 3.2

Summary of accuracy assessments for soil fraction images derived from SMA

	2020		2022		2023		2024	
	Forest	Soil Fraction	Forest	Soil Fraction	Forest	Soil Fraction	Forest	Soil Fraction
UA (%)	86.6	85.45	84.62	88.24	85.59	85.85	87.25	85.05
PA (%)	85.84	86.24	88.00	84.91	86.36	85.05	84.76	87.50
OA (%)	86.04		86.41		85.71		86.12	

UA, User's Accuracy; PA, Producer's Accuracy; OA, Overall Accuracy

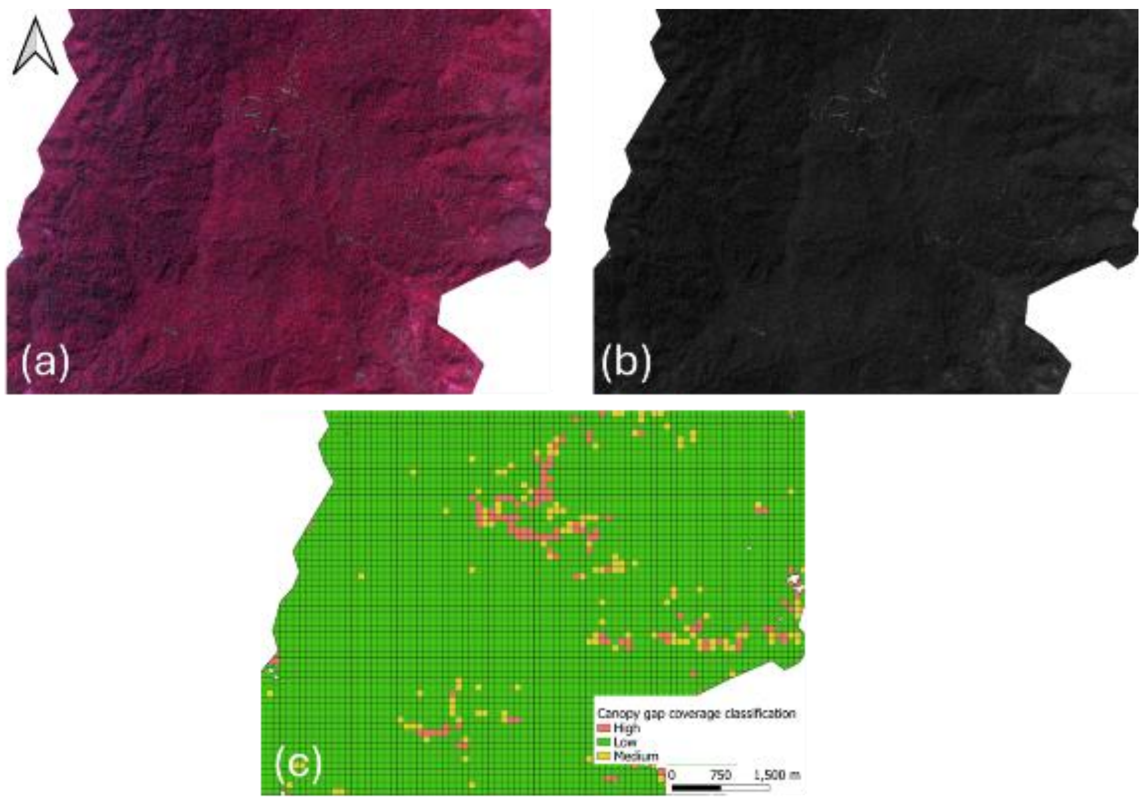

Fig. 3.3. A portion of the ARFR showing **(a)** false colour composite of Sentinel-2 image; **(b)** soil fraction image; **(c)** canopy gap coverage classification

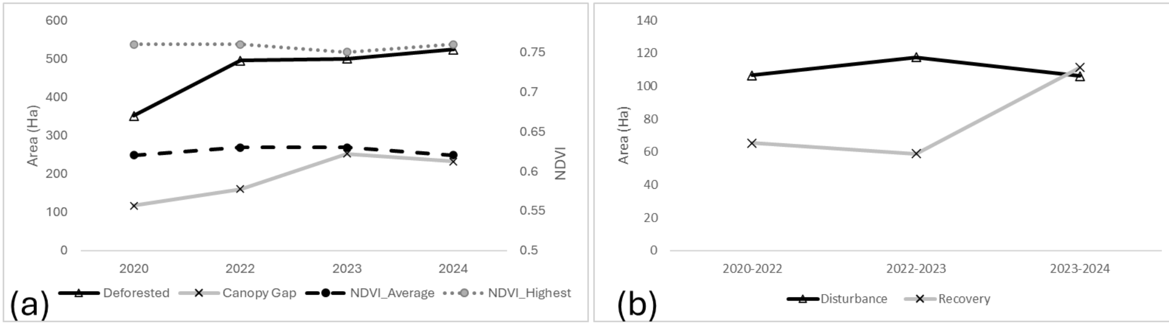

Fig. 3.4. (a) Trends of deforestation, canopy gaps, and NDVI **(b)** Trends of disturbance and recovery

We assessed the areal changes in the canopy gaps annually to map disturbance and recovery in the forest reserve, as discussed in section 2.4. A visual inspection of the maps (Fig. 3.5) reveals that disturbed areas were primarily concentrated along the fringes of the forest reserve, similar to the distribution of deforested regions. This mostly determined the distribution of recoveries. However, between 2020 and 2022, significant regeneration was observed in the forest core, as access roads constructed in 2020 for the now-halted bauxite mining operations had been revegetated by 2022. Across the periods of consideration, disturbance showed an increase-then-decrease trend while recovery showed a decrease-then-increase trend, as seen in Fig. 3.4(b). The lowest disturbance was between 2023 and 2024, with 106.1 ha, and the highest was between 2022 and 2023, with 117.5 ha. These represent 0.45 and 0.50% of the reserve area, respectively. Comparatively, recovery made up 65.37 and 60% of the disturbed area in 2020-2022 and 2022-2023, respectively. Between 2023 and 2024, recovery exceeded disturbance, representing 106.10% of the disturbed area. Thus, disturbed areas that undergo recovery annually represent more than half the area of the originally disturbed areas in the ARFR. Generally, the area of canopy disturbance was at least a quarter of the total deforested area each year.

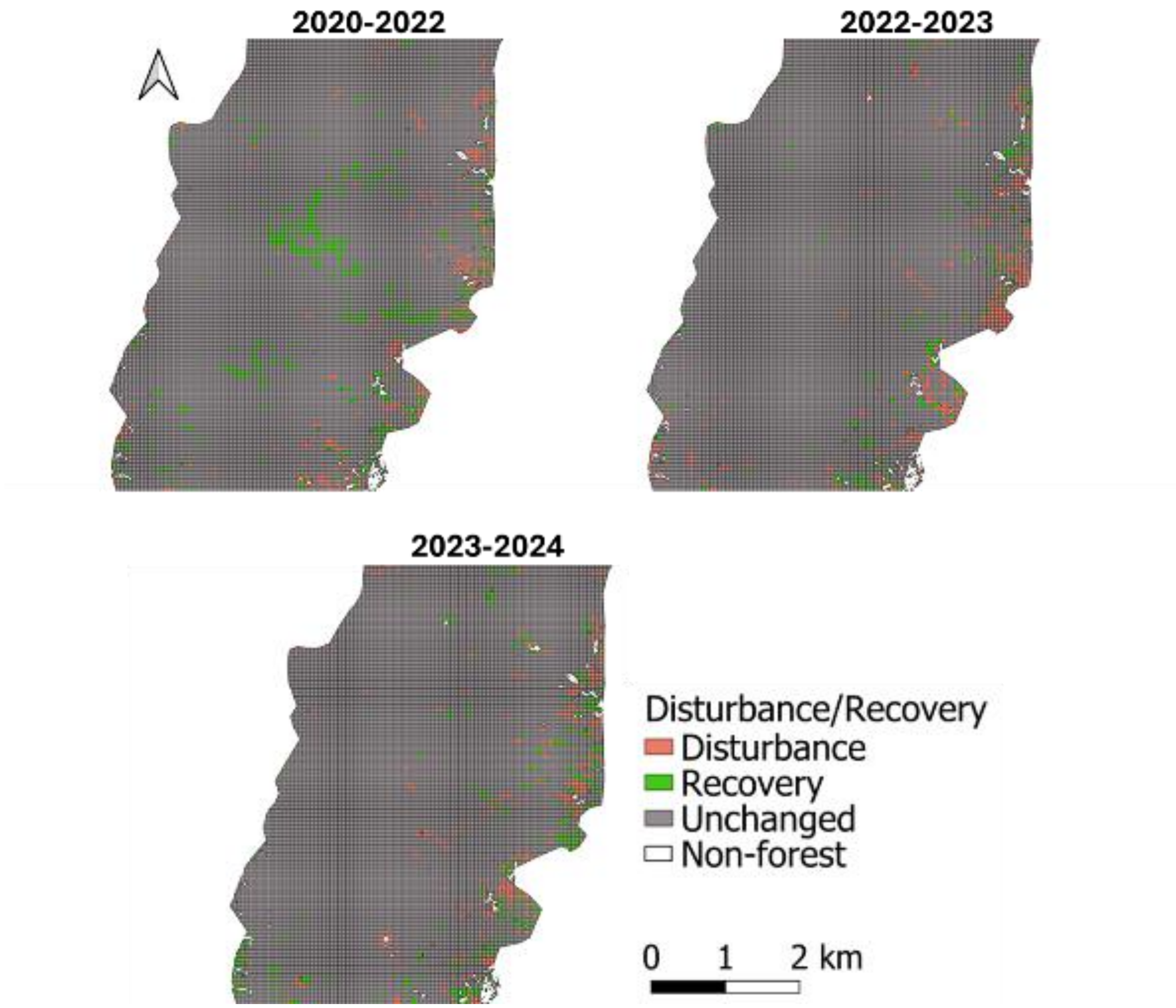

Fig. 3.5. Disturbance/recovery maps from 2020 to 2024

The change trajectories also produced results on the rate of changes in the canopy gaps. From Fig. 3.6, it is observed that most disturbances occur at a faster rate between the years. This is evident from at least 60.7 ha of canopy gaps transitioning from 'low' to 'high' from 2020 to 2024. Disturbances that occurred at a slower rate determined from the 'medium to high' and 'low to medium' transitions recorded the highest values of 31.8 and 25.0 ha, respectively, across the years. Recovery was also mostly at a faster rate annually as the transition from 'high to low' produced the largest coverage across the years. Annually, areas of high canopy gap coverage mostly recorded increased ('high') gaps the following year as seen from the 'high to high' transition under the unchanged class. This was followed by the 'low to low' transition, then the 'medium to medium'.

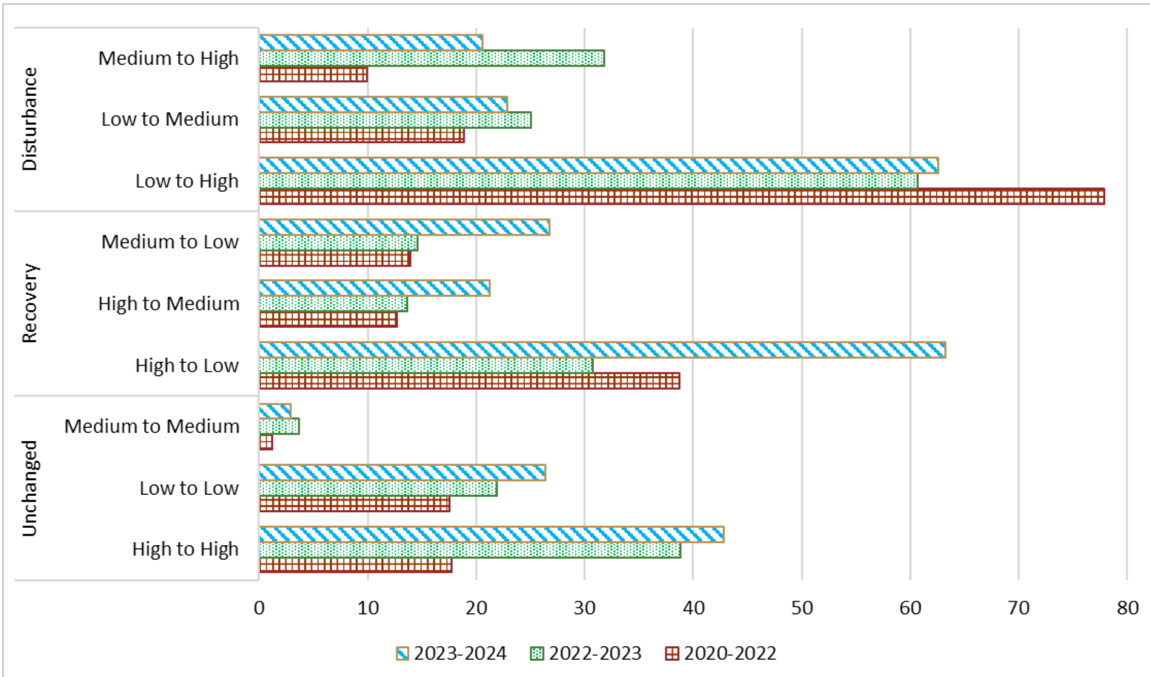

Fig. 3.6. Annual change trajectory area

3.3.2 Relationship between disturbance and topographic and geospatial features

We used the relationship between topographic and geospatial features and the mapped canopy disturbances to infer the possible sources of disturbances in the forest reserve in the absence of spatially explicit proxies that are usually associated with mechanized large-scale logging. Scatter plots were used to evaluate these relationships by analysing the distribution trends of canopy disturbances in relation to elevation, slope, distance from the forest edge to the core, and distance from river channels. Pie charts were used to analyse the distribution of disturbances across different aspects. Mapped disturbances exhibited an increase-then-decrease pattern in relation to increasing elevation and slope while predominantly displaying a declining trend with distance from the forest edge to the core and distance from river channels. However, a deviation from this decreasing trend was observed in the 1,500–2,000 m section from the forest edge, where disturbances showed a slight increase. Across the years, disturbances increased from areas of low elevation and peaked at the 500-600 m region, where it declined with further increase in elevation. A similar trend was observed for disturbances against slope across the years, where disturbances increased from areas with weak slopes to a peak at the 15-20° range and declined with further increase in steepness. The mostly decreasing trend observed in the disturbance-distance-from-forest-edge relationship (Fig. 3.7(c)) is due to the general decline in disturbance as one moves from the forest edge to the core. Disturbances were generally observed to decrease with increasing distance away from river channels except between 2022 and 2023, where a deviation was observed at the 100-200 m zone, and in 2023-2024 in the 300-400 m zone (Fig. 3.7(d)). The relationship between disturbance and aspect showed that west-facing disturbances were the most dominant, accounting for at least 37% of all disturbance directions across the periods. South-facing disturbances followed as the next most prominent, with east-facing disturbances ranking third. North-facing disturbances were consistently the least common, reaching their highest distribution of 16% between 2020 and 2022. The relationships between canopy disturbances and topographic and geospatial features are represented in Fig 3.7.

3.4 Discussion

3.4.1. Disturbance and recovery dynamics

From the results, it is observed that deforestation and canopy gap coverage exhibit a similar trend of annual increase, except in 2024, when there was a decrease in canopy gap coverage. The divergence in trends observed in 2024 may highlight the ongoing challenges in controlling relatively large-scale deforestation activities, such as mining and farming in the Atewa Range

Forest Reserve (ARFR; Kusimi, 2015; Nyamekye et al., 2021; Amponsah et al., 2022), despite efforts from both governmental and non-governmental organizations. Generally, disturbance activities in the forest were on a small scale compared to deforestation activities, as canopy disturbances were only about a quarter of deforested areas. The limited scale and occasionally sub-pixel nature of the disturbances may account for the minimal changes observed in NDVI values across the forested areas of the reserve. Despite the scale of the canopy disturbance, the findings are concerning, as the number of grids transitioning from 'low' to 'high' canopy gap coverage was the highest across all the years. Also, the grids that were classified as showing high canopy gap coverage annually showed further increase in 'high' canopy gaps (Fig 3.6). This implies the possibility of these disturbed areas eventually transitioning into permanently deforested sites like those already on the edges of the forest. The annual transitions from 'low' to 'high' and from 'high' to 'high' may account for the insufficient recovery observed between 2020-2022 and 2022-2023 (Fig 3.4(b)). This suggests that the activities responsible for the disturbances were likely persistent and concentrated in the same areas, primarily along the forest edge. The prevalence of canopy disturbances in these regions further supports this observation.

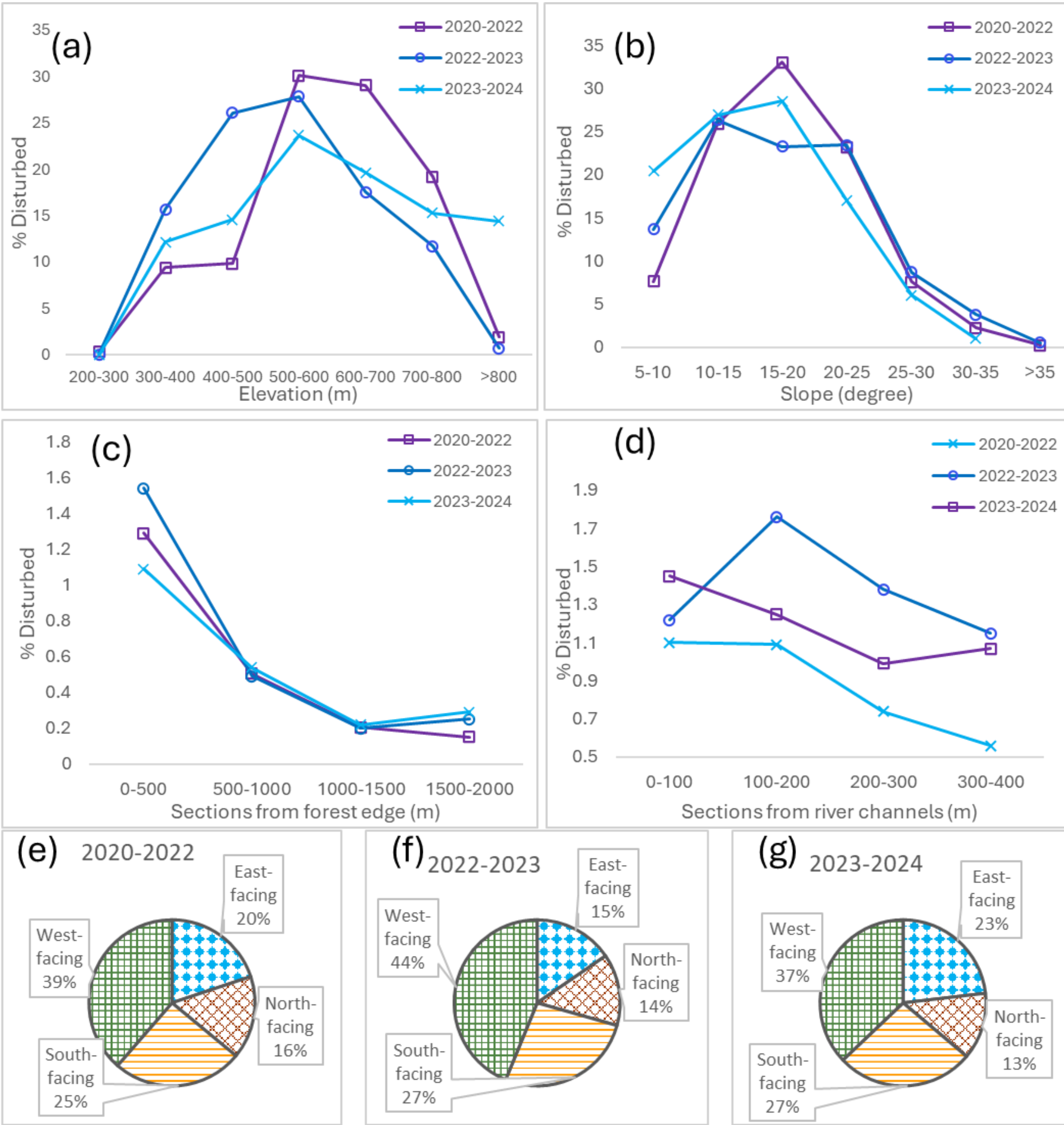

Fig. 3.7. (a-d) Relationship between disturbances and topographic and geospatial features, **(e-g)** Distribution of disturbances in relation to aspect

3.4.2 Inferring canopy disturbance sources

Visual analysis of disturbance and recovery maps reveals that most disturbances and recoveries occur along the edges of the reserve. This pattern aligns with the observed trend of increasing disturbance as one moves outward from the forest core. The study area is bordered by settlements on all sides (see Fig. 3.1), where communities rely on the forest for firewood, agriculture, game meat, mining, and timber, among other resources. While some of these activities extend into the forest interior, the most accessible areas, those closest to settlements, remain the most affected. As a result, persistent canopy disturbances at the forest edges hinder full recovery, raising concerns about the potential for permanent forest loss in these regions. Mon et al. (2012) conducted a study in a tropical forest in Myanmar, where they used logistic regression to analyze the relationship between forest degradation and the distance to the nearest settlement. Their findings highlighted how proximity to settlements increases the likelihood of forest degradation, emphasizing the influence of human activities on forest ecosystems. Persistent canopy disturbance along forest edges can contribute to forest fragmentation, a phenomenon Haddad et al. (2015) found to commonly occur within 1 km of forest edges worldwide. According to their study, fragmentation has long-term impacts on forest ecosystems, including reduced biodiversity, diminished biomass, and disrupted nutrient cycles.

The Atewa landscape, within which the ARFR lies, is known to have river channels along which alluvial mining activities occur (Adams and Hayakawa, 2025). With alluvial mining as one of the drivers of deforestation in the forest reserve, it was important to investigate if it remained a driver for canopy disturbances as well. The mostly increasing pattern in canopy disturbances in relation to river channel proximity infers the possibility of disturbances related to early-stage mining exploration activities, which usually cause little disturbance before the main mining activities. In the Ghanaian Artisanal Small-Scale Mining (ASM) sector, mineral prospecting usually begins with non-mechanized pitting and sampling, which comes after vegetation clearing on a small scale. In subsequent years, such sites could be expanded to begin the main mining processes in the ARFR.

This could also be explained by the transition from areas with low canopy gap coverage to high, as well as the persistence of high-to-high transitions. These patterns suggest that once canopy gaps form, they are likely to remain without significant recovery where human activities persist. Vegetation disturbances near river channels cannot be solely attributed to human activities, as natural factors like flooding (Chen et al., 2023), and erosion and deposition (Jiao et al., 2009) also contribute to these changes. However, the pronounced annual transitions from 'low' to 'high' and 'high' to 'high' suggest a strong likelihood of anthropogenic disturbances in these areas each year.

Human activities tend to concentrate at low elevations and on gentle slopes, where accessibility and ease of construction are greater (Xu et al., 2020). Natural disturbances, including windthrow, bark beetle outbreaks, and forest fires, are also more common in these areas (Stritih et al., 2021). In contrast, high elevations often experience fewer vegetation disturbances due to factors like sparse vegetation, rocky substrates, and low temperatures, which limit insect and disease outbreaks (Logan and Powell, 2001; Heavilin et al., 2007). Additionally, the increased precipitation and nitrogen deposition at higher altitudes generally support plant growth better than at lower elevations (Kane and Kolb, 2014). Consequently, canopy disturbances in tropical forests are expected to be minimal at high elevations, as seen from the disturbance-elevation relationship (Fig. 3.7(a)). However, steep slopes are particularly prone to natural disturbances, as they promote erosion, landslides, and reduced soil stability, leading to vegetation disruption (Kenderes et al., 2007; Nagel et al., 2017). In the Atewa landscape, human activities such as farming, logging, and mining are predominant, and these activities are conveniently carried out at low elevations and on gentle slopes. In the absence of any significant insect and disease outbreaks as well as extreme drought or weather occurrence in the study area during the period of study, it is inferred that human activities are most likely responsible for the canopy disturbances at low to intermediate elevations and slopes which diminish as these factors increase, consistent with findings from Feng et al. (2021) and Chen et al. (2023). It is important to note, however, that this inference may not apply universally. For example, Hamunyela et al. (2020) observed significant forest degradation at higher elevations in the montane forests of Eastern Tanzania, highlighting the influence of regional variation in disturbance patterns. Figure 3.8 shows sites where trees had been logged in the ARFR.

Research suggests that the effects of aspect on vegetation growth and variation depend on the hemisphere. In the northern hemisphere, south-facing slopes receive more sunlight, making them warmer and less conducive to tree growth, while north-facing slopes are typically cooler, more humid, and favorable for vegetation (Måren et al., 2015). Conversely, in the southern hemisphere, north-facing slopes tend to be warmer (Schulze and McGee, 1978). Given these patterns, natural disturbances in the ARFR would be expected to occur predominantly on south-facing slopes, where solar illumination and moisture conditions may create weaker vegetation that is more susceptible to windthrows and other natural factors. While a notable portion of the disturbed forest was indeed south-facing, the majority of disturbances were west-facing, indicating that the north-south aspect orientation may have had little to no influence on the disturbances observed if they occurred naturally. This observation aligns with Singh (2018), who noted that latitude affects the extent to which aspect influences vegetation growth. In low-latitude regions like Ghana (4°N to 11°N), vegetation generally shows minimal variation between northern and southern aspects, unlike mid-latitude regions where northern aspects often support denser vegetation. Consequently, the aspect-related disturbances in the ARFR are more likely attributed to anthropogenic activities than natural factors, even though some natural disturbances could occur on the south-facing slopes.

Fig. 3.8. Tree logging sites in the ARFR

3.5 Study limitations

The study aimed to evaluate Sentinel-2's capability in mapping low-scale canopy disturbances in the Atewa Range Forest Reserve (ARFR) and used the relationship between these disturbances and topographic and geospatial features to infer potential sources. However, the study faced limitations due to the inconsistent availability of annual satellite data caused by frequent cloud cover, a common challenge in forested regions. Consequently, data from 2021 was omitted, potentially impacting the assessment of how topographic and geospatial factors influenced the distribution of canopy disturbances annually. Additionally, the relatively short operational period of the Sentinel-2 Multispectral Imager (MSI) restricted the ability to analyse long-term disturbance trends.

3.6 Conclusions

Through the application of Spectral Mixture Analysis (SMA) on Sentinel-2 satellite imagery, small-scale canopy disturbances that often precede deforestation in tropical forests were mapped with high accuracy in the Atewa Range Forest Reserve (ARFR). Canopy gap coverage was found to increase from 2020 to 2023 while showing a slight dip in 2024. This reflected an increase in canopy disturbances from 2020 to 2023, with a decrease in 2024, which was the only year when recovery exceeded disturbance. Deforestation was, however, found to maintain an increasing trend even in 2024, emphasizing the difficulties in controlling relatively large-scale deforesting activities such as mining and farming in the forest reserve. The relationship between the mapped disturbances and topographic and geospatial features suggested that the disturbances were likely human induced. This inference was supported by the observation that geospatial features, such as the distance from the forest core to the edge and the proximity to river channels, mostly showed a positive correlation with the occurrence of disturbances. Canopy disturbances showed an increase-then-decrease trend with increasing elevation and slope that mostly correspond to human activities, while aspect, mostly west-facing, inferred mostly human-induced disturbances. The study shows that Sentinel-2 satellite imagery combined with topographic and geospatial data is ideal for mapping small-scale disturbances that leave no proxies for source identification rather than large-scale disturbances, such as selective logging activities, which usually exhibit spatially explicit proxies for source identification. Results from the study suggest increased monitoring of small-scale disturbance activities within the ARFR.

Chapter 4

Estimating above-ground biomass of the Atewa Range Forest Reserve in Ghana using Sentinel-2 imagery

4.1 Introduction

The increase in global temperature in recent times is an indication of global climate change to which greenhouse gases (GHGs) are key contributors (Abbass et al. 2022; Al-Ghussain 2019; Song et al. 2023; Stips et al. 2016). Climate change, characterized by irregular weather patterns, rising sea levels, and perceivable increased temperature among others (Kowal, Gough, and Butler 2023; Michel et al. 2021) is a phenomenon that has been known to have occurred throughout Earth's history even before the dawn of humans (National Geographic 2024). However, since the Industrial Revolution, the rate of change in climatic conditions has increased owing to the anthropogenic release of high concentrations of GHGs into the atmosphere (Hansen et al. 1998; Skeie et al. 2017). Carbon dioxide (CO_2), characterized by relatively long residence time and high atmospheric concentrations, has a high Global Warming Potential (GWP) and thus has become topical in issues relating to climate change (Archer et al. 2009; Lashof and Ahuja 1990).

Forests serve as important carbon sinks for CO_2 as they are the largest carbon storage in terrestrial ecosystems accounting for about 46.6% of global terrestrial carbon (Chen, et al. 2021; Whitehead 2011). Studies by DeFries et al. (1999), Hurteau (2021), Murdiyarso, Hergoualc'h, and Verchot (2010), and Pan et al. (2011) highlight the importance of monitoring and conserving forest resources towards achieving carbon neutrality. Accurately estimating forest above-ground biomass (AGB) is an important requirement for the monitoring, conservation, evaluation, and valuation of productivity, biodiversity, and carbon cycle and storage (Alvarez et al. 2012; Geng et al. 2017; Huang et al. 2013). Scientists have over the years estimated AGB using techniques that involve direct calculation through measured tree structures and corresponding allometric equations. These methods may involve the destruction of parts or whole trees, are labour intensive, expensive, and typically apply to only a limited area (Aabeyir et al. 2020; Djomo et al. 2010; Henry et al. 2011).

Though not as accurate as the direct field calculation method, the use of remotely sensed satellite data provides a low-cost and timesaving means of estimating AGB over large areas (Anand 2022). This coupled method is based on the relationship between field-measured data and vegetation parameters obtained through spectral reflectances. Satellite remote sensing data applied in AGB estimation include radar backscatter polarizations, vegetation indices, vegetation biophysical variables, and multispectral bands, which provide vegetation data on height, volume, leaf area index (LAI), and vegetation vigor, among others (Hojo et al. 2023; Malhi et al. 2022; Muhe and Argaw, 2022; Shen et al. 2016). The remote sensing methods do not come without their demerits. Satellite data may be plagued with factors such as low spatial and temporal resolutions, inaccessibility due to cloud coverage and high cost, and canopy penetration capacity, among others (Tadese et al. 2019)

Developed by the European Space Agency (ESA), Sentinel-2 satellite imagery has been considered to be an ideal option for the estimation of AGB through the use of vegetation indices and biophysical variables derived from its 13-band spectral images (Castillo et al. 2017; Chen et al. 2018; de Moura Fernandes et al. 2023; Marcone et al. 2024; Muhe and Argaw 2022; Pandit, Tsuyuki, and Dube 2018). The presence of the red-edge band, which is crucial in the monitoring of photosynthetic activities of plants without the setback of oversaturation (Mutanga and Skidmore 2004) gives Sentinel-2 an edge over other satellite data that lacks this band. A combination of its high spatial resolution (10, 20, and 60 m) and temporal resolution (5 days) also makes it the ideal freely accessible vegetation monitoring data.

As a signatory to the United Nations Framework Convention on Climate Change (UNFCCC) and the Paris Agreement, Ghana is committed to combating climate change by reducing carbon emissions through their sequestration by forest resources. This is evident by the number of forest reserves established throughout the High Forest Zone (HFZ) in the southern part of the country. These forest reserves are usually highly diversified in flora and fauna and are considered sensitive biodiversity hotspots (Afele et al. 2022; Damnyag 2012; Damnyag et al. 2012). With the growing demand of society, these forest reserves have recently been under the pressure of anthropogenic activities such as logging, mining, and illegal farming activities which have increased deforestation, and consequently the CO_2 emission rates in the country (Tsai et al. 2019; National REDD+ Secretariat and Forestry Commission 2017; Appiah et al. 2009; Yiridoe and Nanang 2001). National strategies designed under programs like the Forest Carbon Partnership Facility (FCPF) under the Reduced Emissions from Deforestation and Forest Degradation (REDD+) program in Ghana have already been in motion towards reducing CO_2 emissions from deforestation. However, in the absence of consistent National Forest Inventory (NFI) data for most of these forest reserves (Ghana Forestry Commission 2018), the accurate estimation of forest AGB, especially on a large scale has remained a challenge. To better quantify the stock and emissions of carbon to meet the needs of the REDD+ program, it is imperative that the AGB and carbon accumulation (CAc) of the designated forest reserves in Ghana are estimated and constantly updated.

The Atewa Range Forest Reserve (ARFR) is a sensitive biodiversity hotspot that has gained a lot of attention from conservationists in recent times due to the threat of degradation by miners, loggers, and farmers, among others. As the largest rainforest in West Africa, it has provided habitat for over 100 globally threatened species and many species of birds and butterflies (Akomaning et al. 2021). However, like most forest reserves in Ghana, the lack of consistent NFI data has deprived the reserve of an accurate AGB estimation. To understand and appreciate the role of the ARFR in combating climate change, its carbon accumulation and sequestration capacity must be determined. In this study, the AGB and CAc of the ARFR are estimated through a combination of remote sensing and field-acquired data. The objectives of the study are (i) to establish the relationship between field-observed AGB and satellite-derived vegetation indices and tree biophysical variables, and (ii) to model AGB and CAc for the ARFR based on the best-performing predictor variables.

4.2 Materials and methods

4.2.1 Study area

The study was conducted in the Atewa Range Forest Reserve (ARFR) which is an upland evergreen forest located in the Eastern Region of Ghana between latitudes 5° 58' to 6° 20' North and longitudes 0°31' to 0°41. The ARFR occurs on the north-south oriented Atewa range of mountains characterized by an undulating and rugged terrain. The highest elevation of the Atewa range is recorded to be 842 m above sea level. The Birim, Densu, and Ayensu rivers which are known to take their sources from the ARFR have popularized alluvial gold mining activities in the surroundings of the reserve, even though agriculture remains the common economic activity (Kusimi 2015; Nyamekye et al. 2021). The area is characterized by temperatures ranging between 22 and 33° C while experiencing bimodal rainfall with mean annual intensities ranging from 1200 to 1600 mm. The major rainfall season typically starts in March and ends in July, while the minor begins in September and ends in November. The dry season occurs from November to March (MOFA 2024). Figure 4.1 is a study area map showing the field sample plot locations.

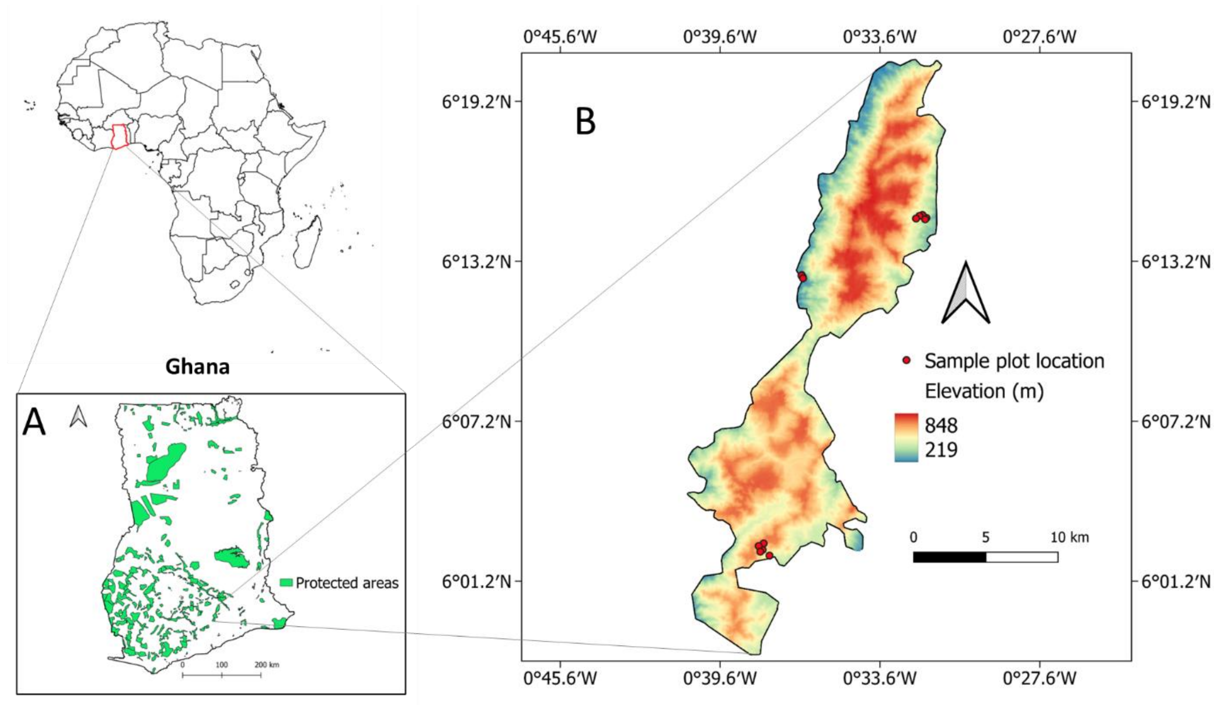

Fig. 4.1. (A) Distribution of protected areas in Ghana **(B)** Study area elevation and field sample plots

4.2.2 Field data collection

A total of 15 field sampling plots were established within the ARFR in March of 2024. Suitable sites for establishing the sample plots were guided by the area's Shuttle Radar Topography Mission (SRTM) Digital Elevation Model (DEM). As the reserve has a homogeneous coverage of vegetation type, the DEM was crucial in selecting areas of relatively flat topography to aid in producing accurate tree height measurements. The sample plot locations were selected based on accessibility to the forest reserve and the selection of less rugged areas. Inside each of the 30 × 30 m plots, tree height and diameter at breast height (DBH) measurements were taken for all trees with diameters ≥10 cm. A Clino Master clinometer and a DBH tape were used for measuring tree height and DBH, respectively. Field AGB was calculated for each tree by using allometric equations developed by Chave et al. (2014) as shown in Equation **(1)**:

$$AGB = 0.0673\,(\rho D^2 H)^{0.976} \qquad \textbf{(1)}$$

Where AGB is Above-ground biomass; ρ is specific wood density obtained from the global wood density database (Zanne et al. 2009); "D" is diameter at breast height; and "H" is tree height.

The total AGB calculated for each plot was obtained by summing up the AGB calculated for each tree and multiplying by a biomass expansion factor (BEF) of 3.4 as provided by the Food and Agriculture Organization (FAO 2004). The final AGB value was then represented in Mg/ha (Table 4.1). To calculate CAc, the following equation was applied:

$$CAc = AGB \times CF \qquad \textbf{(2)}$$

Where CAc is carbon accumulation, and CF is the conversion factor value of 0.47 (IPCC, 2006).

Table 4.1

Sample plots with measured parameters and corresponding measured AGB

Sample plot location	Sample Plot	Latitude	Longitude	Trees with dbh > 10cm	Trees with dbh < 10cm	AGB Mg/ha	Mean height (m)	Mean DBH (cm)
Anyinam	1	6.21030	-0.60831	54	49	211.57	22.66	32.05
	2	6.21141	-0.60889	44	53	93.79	18.08	23.12
	3	6.21024	-0.60861	50	47	112.59	18.76	24.49
	4	6.21116	-0.60910	45	46	171.73	24.18	31.72
	5	6.20941	-0.60812	47	25	138.71	18.67	25.33
Sagyimase	6	6.24717	-0.53095	55	29	224.68	25.01	36.74
	7	6.24902	-0.53342	58	23	207.07	22.60	33.83
	8	6.24627	-0.53177	36	35	85.18	21.56	29.08
	9	6.24838	-0.53538	39	34	109.02	22.84	29.78
	10	6.24678	-0.53744	34	30	85.86	21.37	30.10
Obuoho	11	6.04361	-0.63278	36	86	54.45	21.15	21.00
	12	6.03604	-0.62912	27	87	49.60	16.12	24.12
	13	6.03964	-0.63345	24	104	148.76	23.74	35.10
	14	6.04201	-0.63592	31	82	74.07	20.33	26.98
	15	6.03846	-0.63484	33	84	71.54	19.92	24.35

4.2.3 Satellite data pre-processing

Sentinel-2 level 1-C satellite image for January 31st, 2024, was obtained for the study area via the Copernicus Data Space Ecosystem website (https://dataspace.copernicus.eu). The difference in data acquisition periods for the field and satellite data resulted from the limited number of cloud-free satellite imagery for the study area. However, since both field and satellite data were collected during the dry season, discrepancies in the data were expected to be insignificant. Radiometric and atmospheric correction was applied to the satellite image to convert the top-of-atmosphere (TOA) reflectance to bottom-of-atmosphere (BOA) reflectance in the Sentinel Application Platform (SNAP) software. To match the dimensions of the field sample plots, all bands of the Sentinel-2 image relevant to the study were resampled to 30 m spatial resolution using the nearest neighbour algorithm in QGIS. The satellite image was then clipped to a shapefile of the ARFR.

4.2.4 Vegetation indices and Biophysical variable extraction

To model the AGB of the ARFR, the relationship between the field-measured AGB and the predictor variables had to be established. The predictor variables comprised vegetation indices and biophysical variables of the study area as applied by Castillo et al. (2017), Chen et al. (2018), and Muhe and Argaw (2022). The use of vegetation indices as predictor variables follows the logic that forest biomass has a direct relationship with forest health and vigor which are measured using a combination of the red (band 4), near-infrared (NIR; band 8), and red-edge (bands 5, 6, 7, and 8A) bands in various mathematical transformations to assess photosynthetic activities of plants (Patel, Saha, and Dadhwal 2007; Verrelst et al. 2008; Wahlang and Chaturvedi 2020). Forest biophysical variables, like the vegetation indices, have been used as indicators of the photosynthetic capacity of plants (Wang et al. 2019) as they carry vegetation surface information on the interactions between plants and solar radiations (Muhe and Argaw 2022). The vegetation indices and biophysical variables used as predictor variables in the study are shown in Table 4.2. The geographic coordinates of each plot were used to extract the corresponding pixel values of the predictor variables in QGIS to model the relationship between field-measured AGB and the predictor variables.

4.2.5 Statistical models and model evaluation

The predictor variables derived from the Sentinel-2 bands were first correlated with the field-measured AGB using a pairwise Pearson's product-moment correlation. This was necessary to determine and eliminate multicollinearity. To create a model for predicting AGB for the area, linear and non-linear (polynomial and logarithmic) regressions were used to assess the strength of the relationship between the selected predictor variables and the response variable. The selected predictor variables were evaluated based on the coefficient of determination (R^2) and their correlation coefficients (r; Askar et al. 2018). The best prediction model was selected by assessing the Root Mean Square Error (RMSE), R^2, and the significance at $P \leq 0.05$. The RMSE was calculated as follows:

$$\text{RMSE} = \sqrt{\frac{\sum_{i=1}^{n}(B_{\mathrm{m}}-B_{\mathrm{o}})^2}{n}} \qquad (3)$$

Where RMSE is Root Mean Square Error; B_{m} is the modeled AGB; B_{o} is the field-measured AGB; and n is the number of samples.

A summary of the steps applied in the methodology is shown in Figure 4.2.

Table 4.2

Vegetation indices and biophysical variables used as predictor variables. Biophysical variables were calculated using neural networks in the SNAP software (Kamenova and Dimitrov, 2021)

Predictor variable	Equation/Description
Vegetation indices	
NDVI (Normalized Difference Vegetation Index)	(Band 8-Band 4)/(Band 8+Band 4)
TNDVI (Transformed Normalized Difference Vegetation Index)	$[(\text{Band } 8-\text{Band } 4)/(\text{Band } 8+\text{Band } 4)+0.5]^{1/2}$
SAVI (Soil Adjusted Vegetation Index)	(Band 8-Band 4)/(Band 8+Band 4+0.5) * 1.5
NDVI45 (Normalized Difference Vegetation Index with bands 4 and 5)	(Band 5-Band 4)/(Band 5+Band 4)
IRECI (Inverted Red-Edge Chlorophyll Index)	(Band 7-Band 4)/(Band 5/Band 6)
Biophysical variables	
FCOVER	Fraction of vegetation cover
LAI	Leaf Area Index
LAI_CAB	Canopy chlorophyll content
LAI_Cw	Canopy water content
FAPAR	Fraction of Absorbed Photosynthetically Active Radiation

Band 4 – Red; Bands 5, 6, 7 – Vegetation Red Edge at 0.705, 0.740, and 0.783 µm wavelengths respectively; Band 8 – NIR

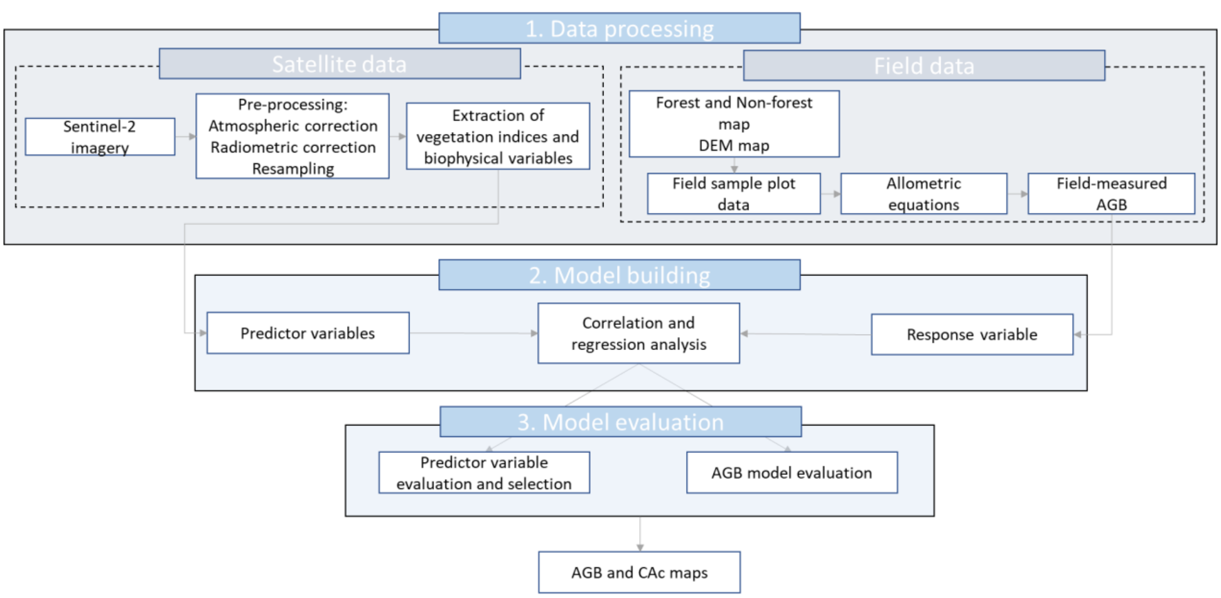

Fig. 4.2. Steps applied in model development

4.3 Results

4.3.1 Field-measured AGB of the ARFR

A total of 613 trees comprising 34 species were recorded from the 15 sample plots (Table 4.3). Contributing 27.90 and 23.33% respectively, *Funtumia elastica* and *Cedrela odorata* were the dominant tree species recorded. The measured AGB from the sample plots ranged from 49.60 to 224.68 Mg/ha. With the homogeneity in vegetation coverage in the ARFR, the AGB values per plot were dependent on the plot tree density rather than the variation in vegetation cover.

4.3.2. Model development and evaluation

Correlation and regression analysis were employed to establish the relationship between the predictor variables and the measured AGB and assess multicollinearity. The correlation analysis indicated that all the vegetation indices were strongly correlated to the measured AGB ($r = 0.63 – 0.76$) compared to the biophysical variables ($r = 0.19 – 0.56$; Table 4). The relationship between the predictor variables and the measured AGB was examined in linear and non-linear (second-order polynomial and logarithmic) regressions to characterize the strength and nature of the association between the predictors and the response variable. This step was critical for identifying the most relevant predictors and reducing the dimensionality of the dataset, thereby enhancing the efficiency and performance of subsequent model development. The relationships between the predictor variables and the measured AGB, as evaluated using the R^2, revealed that polynomial models generally exhibited the strongest fit ($R^2 = 0.64 – 0.035$), followed by linear ($R^2 = 0.57 – 0.035$) and then logarithmic models ($R^2 = 0.55 – 0.035$; Table 4.4). Among all three models, the vegetation indices exhibited stronger relationships with the AGB than the biophysical variables. The optimal model for predicting AGB in the ARFR was developed using stepwise linear, polynomial, and logarithmic regression approaches. The performance of the resulting models was evaluated based on the R^2, RMSE, variance inflation factor (VIF), and ecological plausibility. In developing models to predict above-ground biomass (AGB), particular attention must be paid to the sign and magnitude of the intercept term, especially in linear and non-linear regression models. A negative intercept implies that the model could predict negative biomass values when predictor variables, such as vegetation indices, approach zero, an outcome that is ecologically unrealistic, as biomass cannot be negative. It also implies that the model underestimates AGB in areas of low biomass levels. This issue is most evident in linear models, but it can also arise in polynomial and logarithmic models if the intercept and coefficient combinations lead to negative predictions within the range of observed data (Paine et al., 2012). To ensure ecological validity, the models were constrained to produce non-negative predictions that reflect realistic biomass conditions across all predictor ranges. Such precautions help to maintain the interpretability and applicability of the model in real-world forest and vegetation monitoring contexts. Table 4.5 represents the final selected models for the linear, polynomial, and logarithmic regressions. The inclusion of multiple vegetation indices in a single model introduced multicollinearity due to the high degree of correlation among these indices, as they are mostly derived from similar bands. Additionally, the incorporation of biophysical variables, many of which exhibited weak individual relationships with the measured AGB, led to statistically insignificant coefficient estimates. To enhance model performance and minimize multicollinearity, NDVI was identified as the most effective single predictor and consistently produced the best-fitting models across all regression approaches.

To evaluate the accuracy of the predicted AGB, a linear regression was conducted between the measured and predicted AGB to assess the strength of the relationship. An RMSE of 45.70 Mg/ha and an R^2 value of 0.52 were obtained as shown in the scatter plot in Figure 4.3. The selected prediction model is shown in equation (4).

$$AGB = 421.61 \times \ln(NDVI) + 287.15 \qquad (4)$$

Table 4.3

Tree species information from sample plots

Scientific Name	Number of Trees	Percentage	Height (m)			DBH (cm)		
			Min	Max	Mean	Min	Max	Mean
Afzelia africana	3	**0.49**	9.75	33.81	17.84	10.5	22.2	14.5
Albizia glaberrima	2	**0.33**	22.77	25.77	24.27	21.0	22.9	22.0
Albizia zygia	7	**1.14**	12.47	25.55	21.04	11.2	62.1	39.5
Alchornea cordifolia	15	**2.45**	9.05	32.62	19.35	10.0	45.3	22.5
Alstonia boonei	29	**4.73**	9.25	43.64	23.71	10.1	128.2	30.6
Antiaris toxicaria	3	**0.49**	14.09	43.64	24.27	13.2	128.2	52.5
Antrocaryon	7	**1.14**	7.24	34.99	20.63	10.0	22.2	14.1
Buchholzia coriacea	1	**0.16**	24.22	24.22	24.22	29.1	29.1	29.1
Cedrela odorata	143	**23.33**	10.86	34.80	23.33	10.4	140.0	31.8
Ceiba pentandra	17	**2.77**	9.25	34.80	22.87	15.0	129.0	38.9
Celtis mildbraedii	5	**0.82**	12.07	24.77	17.53	10.2	128.2	36.7
Celtis zenker	8	**1.31**	8.85	29.77	17.00	12.6	40.1	22.5
Cola gigantea	29	**4.73**	4.43	33.10	20.13	14.0	92.2	32.7
Cola gigantia	3	**0.49**	17.44	29.77	22.74	16.2	40.1	24.8
Cordia millenii	13	**2.12**	4.43	27.03	14.68	12.0	40.5	18.9
Duboscia viridiflora	2	**0.33**	24.16	28.16	26.16	45.1	45.1	45.1
Elaeis guineensis	4	**0.65**	5.23	40.23	17.18	11.1	40.4	21.8
Eucalyptus acmenoides	4	**0.65**	17.11	18.11	17.36	18.2	46.3	29.6
Funtumia Africana	6	**0.98**	9.25	38.22	21.93	16.2	100.1	37.9
Funtumia elastica	171	**27.90**	8.05	33.19	19.99	10.0	50.0	22.5
Glyphaea brevis	18	**2.94**	13.08	31.09	21.43	10.3	60.0	28.1
Macaranga barteri	18	**2.94**	8.25	29.77	16.30	12.6	40.1	21.0
Margaritaria discoidea	1	**0.16**	24.14	24.14	24.14	100.1	100.1	100.1

Milicia excelsa	4	**0.65**	13.08	29.17	23.63	17.6	60.0	31.4
Morinda lucida	3	**0.49**	14.28	15.09	14.62	87.2	100.6	92.4
Musanga cecropioides	3	**0.49**	13.08	18.46	15.00	15.9	17.6	16.7
Nesogordonia papaverifera	2	**0.33**	30.00	30.02	15.06	11.4	12.0	11.7
Piptadeniastrum africanum	33	**5.38**	12.07	43.64	24.04	10.2	128.2	38.2
Ricinodendron heudelotii	13	**2.12**	9.86	34.60	18.22	8.0	43.2	23.4
Terminalia ivorensis	5	**0.82**	9.25	38.22	18.06	16.2	100.1	33.6
Terminalia superba	2	**0.33**	29.72	29.77	29.75	25.2	27.2	26.2
Trichilia monadelpha	28	**4.57**	4.43	38.22	16.23	12.0	100.1	24.9
Triplochiton scleroxylon	7	**1.14**	22.00	32.19	26.71	27.2	48.5	36.4
Vernonia conferta	4	**0.65**	27.37	29.37	28.50	28.5	50.3	39.0

Table 4.4

r and R^2 values of correlation and regression analyses between AGB and predictor variables

	r	R^2		
		Linear	Polynomial	Log
NDVI	0.76	0.57	0.64	0.55
TNDVI	0.75	0.57	0.67	0.56
IRECI	0.69	0.48	0.48	0.47
SAVI	0.67	0.45	0.45	0.45
NDVI45	0.63	0.4	0.41	0.41
LAI_Cw	0.56	0.31	0.6	0.44
LAI	0.54	0.3	0.31	0.31
FAPAR	0.53	0.28	0.29	0.28
LAI_CAB	0.42	0.17	0.28	0.2
FCOVER	0.19	0.035	0.037	0.035

4.3.3. Spatial distribution of estimated above-ground biomass and carbon accumulation in the ARFR

The resulting AGB and CAc maps from the model in equation (4) are shown in Figures 4.4A, 4.4B, and 4.5. From the predicted AGB map, the ARFR recorded a high AGB value of 188.92

Mg/ha with a mean value of 115.12 Mg/ha. The spatial distribution of AGB within the ARFR is such that intermediate to high AGB values (>100 Mg/ha) are mostly found deeper within the forest reserve. The resulting CAc map followed a similar spatial distribution as the AGB, with a high of 88.79 Mg/ha and a mean of 54.12 Mg/ha.

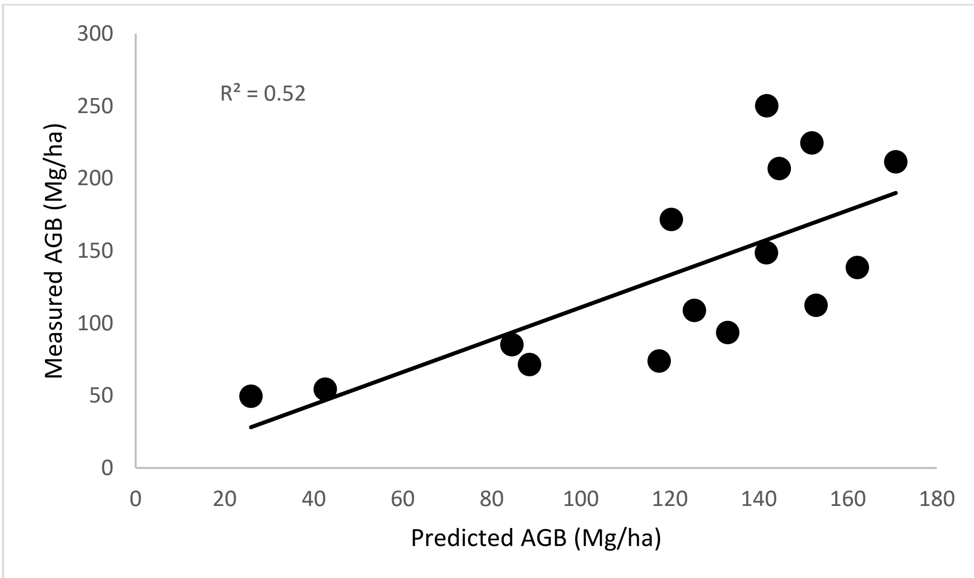

Fig. 4.3. Relationship between predicted and measured AGB

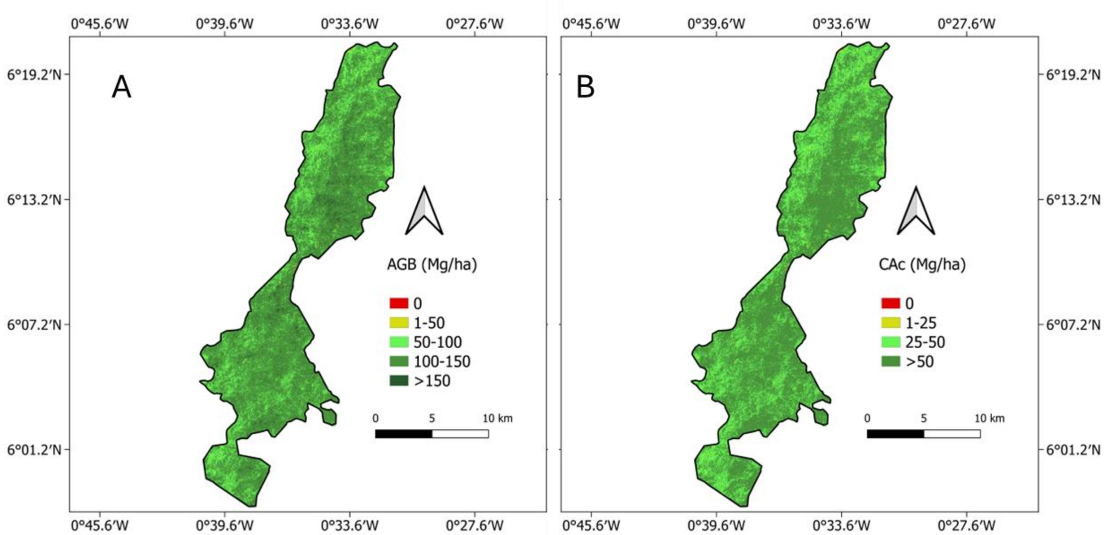

Fig. 4.4. (A) Map of predicted AGB **(B)** CAc map

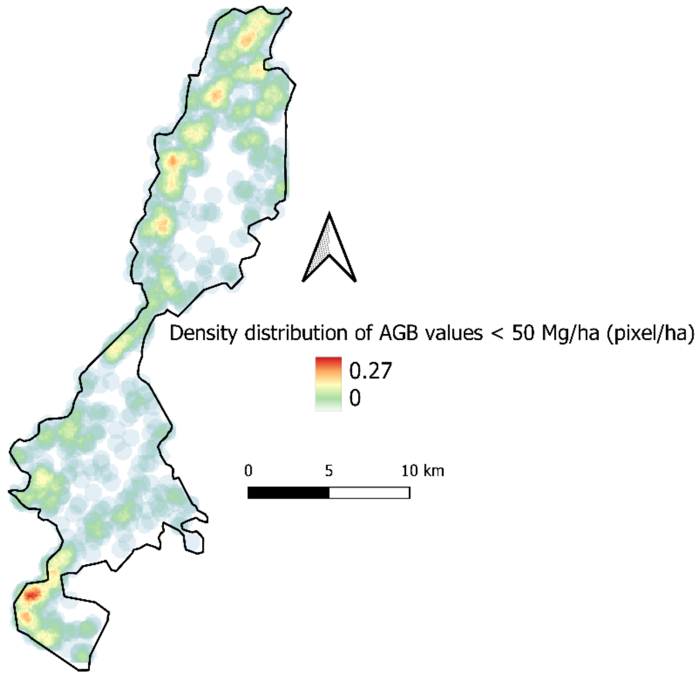

Fig. 4.5. Density distribution of pixels with AGB values less than 50 Mg/ha

Table 4.5. AGB model statistics

Model variable	R^2	Adjusted R^2	Coefficients	t-value	Significance	VIF	RMSE
			Linear				
(n = 15)	0.87	0.86					49.79
Constant			Constrained to 0				
NDVI			184.52	9.8	<0.001	1	
			Polynomial				
(n = 15)	0.9	0.89					43.25
constant			Constrained to 0				
$NDVI^2$			270.64	11.49	<0.001	1	
			Logarithmic				
(n = 15)	0.56	0.52					
Constant			287.15	6.81	<0.001		40.37
ln (NDVI)			421.61	4.03	0.001	1	

VIF = Variance Inflation Factor

4.4 Discussion

4.4.1. Model validation and contributing factors

Above-ground biomass data collected from the sample plots served as the response variable in the model development. The absence of a variable vegetation cover in the ARFR resulted in sample plot AGB values depending on tree density rather than vegetation type. Thus, plots with high tree count recorded high biomass values and vice versa.

The vegetation indices and biophysical variables were used as predictors for the model development. Contrary to similar studies conducted by Chen et al (2018), and Muhe and Argaw (2022), where the biophysical variables showed a stronger linear relationship with the measured AGB over the vegetation indices, the vegetation indices in this study showed stronger relationships (linear, polynomial, and logarithmic) with the measured AGB. The IRECI and NDVI45 function through the absorption of the red-edge band by plants to determine the robustness of their photosynthetic activities. In this study, the IRECI and NDVI45 indices exhibited positive linear relationships with the measured AGB, highlighting their demonstrated utility in estimating AGB (Frampton et al., 2013; Li, Zhou, and Xu, 2021; Suardana et al., 2023). The traditional vegetation indices, NDVI, TNDVI, and SAVI, which are mostly used across various satellite imagery to estimate AGB, showed the best relationship with the measured AGB in the ARFR. Thus, even though the NDVI was the only predictor variable applied in this study, the significance of the other vegetation and biophysical indices in the estimation of AGB globally cannot be overlooked.

Although the quadratic model exhibited a higher R^2 value (0.90) compared to the linear (0.87) and logarithmic (0.56) models, the logarithmic regression yielded the lowest RMSE, indicating superior predictive accuracy. This outcome can be attributed to the constraints applied to the linear and quadratic models to prevent ecologically implausible negative AGB predictions, such as forcing negative intercepts to zero. While these adjustments improved the realism of the models, they also reduced their statistical flexibility, slightly compromising their fit and increasing prediction error. In contrast, the logarithmic model inherently maintained positive predictions across the full NDVI range without requiring such constraints, thereby offering a more balanced trade-off between model fit and ecological validity. Thus, while R^2 indicates the proportion of variance explained by a model, it does not account for ecological plausibility or prediction error. High R^2 values can result from overfitting, especially in complex models that capture noise rather than meaningful patterns. Therefore, relying solely on R^2 may lead to selecting models that perform poorly in real-world, ecologically grounded scenarios.

The selection of the final model was crucially dependent on the VIF. Where VIF is greater than 10, there is a high possibility of collinearity, which could lead to model overfitting and unreliable coefficient estimates (Hair 2009). Thus, the VIF value of 1.00 for the selected predictor variable, NDVI, is an indication of a reliable model. With an RMSE of 45.70 Mg/ha and an R^2 value of 0.52 between the measured and predicted AGB, the model produced a good prediction performance. The values from the predicted AGB of the ARFR were lower than what was reported by Asare et al. (2012) in the biomass map of Ghana, which was between 275.1 and 400 Mg/ha for the ARFR. Asare et al. (2012)'s values, however had an uncertainty of ± 70-80 Mg/ha, which indicates that values from this study are more accurate.

4.4.2. Distribution of low above-ground biomass areas

Areas with AGB values of 0 typically represent the non-forest portions of the reserve which have been increasing over the years. The conversion of forest resources to non-forest has remained a threat to the sustainable existence of the ARFR (Amponsah et al. 2022; Nyamekye et al. 2021). Illegal anthropogenic activities such as mining, farming, and logging have remained menace to the forest's productivity and have the potential of rather increasing carbon emissions from the forest reserve. From the density distribution map (Fig. 4.6), high densities of AGB values less than 50 are mostly closer to the forest reserve's fringes, which is an indication of the prevalence of human activities along tropical forest edges and its accompanying reduction in AGB as indicated by Brinck et al. (2017) using remote sensing. Nunes et al. (2023) also found that edge effects negatively affected tree architecture and allometry which in turn lowered the AGB of edge forests in Central Amazonia as observed in this study. The ARFR is surrounded on the fringes by communities that depend on it for food materials, timber, game meat, and the mining of minerals, among others. The distribution of AGB values below 50 Mg/ha along the fringes of ARFR can be attributed to a combination of local anthropogenic pressures and edge-related ecological dynamics. The ARFR is surrounded by rural communities and areas with ongoing small-scale agricultural and artisanal mining activities (Chapter 2), particularly in the eastern peripheries. These activities often result in forest fragmentation, selective logging, and vegetation clearing, all of which contribute to biomass depletion (Laurance, 2004). In addition to these human-induced pressures, edge habitats experience altered microclimatic conditions, such as increased solar radiation, wind desiccation, and temperature variability, that can suppress vegetation productivity and favor the dominance of low-biomass, disturbance-adapted species (Hofmeister et al., 2019). These environmental stressors, combined with proximity to human settlements, create conditions that inhibit the accumulation of mature forest biomass. As such, the low AGB values observed at the forest margins reflect both the direct impact of land use practices (Chapters 2 and 3) and the ecological consequences of forest edge effects, which are particularly pronounced in a biodiversity-rich yet increasingly fragmented landscape like the ARFR.

Areas characterized by rugged terrains such as the ARFR are likely to produce less accurate AGB estimates with SAR data even though they are known to interact with tree structures and hence produce more accurate estimates. The complex topography of such rugged terrains results in variable radar backscattering, and shadowing among other complications that affect its accuracy (Hoekman and Reiche 2015; Hojo et al. 2023; Ling et al. 2022; Loew and Mauser,2007). In the rugged Afromontane forests of Ethiopia, the optical methodology applied in this research as used by Muhe and Argaw (2022) produced accurate AGB estimates with an R^2 value of 0.733 and an RMSE of 0.16 ton C/pixel. However, when the performance of different predictor variables was tested in a variable importance analysis toward the estimation of AGB in the rugged terrain of the Teshio Experimental Forest of Hokkaido University in Japan, Hojo et al. (2023) found that the non-SAR variables came out on top. The relatively weak performance of the SAR variables was attributed to the rugged nature of the terrain. Thus, the application of optical remote sensing in estimating AGB is ideal for rugged terrains where the predictive performance of SAR may be affected.

In Ghana and other developing countries where there is a lack of expertise in the application of SAR for the measurement, reporting, and verification (MRV) of changes in forest resources (Reiche et al. 2016), the coupled method of forest biophysical parameters and indices with measured AGB will play an important role in keeping countries in these regions updated with the rest of the world.

4.5. Potential sources of errors in the AGB estimation

Several sources of uncertainty may have influenced the estimation of AGB in the ARFR, spanning from field data collection to remote sensing-based modeling. Errors in field sampling can arise from inaccuracies in tree diameter measurements, species misidentification, and height estimation, all of which affect the calculation of tree-level biomass using allometric equations. Also, the allometric equations adopted from the study by Chave et al (2014) reported a residual standard error (RSE) of about 0.36, which reflected errors in the predictions of individual tree AGB in the best pan-tropical model. Thus, even with precise field data collection, errors could arise from the development of the allometric equation applied in the measured AGB calculation in this study.

Additionally, the use of generalized biomass expansion factors (BEFs) introduces further uncertainty, as these factors are often derived from different ecological contexts and may not fully capture the structural variation and species composition unique to the ARFR. The spatial mismatch between field plot locations and the corresponding satellite image pixels used for model calibration also contributes to estimation error. Slight misalignments due to GNSS inaccuracy, topographic variation, or canopy heterogeneity can result in the extraction of vegetation index values that do not accurately represent the sampled plot area.

Moreover, spectral mixing within satellite pixels, especially in transitional zones where forest edges meet non-forest land cover, can reduce the precision of vegetation indices, thereby weakening the relationship between spectral data and field-measured AGB. Temporal mismatches between field data collection and image acquisition dates can further exacerbate these discrepancies, particularly in dynamic forest environments subject to seasonal or anthropogenic changes.

Collectively, these sources of error highlight the challenges of integrating field and remotely sensed data for AGB estimation in complex, heterogeneous landscapes like the ARFR and underscore the need for rigorous field protocols, locally calibrated expansion factors, and high-resolution spatial data to improve model reliability.

4.6. Conclusions

To the best of our knowledge, this is the first study to locally estimate the AGB of the ARFR using the coupled method of field-measured data and remote sensing. The Sentinel-2-derived vegetation indices and biophysical variables used as the predictors produced accurate results ($R^2 = 0.52$) and confirmed the reliability of remote sensing in estimating AGB over large areas. The vegetation indices showed a stronger general relationship with the measured AGB, especially in a quadratic relationship with R^2 values ranging between 0.41 and 0.67, while the biophysical variables recorded R^2 values in the range 0.035 – 0.60. The NDVI produced the model with the best performance across all the models that were explored, leading to its ultimate application in the logarithmic function model used for the AGB estimation.

Findings from the study bring to light the value of the ARFR in terms of its biomass and carbon accumulation, as it remains a crucial forest resource for the sequestration of carbon towards the reduction of global warming and climate change. However, the forest reserve could become a source of carbon emissions if the activities of humans that lead to tree loss are not controlled. It is therefore imperative that policymakers and relevant monitoring bodies, such as the Forestry Commission, increase monitoring and protection of the forest. The research was limited by a reduced number of sample plots, which could have been supplemented by NFI data if available. For improved accuracy of future works in the ARFR and in other forest reserves in Ghana, the collection and application of NFI data is highly recommended.

Chapter 5

General discussion

5.1 Anthropogenic activities in the Atewa landscape and the Atewa Range Forest Reserve (ARFR)

Globally, areas where human activities such as mining, farming, and logging, among other human activities, are undertaken are usually faced with environmental challenges that affect important ecosystems, usually the forest and aquatic ecosystems (Dar et al., 2022; Muruganandam et al., 2023). The Atewa landscape in Ghana, where these activities have been taking place over the years, is no exception. Considering the relevance of the study area to biodiversity conservation, as it hosts the Atewa Range Forest Reserve (ARFR), the study was focused on mapping and assessing the dynamics of these human activities on an annual basis, focusing on discernible activities and those that are not readily discernible at the pixel level in satellite images. This study was necessary as annually consistent research on the effects of human activities in the study had not been focused on in past research.

The dominant large-scale human activity in the study area was found to be alluvial mining, followed by farming activities. Alluvial mining activities in the landscape were seen to increase annually at a growth rate of 12.3% between 2018 and 2023, which emphasizes the ineffectiveness of government policies in recent years, which have mostly been manual and ground-based, including Operation Vanguard, where military personnel were deployed to monitor illegal mining activities. The results from Operation Vanguard and alluvial mines coverage mapped in this study show clearly the advantages and accuracy in applying remote sensing and GIS techniques in mapping land use pattern changes over manual methods. The results also emphasize the recent trends in pollution in the form of sedimentation in river bodies owing to mining activities in Ghana.

With the spatial interconnectedness among vegetation, settlements, and river channels in the study area, there is the potential for mining-related heavy metals such as mercury (Hg) and cyanide (CN) to be absorbed by food crops, thereby initiating accumulation, then biomagnification along the food chain.

Agriculture has remained an important aspect of the primary sector of the country, which accounts for about 19% of the country's GDP while employing about 34% of the workforce (Ferreira et al., 2022). This is reflected in the LULC mapped in the landscape in Chapter 2, where the herbaceous cover, which comprises, among others, young-stage agricultural fields, constituted at least 16% of the total area, with oil palm and coca plantations constituting part of the closed-canopy vegetation (Table 2.5). However, despite the clear delineation of the boundaries of the forest reserve, some farms have been established within the confines of the reserve, while others have expanded over the years to encroach on the reserve. This issue sometimes becomes more complex with some community members feeling entitled to the resources in the forest reserve.

The ARFR, located within the broader Atewa landscape, has long been under the protection and surveillance of the Ghana Forestry Commission (GFC). The GFC has consistently combated the persistent threat of illegal mining and logging within the reserve. However, the rapidly expanding economic activities in the areas surrounding the forest pose significant environmental challenges and continue to undermine the effectiveness of the GFC's protective efforts. Even though the reserve does not experience as much degradation as outside of its borders in the landscape, the irregular pattern of mining and farming activities highlights a vulnerability in the dependence of ground-based monitoring methods in the forest reserve.

Characteristic of the ARFR is the persistence of degradation in the form of canopy disturbances, which are small in scale and sometimes not readily discernible even in high-resolution satellite images. These disturbances are likely a result of human activities such as the small-scale non-mechanized logging that takes place in the forest (Chapter 3). As indicated by the results from the canopy disturbance mapping in the ARFR, disturbed canopies are mostly concentrated at the fringes of the forest reserve, near human settlements. This suggests the possibility that the permanent conversion of the forest to bare and farmlands begins with such small-scale disturbance activities occurring where there is the ease of accessibility by settlers close to the forest reserve.

The study highlights the prevalence of three disturbance activities in the Atewa landscape, namely, mining, farming, and tree logging. The difference in these activities within and outside the ARFR is mostly in the scale at which they occur. Outside the ARFR, Artisanal Small-scale miners (ASM) operate both legally and illegally, employing the use of heavy-duty machinery at a relatively large scale, where large areas of vegetation are removed. Farmlands cover noticeably larger areas outside the forest reserve, where they are legally operated seasonally. In the ARFR, mining is prohibited; thus, its characteristic small coverage compared to mines outside the reserve. Mining activities within the ARFR could be undertaken using heavy-duty machines or by manpower using rudimentary tools and techniques. Also, mineral prospecting activities, which usually occur at a small scale prior to the main mining stage, could contribute to the small-scale mines identified in the ARFR. Farmlands in the ARFR are mostly at the fringes and are usually extensions of those existing outside the reserve's boundaries. This results in their characteristic small coverage. It is worth noting that farmlands represented tilled bare lands and herbaceous cover, making the clear delineation of farmlands from bare non-farmlands and other herbaceous cover difficult. While no large-scale tree logging activity was identified in the Atewa landscape, small-scale or individual tree felling, which has been a challenge for the GFC over the years, was identified in the ARFR.

Aside from the ARFR, several other forest reserves in the country, especially those in the High Forest Zone (HFZ), have been reported to face threats of degradation and deforestation from farming, mining, and logging, among other human activities (Appiah et al., 2009). A study by Sakyi and Ameko (2025) highlighted how the dependency of fringe communities on non-timber resources from the Yenku Forest Reserve in Ghana affects the forest ecosystem. This, along with a study by Ankomah et al (2020) which emphasizes the effects of mining among other activities in Ghana's HFZ, paints a clear picture of the threats forest resources in southern Ghana face. While focusing on mapping disturbances on different scales resulting from different human activities, this case study presents an effective methodological approach for understanding the dynamics of such human-mediated forest disturbances in forests in the HFZ and the entire country. The study, while mostly employing the use of freely accessible satellite imagery like the Sentinel-2A, eliminates the constraint of data unavailability due to high cost of data acquisition. Thus, the study underscores the critical role of remote sensing and GIS in detecting and mapping forest disturbances, while simultaneously evaluating their impacts on AGB and CAc, an area of research that remains underexplored within the Ghanaian context.

The integration of GIS techniques with remote sensing significantly enhanced the spatial and analytical depth of this study, enabling a more nuanced understanding of forest disturbance dynamics in the ARFR. GIS provided spatially explicit analyses that satellite imagery alone could not achieve, offering tools to quantify, contextualize, and visualize the impacts of anthropogenic activities on key forest metrics such as AGB and carbon accumulation CAc. Multiple ring buffer analysis was applied to measure the proximity of mining operations to sensitive areas like the ARFR boundaries and river channels, revealing spatial gradients of disturbance risk. The 100 m ×

100 m grid framework also facilitated standardized annual change detection of soil fraction, allowing for the identification of both persistent degradation and vegetation recovery.

Kernel density estimation (KDE) further improved result visualization by mapping the spatial distribution of low-biomass areas (<50 Mg/ha), producing continuous surfaces that highlight clusters of forest degradation. Together, these GIS-based approaches provided a robust, scalable framework for integrating spatial measurements, temporal change detection, and landscape-level pattern analysis. This combined methodology not only improved the ecological interpretability of remote sensing outputs but also strengthened their applicability for forest conservation in data-scarce contexts like Ghana.

The Sub-Saharan region of Africa has long been a region for mining precious minerals, with different countries producing different minerals for the international markets. This has led to a more than doubled increase in the areal extent of mines between 2000 and 2018 (Ahmed et al., 2021). Outside of these mining areas, a decrease of 17.7% of off-site forest cover has been recorded from 2001 to 2020 (Ahmed et al., 2025). This warns of a continued increase in mining activities and their associated forest degradation and deforestation in the region. Many studies have employed the use of remote sensing in mapping mining and other human activities and their effects on forest resources in the Sub-Saharan region (Potapov, et al., 2012; Luethje et al., 2014; Dlamini and Xulu, 2019; Mufungizi, 2024). However, several studies applied remote sensing in isolation without the integration of GIS. Results from this case study confirm the significance of the integration of GIS in such forest monitoring studies, as GIS-based data visualization, resampling, and buffer analysis, among others, facilitated the mapping process as a whole. Also, several studies have paid attention mostly to disturbances that are discernible at the pixel level, with little focus on the small-scale sub-pixel disturbances that usually contribute to deforestation in the long term.

Through the application of Spectral Mixture Analysis (SMA) and GIS, this case study presents the methodology for mapping both large- and small-scale forest disturbances resulting from human activities in the African region and globally. The study also contributes to the mapping and modeling of global ecosystem parameters such as AGB, as it could serve as a source of ground truth data for validating satellite-based models such as those provided by NASA's BigFoot (1999 to 2004) and Global Ecosystem Dynamics Investigation (GEDI) projects, as well as JAXA's Multi-sensing Observation Lidar and Imager Demonstration (MOLI) project.

5.2 The implications of disturbances in the ARFR on biodiversity

The most immediate implication of disturbances within the ARFR is habitat fragmentation. Fragmentation disrupts the contiguous forest cover, which is essential for many species whose survival depends on the forest, particularly those with limited dispersal abilities (Pfeifer et al., 2017). Canopy disturbances and edge encroachments are known to reduce core forest areas and create microhabitats that differ significantly in temperature, humidity, and light exposure from the forest interior (Hofmeister et al., 2019). The changes in microhabitats are usually not suitable for sensitive species, thus leading to localized extinctions or forced migration (Stratford and Stouffer, 2015). In highly biodiverse ecosystems such as the ARFR, where species richness is linked to habitat continuity, such fragmentation can result in irreversible biodiversity loss. Additionally, with the presence of forest edge activities such as farming and illegal logging near human settlements, generalist and invasive species that thrive in disturbed habitats may outcompete native forest species. This shift in species composition not only reduces biodiversity but can also lead to instabilities in the ecosystem and a decline in the provisioning of ecosystem services (Leidinger et al., 2021).

The ARFR is home to many endemic and threatened species, including amphibians, birds, and plants that have not been recorded in other parts of the world (McCullough et al., 2007). The cumulative effect of localized but persistent degradation, including tree logging and artisanal prospecting, threatens the microhabitats critical for these species. Small canopy gaps created by the removal of trees can alter microclimatic conditions necessary for the survival of amphibians and epiphytic plant species, which are especially sensitive to humidity and temperature changes (Burrow and Maerz, 2022). Moreover, species in ARFR may rely on specific plant-host relationships or require large, undisturbed territories to maintain viable populations. The increasing encroachment along the fringes of the reserve, as reported, can isolate populations, reduce gene flow, and increase susceptibility to stochastic events such as disease or drought (Rajora and Mosseler, 2001). These factors, compounded by human-induced stressors, place the survival of endemic and range-restricted species at critical risk.

The study's findings emphasize the increasing threat of pollution from alluvial mining operations. Even at a smaller scale within the ARFR, the use of mercury (Hg) and cyanide (CN) in artisanal mining introduces toxic substances into the ecosystem. These contaminants can leach into the soil and water systems, thereby entering the food web (Johnson, 2015; da Silva and Guimarães, 2024). Plants, including the food crops that are grown within and near the forest, can absorb these toxins, which may then be ingested by herbivores and predators, leading to bioaccumulation and biomagnification. This toxic loading compromises not only faunal health but also reproductive success, leading to long-term declines in species populations. Amphibians and aquatic invertebrates, which are known to be important bioindicators of ecosystem health, are especially vulnerable to this chemical pollution. The contamination of headwater streams originating in

ARFR also has far-reaching implications, potentially affecting aquatic biodiversity downstream and human communities that rely on these water sources.

Forest ecosystems like the ARFR provide a variety of ecosystem services essential for both biodiversity and human wellbeing, including water filtration, carbon sequestration, soil stabilization, and pollination. Even small-scale degradation in the form of tree felling or fringe farming can disrupt these services, especially when such disturbances accumulate over time. The removal of canopy cover accelerates erosion, increases runoff, and reduces the forest's ability to moderate local temperatures and moisture levels. Degradation may further affect critical ecological processes such as seed dispersal and pollination, which depend on diverse and intact animal populations. For instance, the loss of fruit-eating birds and bats due to habitat fragmentation can hinder natural forest regeneration (Fontúrbel et al., 2015). Similarly, the decline of specific insect pollinators, which are usually sensitive to changes in habitat structure, may affect the reproductive success of both wild and cultivated plants. Without these processes, the forest's ability to recover from disturbance is affected, reducing its long-term resilience and productivity.

5.3 The implications of disturbances of the ARFR on climate change mitigation

With limited scientific works on the locally estimated above-ground biomass (AGB) of the ARFR, the study involved estimating the AGB and the corresponding carbon accumulation (CAc) of the ARFR through the application of a logarithmic regression (Chapter 4). This aspect of the research was important in highlighting the relevance of the ARFR in carbon sequestration, and hence the mitigation of climate change.

Tropical forests, such as the ARFR, are globally recognized as critical carbon sinks that significantly contribute to climate regulation through carbon sequestration. The capacity of these ecosystems to store atmospheric carbon in both AGB and soil pools plays a vital role in climate change mitigation. However, anthropogenic degradation in the form of mining, farming, and selective logging within and around the ARFR has profound implications for this regulatory function, primarily through alterations in forest structure, biomass loss, and subsequent carbon emission dynamics (Kronseder et al., 2012; Meyer et al., 2019).

Degradation of forest biomass through direct vegetation removal or indirect canopy disturbances fundamentally alters the carbon balance of forest ecosystems. The ARFR exhibits a spatial gradient in AGB values, with lower biomass at the forest fringes and higher values in the core and elevated areas (Fig. 4.5). This pattern reflects the susceptibility of edge zones to anthropogenic intrusion (Chapters 2 and 3). Edges are typically more accessible to local populations and more exposed to extrinsic stressors such as temperature fluctuations, desiccation, and wind damage, all of which exacerbate biomass loss (Laurance, 2004). Reduced AGB in these transition zones leads to diminished carbon storage capacity, both in living biomass and in litter and soil organic matter, thus compromising the ARFR's function as a carbon sink.

Furthermore, the fragmentation and progressive encroachment of the forest increase the decomposition rates of organic matter due to higher exposure to sunlight and temperature variability (Schröder and Fleig, 2017). This accelerates the release of previously sequestered carbon back into the atmosphere in the form of CO_2. Forest degradation also diminishes forest canopy cover, reducing photosynthetic activity across affected areas and thereby lowering net primary productivity (NPP). The cumulative consequence is a shift in the ARFR's carbon budget, potentially transforming sections of the reserve from net carbon sinks into net carbon sources, a feedback loop that exacerbates global warming.

Another critical implication of degradation in the ARFR is its impact on carbon sequestration potential over time. The structural complexity of undisturbed tropical forests, characterized by multilayered canopies and high species diversity, supports enhanced carbon accumulation (Poorter et al., 2015). Disturbance events, including artisanal mining and selective logging, simplify forest structure and reduce species heterogeneity, which are both positively correlated with biomass productivity. As pioneer species dominate disturbed patches, their fast growth rates may initially suggest recovery; however, their lower wood density and shorter lifespans reduce the long-term carbon storage potential compared to late-successional, high-biomass species. This simplification limits the reserve's capacity to offset carbon emissions on decadal scales (Poorter et al., 2017).

Additionally, degradation disrupts the vertical and horizontal continuity of forest cover, impeding ecosystem processes such as seed dispersal, succession, and recruitment—factors crucial for maintaining long-term carbon dynamics. In areas where regeneration is impaired, forest recovery trajectories are delayed or altered, resulting in semi-permanent carbon deficits. This is particularly relevant in the ARFR, where forest recovery may be hindered by persistent anthropogenic disturbances (as reported in Chapter 3), and the introduction of invasive species that compete with native flora, further diminishing future biomass potential.

Soil carbon dynamics are also adversely affected by degradation. Mining and intensive farming near or within the ARFR disturb the topsoil and subsoil layers, leading to erosion and loss of organic carbon content (Nogueira Jr et al., 2011). In tropical environments, where a significant portion of the ecosystem's carbon is stored below ground, such disturbances can result in substantial emissions of CO_2 and methane (CH_4), especially when soils are exposed to oxidation processes (Mchunu and Chaplot, 2012). Mercury and cyanide contamination from mining exacerbate this issue by disrupting soil microbial communities that are integral to carbon cycling and nutrient retention (Zheng et al., 2022).

Moreover, the degradation-induced reduction in ARFR’s carbon sequestration capacity has implications beyond its boundaries. The forest is hydrologically significant, hosting headwaters of several rivers. Changes in forest cover affect evapotranspiration and local precipitation patterns, potentially reducing moisture recycling and altering regional climate regulation services. These cascading impacts can influence climate resilience in adjacent agricultural and urban areas, underscoring the interconnectedness of forest integrity and regional climate stability. Figure 5.1 shows a summary of the application of remote sensing and GIS in assessing the effects of human activities in the Atewa landscape and its effects on the environment.

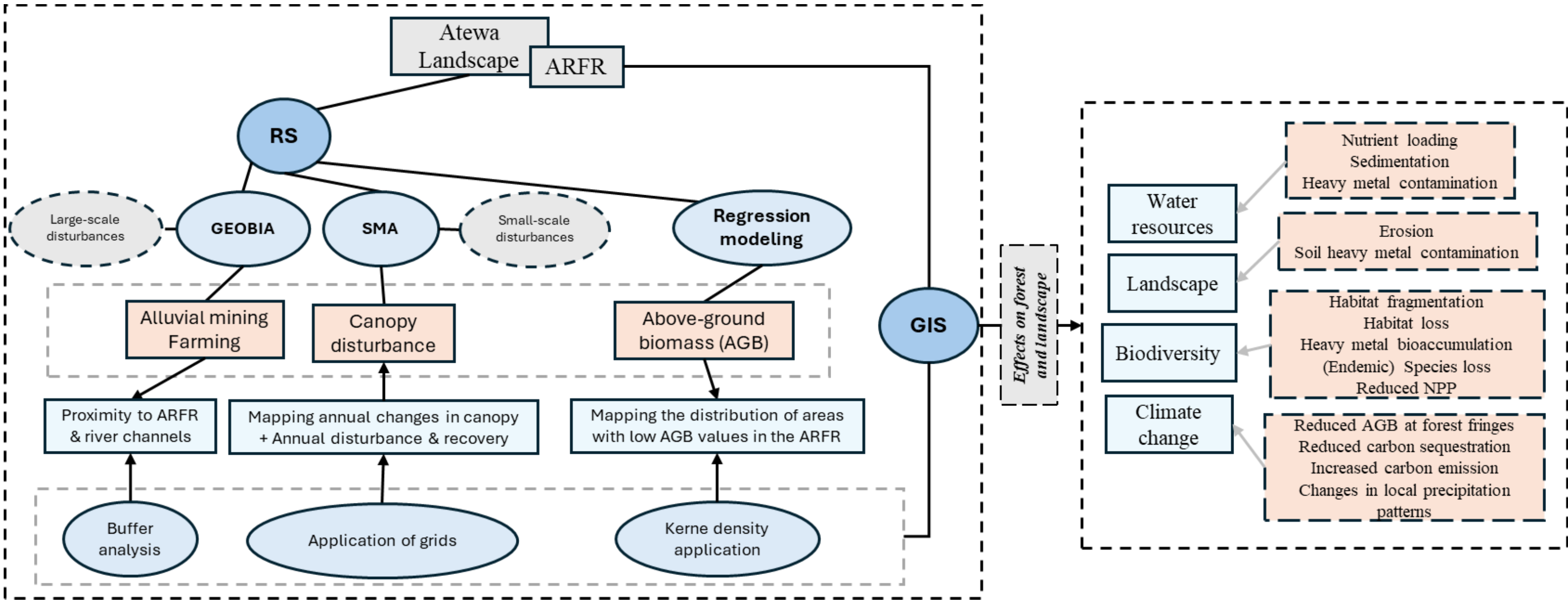

Fig. 5.1. Summary of the application of remote sensing and GIS in assessing human activities in the Atewa landscape and its effects on the environment

5.4 Study limitations and ways forward

The application of optical remote sensing in forest monitoring studies has proven to be crucial in assessing the effects of human activities on forests and the effects on biodiversity and climate change in the grand scheme. The application of optical remote sensing in such studies, however, comes with some constraints. One of the common limitations is the constraint of cloud cover over forested regions, which affects, especially, studies that require annually consistent data for analysis (Whitcraft, 2015). In this regard, the use of Synthetic Aperture Radar (SAR) data has proven to be an effective solution where microwaves actively emitted by SAR sensors penetrate cloud cover, making it ideal for areas that have persistent cloud cover (Ling et al., 2021). However, the suitability of SAR data for the study area is also met with the challenge of the ruggedness of the study area. The ARFR is the dominant highland area within the Atewa landscape as seen in Figure 1.1. The characteristic ruggedness of the terrain is known to reduce the effectiveness of SAR data due to issues of geometric distortions, radiometric calibrations, and speckle noise enhancements, among others (Park, 2015). This made the application of optical remote sensing data ideal for the study area. As such, analysis like the annual dynamics of alluvial mines in the study area (Chapter 2) was affected by the lack of data for the year 2019. Also, the annual consistency in the mapping of small-scale canopy disturbances in the ARFR (Chapter 3) was affected, leading to missing data in 2022. This might have affected the results of the intended annual mappings in small and large-scale degradations. The rugged nature of the terrain not only affected remotely sensed data but also field data collection. This limitation was much apparent in taking tree structural measurements for the calculation of field-observed AGB, where data collection was mostly at areas at low elevation. This biased sampling method introduces the issue of possible underestimation or overestimation of AGB in the high elevation regions of the forest reserve.

Overcoming the challenge of persistent cloud cover in the study area is particularly complex due to the area's rugged topography. To enhance data reliability and continuity, future research should consider integrating optical and SAR remote sensing through data fusion techniques, allowing the complementary strengths of both datasets to be effectively leveraged. To achieve more accurate estimates of AGB in the ARFR, future studies are encouraged to incorporate remotely sensed LiDAR data, particularly from airborne platforms. While satellite-based LiDAR coverage remains limited in the region, airborne LiDAR offers a valuable alternative by significantly reducing the influence of complex topography. Its ability to generate detailed three-dimensional point clouds enables precise characterization of forest structure, thereby enhancing the accuracy of biomass estimation.

Chapter 6

6.1 Conclusions

This study presents an integrated remote sensing and GIS approach in monitoring the Atewa Range Forest Reserve (ARFR), which is a crucial biodiversity hotspot in Ghana. The study proved that the application of high-resolution satellite imagery (4.77 m PlanetScope) through the Geographic Object-based Image Analysis (GEOBIA) increases the mapping accuracy of alluvial mining activities (Chapter 2). The application of GEOBIA was useful in identifying the trends in alluvial mining activities in the ARFR and the Atewa landscape in general where an increasing and irregular trend was observed for the landscape and the ARFR, respectively. An average of 10.8 ha of the ARFR was lost to mining activities annually, mostly contributed by operations in the landscape extending to the fringes of the reserve. Alluvial mining activities typically occurred along the course of river channels with disregard to the Riparian Buffer Zone Policy in Ghana, which is meant to protect the first 100 m of rivers from human activities.

While mining activities, which typically occur at a relatively large scale, are easy to map from satellite images, small-scale disturbances from tree logging and other natural factors, such as windthrows, are difficult to map. Through the application of Spectral Mixture Analysis (SMA), the soil fraction from the ARFR was extracted and used to map annual changes in the canopy structure to identify disturbed areas. This method proved to be effective with accuracies of at least 85%. The results indicated the ARFR undergoes more annual disturbances than recoveries, except in 2024. These disturbances were found to occur mostly at the fringes of the forest reserve, mostly a result of human activities, as inferred from their relationship with topographical factors (elevation, slope, aspect, distance from river channels, and distance from forest edge)

With the annual dynamics of disturbances in the Atewa landscape (small-scale and large-scale) established, the above-ground biomass (AGB) of the ARFR was then estimated to fill the gap of the lack of locally quantified AGB for the biological hotspot because of inadequate and inconsistent forest inventory data. The ARFR recorded a mean value of 124.49 Mg/ha and 92.25 Mg/ha for AGB and carbon accumulation (CAc), respectively. It was however found that, the values of AGB were lowered mostly along the fringes of the reserve which emphasizes the effects of human activities on the fringes of the forest.

The study emphasizes the importance of the application of remote sensing and GIS techniques in monitoring forest disturbances that usually precede deforestation; identifying disturbance sources, topographic factors most susceptible to degradation, and hence deforestation, monitoring the annual spatial changes in the proximity of human activities such as mining, farming, and tree logging to forest and water resources, and applying satellite image-derived vegetation and biophysical indices in estimating forest above-ground biomass (AGB) and the corresponding carbon accumulation.

Acknowledgements

I am grateful to God Almighty for making it possible that I had the strength, the motivation, and the desire to pursue the doctoral program, which I had longed for years. The support from my family cannot be overstated, as their encouragement helped me get through the tough times that usually came with the research. I dedicate this thesis to my late father, Mr. Mohammed Adamu Kwakye Adams, who sacrificed everything to get me a good education to the master's level. It was his dream to see me pursue a PhD one day, and I dedicate this work to him, hoping to make him proud as he rests.

I am very grateful to my supervisor, Assoc. Prof. Yuichi S. Hayakawa at the Faculty of Environmental Earth Science, Hokkaido University. He mentored me throughout this research period while training me on what is relevant, acceptable, ethical, and accurate. I am grateful to him for his support, research-related and career-related, anytime I sought it. He gave me the opportunity to learn about and operate Uncrewed Aerial Vehicles (UAVs), as well as other remote sensing data acquisition methods such as structure from motion (SFM), and LiDAR point cloud data processing. I am very thankful to him.

I want to express my gratitude to members of the Faculty of Environmental Earth Science, Hokkaido University, who contributed to making my research better, especially during seminars and mid-seminar poster presentations. My thanks go to the PhD evaluation committee members, Assoc. Prof. Yuichi S. Hayakawa, Prof. Shiro Tsuyuzaki, Prof. Tomonori Sato, and Assoc. Prof. Takayuki Shiraiwa, for their helpful comments, which helped make my thesis acceptable. I want to thank the Management and Staff of the Atewa Range Forest Reserve (ARFR) for their support during my field data collection. Their guidance and training were crucial in collecting field data the right way. I am also grateful to my friend Mr. Alexander Adjatey for his immense support and assistance during my fieldwork in the ARFR. He made my field experience a great one.

I want to thank Prof. Kingsford Adaboh, Dr. S.S. Koranteng, and Dr. K. Karikari for offering professional and non-professional advice during this period. They have been great pillars in my education and social life, and I cannot thank them enough. I am again grateful to Mr. and Mrs. Adaboh in Tokyo, Japan, for their support throughout my PhD period. I am grateful to my lab members, course mates, and the Ghanaian community in Sapporo for their support.

References

Aabeyir, R., Adu-Bredu, S., Agyare, W. A., & Weir, M. J. (2020). Allometric models for estimating aboveground biomass in the tropical woodlands of Ghana, West Africa. *Forest Ecosystems, 7, 1-23*.

Abbass, K., Qasim, M. Z., Song, H., Murshed, M., Mahmood, H., & Younis, I. (2022). A review of the global climate change impacts, adaptation, and sustainable mitigation measures. *Environmental Science and Pollution Research, 29(28), 42539-42559*.

Adams, J. B. (1993). Imaging spectroscopy: Interpretation based on spectral mixture analysis. *Remote geochemical analysis: Elemental and mineralogical composition, 145-166*.

Adams, J. B., Smith, M. O., & Johnson, P. E. (1986). Spectral mixture modeling: A new analysis of rock and soil types at the Viking Lander 1 site. *Journal of Geophysical Research: Solid Earth, 91(B8), 8098-8112*.

Adams, L., & Hayakawa, Y. (2025). Mapping alluvial mine dynamics in the Atewa landscape in Ghana using Geographic Object-Based Image Analysis (GEOBIA) and GIS. *Environ Monit Assess 197, 473 (2025). https://doi.org/10.1007/s10661-025-13892-z*.

Adedire, M. O. (2002). Environmental implications of tropical deforestation. *The International Journal of Sustainable Development & World Ecology, 9(1)*, 33-40.

Afele, J. T., Nimo, E., Lawal, B., & Afele, I. K. (2022). Deforestation in Ghana: Evidence from selected forest reserves across six ecological zones. *International Journal of Forest, Animal and Fisheries Research, 6(1), 1-7*.

Afum, B. O., & Owusu, C. K. (2016). Heavy metal pollution in the Birim River of Ghana. *International Journal of Environmental Monitoring and Analysis, 4(3), 65-74.*

Aguiar, A. P., G., V. I., Assis, T. O., Dalla-Nora, E. L., Toledo, P. M., Oliveira Santos-Junior, R. A., . . . Ometto, J. P. (2016). Land use change emission scenarios: anticipating a forest transition process in the Brazilian Amazon. *Global change biology, 22(5), 1821-1840*.

Ahmed, A. I., Bryant, R. G., & Edwards, D. P. (2021). Where are mines located in sub Saharan Africa and how have they expanded overtime? *Land Degradation & Development, 32(1), 112-122*.

Ahmed, A. I., Massam, M. R., Bryant, R. G., & Edwards, D. P. (2025). How much deforestation in sub-Saharan Africa has been caused by mining? *Biological Conservation, 304, 111040*.

Akabzaa, T. M. (2001). Boom and dislocation: The environmental and social impacts of mining. *Third World Network*.

Akomaning, Y., Hlavackova, P., Darkwah, S., Zivelova, I., & Sujova, A. (2021). Socioeconomic Impact Of Mining In The Atiwa Forest Reserve Of Ghana On Fringe Communities And The Achievement Of SDGs: Analysis From The Residents' Perspective. *Forests, 12 (10)*, 1395.

Al-Ghussain, L. (2019). Global warming: review on driving forces and mitigation. *Environmental Progress & Sustainable Energy, 38(1), 13-21.*

Alvarez, E., Duque, A., Saldarriaga, J., Cabrera, K., de Las Salas, G., d. V., . . . Rodríguez, L. (2012). Tree above-ground biomass allometries for carbon stocks estimation in the natural forests of Colombia. *Forest Ecology and management, 267, 297-308.*

Alvarez-Berríos, N. L., & Aide, T. M. (2015). Global demand for gold is another threat for tropical forests. *Environmental Research Letters, 10(1), 014006*.

Amponsah, A., Nasare, L. I., Tom-Dery, D., & Baatuuwie, B. N. (2022). Land cover changes of Atewa Range Forest Reserve, a biodiversity hotspot in Ghana. *Trees, Forests and People, 9*, 100301.

Amponsah, E., Halvitigala, D., Hwang, H., & Eves, C. (2023). Compensation for farms compulsorily acquired for mining in Ghana: an analysis of the laws, compensation practices and valuation methods. *Property Management, 41(2), 244-260*.

Amponsah-Tawiah, K., & Dartey-Baah, K. (2011). The mining industry in Ghana: a blessing or a curse. *International Journal of Business and Social Science, 2(12).*

Anand, A. (2022). Sentinel SAR Data and In-Situ-Based High-Resolution Above-Ground Carbon Stocks Estimation Within the Open Forests of Ramgarh District. IGI Global.

Ankomah, F., Kyereh, B., & Ansong, M. A. (2020). Forest management regimes and drivers of forest cover loss in forest reserves in the high forest zone of Ghana. *International journal of forestry research, 2020(1), 8865936*.

Appiah, J. O., Ohene, J. B., & Afram, A. (2013). Effects of mining activities on access to potable water: households' perception and practices at Konongo and Odumasi communities in Ghana. *Civil Environ Res, 12*, 2224-5790.

Appiah, M., Blay, D., Damnyag, L., Dwomoh, F. K., Pappinen, A., & Luukkanen, O. (2009). Dependence on forest resources and tropical deforestation in Ghana. *Environment, Development and Sustainability, 11, 471-487.*

Archer, D., Eby, M., Brovkin, V., Ridgwell, A., Cao, L., Mikolajewicz, U., . . . Tokos, K. (2009). Atmospheric lifetime of fossil fuel carbon dioxide. *Annual review of earth and planetary sciences, 37(1), 117-134*.

Asare, R. A., Asante, W., Tutu, D. B., Malhi, Y., Saatchi, S., & Jengre, N. (2012). The biomass map of Ghana: using carbon maps for REDD+. *Ghana Carbon Map Project. Accra, Ghana: Nature Conservation Research Centre.*

Asenso Barnieh, B., Jia, L., Menenti, M., Zhou, J., & Zeng, Y. (2020). Mapping land use land cover transitions at different spatiotemporal scales in West Africa. *Sustainability, 12(20)*, 8565.

Asiedu, J. B. (2013). Technical report on reclamation of small scale surface mined lands in Ghana: a landscape perspective. *American Journal of Environmental Protection, 1(2)*, 28-33.

Askar, Nuthammachot, N., Phairuang, W., Wicaksono, P., & Sayektiningsih, T. (2018). Estimating Aboveground Biomass on Private Forest Using Sentinel-2 Imagery. *Journal of Sensors, 2018(1), 6745629.*

Asner, G. P., & Tupayachi, R. (2017). Accelerated losses of protected forests from gold mining in the Peruvian Amazon. *Environmental Research Letters, 12(9), 094004*.

Asner, G. P., Keller, M., Pereira Jr, R., & Zweede, J. C. (2002). Remote sensing of selective logging in Amazonia: Assessing limitations based on detailed field observations, Landsat ETM+, and textural analysis. *Remote sensing of environment, 80(3), 483-496*.

Attiogbe, F., & Nkansah, A. (2017). The impact of mining on the water resources in Ghana: Newmont case study at Birim North District (New Abirem). *Energy and Environment Research, 7(2)*, 27-36.

Azis, A., Yusuf, H., Faisal, Z., & Suradi, M. (2015). Water turbidity impact on discharge decrease of groundwater recharge in recharge reservoir. *Procedia Engineering, 125, 199-206*.

Baatz, M. (2000). Multiresolution segmentation: an optimization approach for high quality multi-scale image segmentation. *Angewandte geographische informationsverarbeitung*, 12-23.

Bailey, T. C., & Gatrell, A. C. (1995). Interactive spatial data analysis (Vol. 413, No. 8). *Essex: Longman Scientific & Technical.*

Bansa, D. K., Awua, A. K., Boatin, R., Adom, T., Brown-Appiah, E. C., Amewosina, K. K., & ... Okwabi, W. (2017). Cross-sectional assessment of infants' exposure to toxic metals through breast milk in a prospective cohort study of mining communities in Ghana. *BMC public health, 17, 1-12*.

Bansah, K. J., Sakyi-Addo, G. B., & Dumakor-Dupey, N. K. (2016). POST-MINING RECLAMATION IN ARTISANAL AND SMALL-SCALE MINING.

Barenblitt, A., Payton, D., Lagomasino, L., Fatoyinbo, K., Asare, K., Aidoo, H., . . . Wood, D. (2021). The large footprint of small-scale artisanal gold mining in Ghana. *Science of the Total Environment*, 781, 146644.

Blaschke, T., Hay, G., Kelly, M., Lang, S., Hofmann, P., Addink, E., . . . Tiede, D. (2014). Geographic object-based image analysis–towards a new paradigm. *SPRS journal of photogrammetry and remote sensing, 87*, 180-191.

Boadi, S., Nsor, C. A., Antobre, O. O., & Acquah, E. (2016). An analysis of illegal mining on the Offin shelterbelt forest reserve, Ghana: Implications on community livelihood. *Journal of Sustainable Mining, 15(3)*, 115-119.

Bogoliubova, A., & Tymków, P. (2014). Accuracy assessment of automatic image processing for land cover classification of St. Petersburg protected area. *Acta Scientiarum Polonorum. Geodesia et Descriptio Terrarum, 13(1-2)*.

Bourgoin, C., Ceccherini, G., Girardello, M., Vancutsem, C., Avitabile, V., Beck, P. S., . . . Achard, F. (2024). Human degradation of tropical moist forests is greater than previously estimated. *Nature, 631(8021), 570-576.*

Bradley, S. (2020). Mining's impacts on forests aligning policy and finance for climate and biodiversity goals. *Energy, Environment and resources programme*, 1-29.

Brinck, K., Fischer, R., Groeneveld, J., & et al. (2017). High resolution analysis of tropical forest fragmentation and its impact on the global carbon cycle. *Nat Commun 8, 14855 (2017)*.

Brockerhoff, E. G., Barbaro, L., Castagneyrol, B., Forrester, D. I., Gardiner, B., González-Olabarria, J. R., . . . Thompson, I. (2017). Forest biodiversity, ecosystem functioning and the provision of ecosystem services. *Biodiversity and Conservation, 26(13)*, 3005-3035.

Bruno, D., Ruban, D., Tiess, G., Pirrone, N., Perrotta, P., Mikhailenko, A., . . . Yashalova, N. (2020). Artisanal and small-scale gold mining, meandering tropical rivers, and geological heritage: Evidence from Brazil and Indonesia. *Science of the Total Environment*, 715, 136907.

Bullock, E. L., Woodcock, C. E., & Olofsson, P. (2020). Monitoring tropical forest degradation using spectral unmixing and Landsat time series analysis. *Remote sensing of Environment, 238, 110968*.

Burrow, A., & Maerz, J. (2022). How plants affect amphibian populations. *Biological Reviews, 97(5), 1749-1767*.

Campos, J. J., Alpizar, F., Louman, B., & Parrotta, J. A. (2005). An integrated approach to forest ecosystem services. in Mery, G., Alfaro, R., Kanninen, M. and Lovobikov, M.(Eds.)"Forests in the Global Balance–Changing Paradigms". *Vienna, Austria: International Union of Forest Research Organizations*, 185, 97-116.

Castillo, J. A., Apan, A. A., Maraseni, T. N., & Salmo III, S. G. (2017). Estimation and mapping of above-ground biomass of mangrove forests and their replacement land uses in the Philippines using Sentinel imagery. *ISPRS Journal of Photogrammetry and Remote Sensing, 134, 70-85.*

Chaddad, F., Mello, F. A., Tayebi, M., Safanelli, J. L., Campos, L. R., Amorim, M. T., . . . Demattê, J. A. (2022). Impact of mining-induced deforestation on soil surface temperature and carbon stocks: A case study using remote sensing in the Amazon rainforest. *Journal of South American Earth Sciences, 119, 103983.*

Chave, J., Réjou-Méchain, M., Búrquez, A., Chidumayo, E., Colgan, M. S., Delitti, W. B., . . . Vieilledent, G. (2014). Improved allometric models to estimate the aboveground biomass of tropical trees. *Global change biology, 20(10), 3177-3190*.

Chen, J., Shao, Z., Huang, X., Cai, B., & Zheng, X. (2023). Assessing the impact of floods on vegetation worldwide from a spatiotemporal perspective. *Journal of Hydrology, 622, 129715*.

Chen, K., Cai, Q., Zheng, N., Li, Y., Lin, C., & Li, Y. (2021). Forest carbon sink evaluation–An important contribution for carbon neutrality. *In IOP Conference Series: Earth and Environmental Science (Vol. 811, No. 1, p. 012009)*, IOP Publishing.

Chen, L., Ren, C., Zhang, B., Wang, Z., & Xi, Y. (2018). Estimation of forest above-ground biomass by geographically weighted regression and machine learning with sentinel imagery. *Forests, 9(10), 582.*

Chen, S., Ma, M., Wu, S., Tang, Q., & Wen, Z. (2023). Topography intensifies variations in the effect of human activities on forest NPP across altitude and slope gradients. *Environmental Development, 45, 100826*.

Chlot, S. (2011). Nitrogen effluents from mine sites in northern Sweden: nitrogen transformations and limiting nutrient in receiving waters . *Doctoral dissertation, Luleå tekniska universitet*.

Coakley, G. J. (2003). The mineral industry of Ghana. *US Geological Survey Minerals*.

Congalton, R. G., & Green, K. (2019). *Assessing the accuracy of remotely sensed data: principles and practices.* Assessing the accuracy of remotely sensed data: principles and practices.

Copernicus EU. (2023, September 22). *Copernicus Service catalogue*. Retrieved from Copernicus: https://www.copernicus.eu/en/access-data/copernicus-services-catalogue/fraction-absorbed-photosynthetically-active-radiation-0

da Silva, H. A., & Guimarães, J. R. (2024). Mercury cyanide complexes and their relevance as environmental contaminants. *Chemosphere, 350, 141054*.

Damnyag, L. (2012). Valuation of ecosystem services for assessment of cost of deforestation, and analysis of its drivers with implications for sustainable forest management in Ghana. *Dissertationes Forestales, 142, 588-602.*

Damnyag, L., Saastamoinen, O., Appiah, M., & Pappinen, A. (2012). Role of tenure insecurity in deforestation in Ghana's high forest zone. *Forest Policy and Economics, 14(1), 90-98.*

Dar, S. A., Nabi, M., Dar, S. A., & Ahmad, W. S. (2022). Influence of anthropogenic activities on the diversity of forest ecosystems. *In Towards sustainable natural resources: Monitoring and managing ecosystem biodiversity (pp. 33-49). Cham: Springer International Publishing*.

De Marzo, T., Gasparri, N. I., Lambin, E. F., & Kuemmerle, T. (2022). Agents of forest disturbance in the Argentine dry Chaco. *Remote Sensing, 14(7), 1758.*

de Moura Fernandes, M. R., da Silva, G. F., de Almeida, A. Q., Fernandes, M. M., de Mendonça, A. R., Gonçalves, F. G., . . . Silva, J. P. (2023). Aboveground biomass estimation in dry forest in northeastern Brazil using metrics extracted from sentinel-2 data: Comparing parametric and non-parametric estimation methods. *Advances in Space Research, 72(2), 361-377.*

DeFries, R. S., Field, C. B., Fung, I., Collatz, G. J., & Bounoua, L. (1999). Combining satellite data and biogeochemical models to estimate global effects of human-induced land cover change on carbon emissions and primary productivity. *Global biogeochemical cycles, 13(3), 803-815*.

DeFries, R. S., Rudel, T., Uriarte, M., & Hansen, M. (2010). Deforestation driven by urban population growth and agricultural trade in the twenty-first century. *Nature Geoscience, 3(3)*, 178-181.

Dethier, E., Silman, M., Leiva, J., Alqahtani, S., Fernandez, L., Pauca, P., . . . Lutz, D. (2023). A global rise in alluvial mining increases sediment load in tropical rivers. *Nature, 620(7975), 787-793*.

Djomo, A. N., Ibrahima, A., Saborowski, J., & Gravenhorst, G. (2010). Allometric equations for biomass estimations in Cameroon and pan moist tropical equations including biomass data from Africa. *Forest Ecology and Management, 260(10), 1873-1885.*

Dlamini, L. Z., & Xulu, S. (2019). Monitoring mining disturbance and restoration over RBM site in South Africa using landtrendr algorithm and landsat data. *Sustainability, 11(24), 6916*.

Duncan, A. E., de Vries, N., & Nyarko, K. B. (2018). Assessment of heavy metal pollution in the main Pra River and its tributaries in the Pra Basin of Ghana. *Environmental nanotechnology, monitoring & management, 10*, 264-271.

Elmore, A. J., Mustard, J. F., Manning, S. J., & Lobell, D. B. (2000). Quantifying vegetation change in semiarid environments: precision and accuracy of spectral mixture analysis and the normalized difference vegetation index. *Remote sensing of environment, 73(1), 87-102*.

Eng, L. S., Ismail, R., Hashim, W., & Baharum, A. (2019). The use of VARI, GLI, and VIgreen formulas in detecting vegetation in aerial images. *Int. J. Technol, 10(7), 1385-1394.*

FAO. (2002, September 11-13). Forest degradation and improvement. *In Proceedings of the Second Expert Meeting on Harmonising Forest-Related*.

FAO. (2004). Update of the Global Forest Resources Assessment to 2005 Guidelines for national reporting for FRA 2005. *Forest Resources Assessment WP 82*.

FAO. (2020). Global Forest Resource Assessment 2020: Main Report. *Food and Agriculture Organization of the United Nations*.

FAO. (2024, July 28). *Default values of biomass expansion factors (BEFs)*. Retrieved from https://www.fao.org/4/j2132s/J2132S18.htm

Faria, D., Morante-Filho, J. C., Baumgarten, J., Bovendorp, R. S., Cazetta, E., Gaiotto, F. A., . . . Benchimol, M. (2023). The breakdown of ecosystem functionality driven by deforestation in a global biodiversity hotspot. *Biological Conservation, 283, 110126*.

Feng, Y., Ziegler, A. D., Elsen, P. R., Liu, Y., He, X., Spracklen, D. V., & Zeng, Z. (2021). Upward expansion and acceleration of forest clearance in the mountains of Southeast Asia. *Nature Sustainability, 4(10), 892-899.*

Ferreira, V., Almazán-Gómez, M. Á., Nechifor, V., & Ferrari, E. (2022). The role of the agricultural sector in Ghanaian development: A multiregional SAM-based analysis. *Journal of Economic Structures, 11(1), 6.*

Fianko, Y., & Boadua, A. (2021). Impact of Artisanal and Small-Scale Mining on Water bodies and Treatment: The Case of Birim River Basin in Ghana. *Electronic Thesis and Dissertation Repository.*

Fischer, R., Taubert, F., Müller, M. S., Groeneveld, J., Lehmann, S., Wiegand, T., & Huth, A. (2021). Accelerated forest fragmentation leads to critical increase in tropical forest edge area. *Science advances, 7(37), eabg7012.*

Flores, B. M., Montoya, E., Sakschewski, B., Nascimento, N., Staal, A. B., & Hirota, M. (2024). Critical transitions in the Amazon forest system. *Nature, 626(7999), 555-564.*

Fontúrbel, F. E., Candia, A. B., Malebrán, J., Salazar, D. A., González-Browne, C., & Medel, R. (2015). Meta-analysis of anthropogenic habitat disturbance effects on animal-mediated seed dispersal. *Global Change Biology, 21(11), 3951-3960.*

Forkuor, G., Ullmann, T., & Griesbeck, M. (2020). Mapping and monitoring small-scale mining activities in Ghana using Sentinel-1 Time Series (2015–2019). *Remote Sensing, 12(6), 911.*

Frampton, W. J., Dash, J., Watmough, G., & Milton, E. J. (2013). Evaluating the capabilities of Sentinel-2 for quantitative estimation of biophysical variables in vegetation. *ISPRS journal of photogrammetry and remote sensing, 82, 83-92.*

Gallwey, J., Robiati, C., Coggan, J., Vogt, D., & Eyre, M. (2020). A Sentinel-2 based multispectral convolutional neural network for detecting artisanal small-scale mining in Ghana: Applying deep learning to shallow mining. *Remote Sensing of Environment, 248, 111970.*

García Chevesich, P., Neary, D. G., Scott, D. F., Benyon, R. G., & Reyna, T. (2017). Forest management and the impact on water resources: a review of 13 countries.

Geng, A., Yang, H., Chen, J., & Hong, Y. (2017). Review of carbon storage function of harvested wood products and the potential of wood substitution in greenhouse gas mitigation. *Forest Policy and Economics, 85, 192-200.*

Ghana Forestry Commission. (2018). Framework for National Forest Monitoring System.

Ghana Water Resource Commission. (2021). *State of the water bodies*. Retrieved from Ghana Water Resource Commission: https://wrc-gh.org/dmsdocument/133

Ghazoul, J., Burivalova, Z., Garcia-Ulloa, J., & King, L. A. (2015). Conceptualizing forest degradation. *Trends in ecology & evolution, 30(10), 622-632*.

Gitelson, A. A., Kaufman, Y. J., Stark, R., & Rundquist, D. (2002). Novel algorithms for remote estimation of vegetation fraction. *Remote sensing of Environment, 80(1), 76-87*.

Grecchi, R. C., Beuchle, R., Shimabukuro, Y. E., Aragão, L. E., Arai, E., Simonetti, D., & Achard, F. (2017). An integrated remote sensing and GIS approach for monitoring areas affected by selective logging: A case study in northern Mato Grosso, Brazilian Amazon. *International Journal of Applied Earth Observation and Geoinformation, 61, 70-80*.

Haddad, N. M., Brudvig, L. A., Clobert, J., Davies, K. F., Gonzalez, A., Holt, R. D., . . . Cook, W. (2015). Habitat fragmentation and its lasting impact on Earth's ecosystems. *Science advances, 1(2)*, e1500052.

Hair, J. F. (2009). Multivariate data analysis.

Hamunyela, E., Brandt, P., Shirima, D., Do, H. T., Herold, M., & Roman-Cuesta, R. M. (2020). Space-time detection of deforestation, forest degradation and regeneration in montane forests of Eastern Tanzania. *International Journal of Applied Earth Observation and Geoinformation, 88, 102063*.

Hansen, J. E., Sato, M., Lacis, A., Ruedy, R., Tegen, I., & Matthews, E. (1998). Climate forcings in the industrial era. *Proceedings of the National Academy of Sciences, 95(22), 12753-12758*.

Hansen, M. C., Potapov, P. V., Moore, R., Hancher, M., Turubanova, S. A., Tyukavina, A., . . . Townshend, J. R. (2013). High-resolution global maps of 21st-century forest cover change. *science, 342(6160), 850-853*.

Hartman, H. L. (2002). *Introductory mining engineering.* Wiley.

Heavilin, J., Powell, J. A., & Logan, J. A. (2007). Development and parametrization of a model forbark beetle disturbance in lodgepole forest. *IN: K. Miyanishi and E. Johnson (eds), Plant Disturbance Ecology, Academic Press, NY*, pages 527-553.

Henry, M., Picard, N., Trotta, C., Manlay, R., Valentini, R., Bernoux, M., & Saint André, L. (2011). Estimating tree biomass of sub-Saharan African forests: a review of available allometric equations.

Hilson, G. (2002). The environmental impact of small-scale gold mining in Ghana: identifying problems and possible solutions. *Geographical Journal 168.1 (2002): 57-72*.

Hilson, G. M. (2002). The future of small-scale mining: environmental and socioeconomic perspectives. *Futures, 34(9-10), 863-872*.

Hilson, G., & Nyame, F. (2006). Gold mining in Ghana's forest reserves: A report on the current debate. *Area*, 175-185.

Hlásny, T., Kocický, D., Maretta, M., Sitková, Z., Barka, I., Konôpka, M., & Hlavatá, H. (2015). Effect of deforestation on watershed water balance: Hydrological modelling-based approach. *Lesnicky Casopis, 61(2)*, 89.

Hoekman, D. H., & Reiche, J. (2015). Multi-model radiometric slope correction of SAR images of complex terrain using a two-stage semi-empirical approach. *Remote Sensing of Environment, 156, 1-10*.

Hofmeister, J., Hošek, J., Brabec, M., Střalková, R., Mýlová, P., Bouda, M., . . . Svoboda, M. (2019). Microclimate edge effect in small fragments of temperate forests in the context of climate change. *Forest Ecology and Management, 448, 48-56*.

Hojo, A., Avtar, R., Nakaji, T., Tadono, T., & Takagi, K. (2023). Modeling forest above-ground biomass using freely available satellite and multisource datasets. *Ecological Informatics, 74, 101973*.

Hosonuma, N., Herold, M., De Sy, V., De Fries, R., Brockhaus, M., Verchot, L., . . . Romijn, E. (2012). An assessment of deforestation and forest degradation drivers in developing countries. *Environmental Research Letters, 7(4)*, 044009.

Huang, W., Sun, G., Dubayah, R., Cook, B., Montesano, P., Ni, W., & Zhang, Z. (2013). Mapping biomass change after forest disturbance: Applying LiDAR footprint-derived models at key map scales. *Remote Sensing of Environment, 134, 319-332*.

Hurteau, M. D. (2021). The role of forests in the carbon cycle and in climate change. *In Climate change (pp. 561-579). Elsevier*.

Ibrahim, E., Lema, L., Barnabé, P., Lacroix, P., & Pirard, E. (2020). Small-scale surface mining of gold placers: Detection, mapping, and temporal analysis through the use of free satellite imagery. *International Journal of Applied Earth Observation and Geoinformation, 93, 102194.*

IPCC. (2006). IPCC guidelines for national greenhouse gas inventories.

Isbell, F., Gonzalez, A., Loreau, M., Cowles, J., Díaz, S., Hector, A., . . . Larigauderie, A. (2017). Linking the influence and dependence of people on biodiversity across scales. *Nature, 546(7656), 65-72*.

IUCN (2016). The Economics of the Atewa Forest Range, Ghana. *IUCN.*

IUCN. (2023, July 28). *The impact of bauxite mining in Ghana's Atewa Forest*. Retrieved from IUCN: https://www.iucn.nl/en/story/the-impact-of-bauxite-mining-in-ghanas-atewa-forest/

IUCN. (2024, November Thursday). *Mining's impact on forests: a growing threat to biodiversity and climate*. Retrieved from IUCN: https://www.iucn.nl/en/news/minings-impact-on-forests-a-growing-threat-to-biodiversity-and-climate/#:~:text=Ghana's%20forests%20are%20under%20immense,both%20human%20health%20and%20ecosystems.

Jiao, J., Zou, H., Jia, Y., & Wang, N. (2009). Research progress on the effects of soil erosion on vegetation. *Acta Ecologica Sinica, 29(2), 85-91*.

Johnson, C. A. (2015). The fate of cyanide in leach wastes at gold mines: An environmental perspective. *Applied geochemistry, 57, 194-205*.

Kahhat, R., Parodi, E., Larrea-Gallegos, G., Mesta, C., & Vázquez-Rowe, I. (2019). Environmental impacts of the life cycle of alluvial gold mining in the Peruvian Amazon rainforest. *Science of the Total Environment, 662, 940-951*.

Kalinaki, K., Malik, O. A., & Lai, D. T. (2023). FCD-AttResU-Net: An improved forest change detection in Sentinel-2 satellite images using attention residual U-Net. *International Journal of Applied Earth Observation and Geoinformation, 122, 103453*.

Kamenova, I., & Dimitrov, P. (2021). Evaluation of Sentinel-2 vegetation indices for prediction of LAI, fAPAR and fCover of winter wheat in Bulgaria. *European Journal of Remote Sensing, 54(sup1), 89-108.*

Kan, Z., Kwan, P., M., & Tang, L. (2022). Ripley's K-function for network-constrained flow data. *Geographical Analysis, 54(4)*, 769-788.

Kane, J., & Kolb, T. (2014). Short- and long-term growth characteristics associated with tree mortality in southwestern mixed-conifer forests. *Canadian Journal of Forest Research. 44(10): 1227-1235. https://doi.org/10.1139/cjfr-2014-0186*.

Kenderes, K., Aszalós, R., Ruff, J., Barton, Z., & Standovár, T. (2007). Effects of topography and tree stand characteristics on susceptibility of forests to natural disturbances (ice and wind) in the Börzsöny Mountains (Hungary). *Community Ecology, 8(2), 209-220*.

Kowal, S., Gough, W. A., & Butler, K. (2023). Temporal and Spatial Evolution of Seasonal Sea Ice of Arctic Bay, Nunavut. *Coasts, 3(2), 113-124*.

Kronseder, K., Ballhorn, U., Böhm, V., & Siegert, F. (2012). Above ground biomass estimation across forest types at different degradation levels in Central Kalimantan using LiDAR data. *International Journal of Applied Earth Observation and Geoinformation, 18, 37-48*.

Kucharczyk, M., Hay, G. J., Ghaffarian, S., & Hugenholtz, C. H. (2020). Geographic object-based image analysis: a primer and future directions. *Remote Sensing, 12(12)*.

Kumah, D., & Nyarko, E. A. (2018). Gold mining and its effects through the lens of an archaeologist: Experiences from the Prestea area, South Western Ghana. *West African Journal of Applied Ecology, 26, 133-148.*

Kumi-Boateng, B., & Stemn, E. (2020). Spatial analysis of artisanal and small-scale mining in the Tarkwa-Nsuaem Municipality of Ghana. *Ghana Mining Journal, 20(1), 66-74*.

Kusimi, J. M. (2015). Characterizing land disturbance in Atewa range forest reserve and buffer zone. *Land Use Policy, 49, 471-482*.

Lapola, D. M., Pinho, P., Barlow, J., Aragão, L. E., Berenguer, E., Carmenta, R., . . . Walker, W. S. (2023). The drivers and impacts of Amazon forest degradation. *Science, 379(6630), eabp8622.*

Lashof, D. A., & Ahuja, D. R. (1990). Relative contributions of greenhouse gas emissions to global warming. *Nature, 344(6266), 529-531*.

Laurance, W. F. (2004). Forest-climate interactions in fragmented tropical landscapes. *Philosophical Transactions of the Royal Society of London. Series B: Biological Sciences, 359(1443), 345-352*.

Leidinger, J., Blaschke, M., Ehrhardt, M., Fischer, A., Gossner, M. M., Jung, K., . . . Weisser, W. W. (2021). Shifting tree species composition affects biodiversity of multiple taxa in Central European forests. *Forest Ecology and Management, 498, 119552*.

Leon, M., Cornejo, G., Calderón, M., González-Carrión, E., & Florez, H. (2022). Effect of Deforestation on Climate Change: A Co-Integration and Causality Approach with Time Series. *Sustainability, 14(18)*, 11303.

Lestari, L., Kusuma, G. J., Badhurahman, A., Dwiki, S., & Gautama, R. S. (2023). Mine void identification using Object-based Image Analysis (OBIA) of satellite imagery Sentinel 2 data. *ournal of Degraded & Mining Lands Management, 10(2)*.

Li, C., Zhou, L., & Xu, W. (2021). Estimating aboveground biomass using Sentinel-2 MSI data and ensemble algorithms for grassland in the Shengjin Lake Wetland, China. *Remote Sensing, 13(8), 1595*.

Li, X. Y., & Chen, X. (2023). New Insights into Urbanization Based on Global Mapping and Analysis of Human Settlements in the Rural–Urban Continuum. *Land, 12(8), 1607.*

Li, Y., Brando, P. M., Morton, D. C., Lawrence, D. M., Yang, H., & Randerson, J. T. (2022). Deforestation-induced climate change reduces carbon storage in remaining tropical forests. *Nature communications, 13(1), 1964.*

Ling, J., Zhang, H., & Lin, Y. (2021). Improving urban land cover classification in cloud-prone areas with polarimetric SAR images. *Remote Sensing, 13(22), 4708*.

Ling, Y., Teng, S., Liu, C., Dash, J., Morris, H., & Pastor-Guzman, J. (2022). Assessing the accuracy of forest phenological extraction from Sentinel-1 C-band backscatter measurements in deciduous and coniferous forests. *Remote Sensing, 14(3), 674.*

Liu, P., Ren, C., Yang, X., Wang, Z., Jia, M., Zhao, C., . . . Ren, H. (2024). Combining Sentinel-2 and diverse environmental data largely improved aboveground biomass estimation in China's boreal forests. *Scientific Reports, 14(1), 27528.*

Loew, A., & Mauser, W. (2007). Generation of geometrically and radiometrically terrain corrected SAR image products. *Remote Sensing of Environment, 106(3), 337-349*.

Logan, J. A., & Powell, J. A. (2001). Ghost forests, global warming, and the mountain pine beetle (Coleoptera: Scolytidae). *American Entomologist, 47(3), 160-173*.

Luethje, F., Kranz, O., & Schoepfer, E. (2014). Geographic object-based image analysis using optical satellite imagery and GIS data for the detection of mining sites in the Democratic Republic of the Congo. *Remote Sensing, 6(7), 6636-6661*.

Mahalik, G., & Satapathy, K. B. (2016). Environmental impacts of mining on biodiversity of Angul-Talcher open mining site, Odisha, India. *Schol Acad J Biosci, 4(3A)*, 224-227.

Malhi, R. K., Anand, A., Srivastava, P. K., Chaudhary, S. K., Pandey, M. K., Behera, M. D., . . . Kiran, G. S. (2022). Synergistic evaluation of Sentinel 1 and 2 for biomass estimation in a tropical forest of India. *Advances in Space Research, 69(4), 1752-1767.*

Manandhar, R., Odeh, I. O., & Ancev, T. (2009). Improving the accuracy of land use and land cover classification of Landsat data using post-classification enhancement. *Remote Sensing, 1(3), 330-344.*

Marcone, A., Impollonia, G., Croci, M., Blandinières, H., & Amaducci, S. (2024). Estimation of above ground biomass, biophysical and quality parameters of spinach (Spinacia Oleracea L.) using Sentinel-2 to support the supply chain. *Scientia Horticulturae, 325, 112641*.

Måren, I. E., Karki, S., Prajapati, C., Yadav, R. K., & Shrestha, B. B. (2015). Facing north or south: Does slope aspect impact forest stand characteristics and soil properties in a semiarid trans-Himalayan valley? *Journal of arid environments, 121, 112-123*.

Masuda, Y., Castro, B., Aggraeni, I., Wolff, N., Ebi, K., Garg, T., . . . Spector, J. (2019). How are healthy, working populations affected by increasing temperatures in the tropics? Implications for climate change adaptation policies. *Global environmental change*, 56, 29-40.

Mati, B. M., Mutie, S., Gadain, H., Home, P., & Mtalo, F. (2008). Impacts of land-use/cover changes on the hydrology of the transboundary Mara River, Kenya/Tanzania. *Lakes & Reservoirs: Research & Management, 13(2)*, 169-177.

Mayani-Parás, F., Botello, F., Castañeda, S., & Sánchez-Cordero, V. (2019). Impact of habitat loss and mining on the distribution of endemic species of amphibians and reptiles in Mexico. . *Diversity, 11(11)*, 210.

McCullough, J., Alonso, E., Naskrecki, P., Wright, E., & Osei-Owusu, Y. (2007). An Ecological And Conservation Overview Of The Atiwa Range Forest Reserve, Ghana. *Conservation International, Center For Applied Biodiversity Science*, Available Online: https://bit.ly/2GP2jW1 (ACCESSED ON MAY 18, 2021).

Mchunu, C., & Chaplot, V. (2012). Land degradation impact on soil carbon losses through water erosion and CO2 emissions. *Geoderma, 177, 72-79*.

Meißner, S. (2021). The impact of metal mining on global water stress and regional carrying capacities—a GIS-based water impact assessment. *Resources, 10(12), 120*.

Meyer, V., Saatchi, S., Ferraz, A., Xu, L., Duque, A., García, M., & Chave, J. (2019). Forest degradation and biomass loss along the Chocó region of Colombia. *Carbon balance and management, 14, 1-15*.

Michel, D., Eriksson, M., & Klimes, M. (2021). Climate change and (in) security in transboundary river basins. In *In Handbook of Security and the Environment* (pp. (pp. 62-75)). Edward Elgar Publishing.

Minerals Commission. (2015, November). *Artisanal and small scale mining (ASM) framework*. Retrieved from MOFEP: https://www.mofep.gov.gh/sites/default/files/reports/ec

Ministry of Lands and Natural Resources. (2012). Ghana investment plan for the forest investment program (FIP). *Ministry of Lands and Natural Resources*. Retrieved from Forestry Commission.

Ministry of water resources, w. a. (2013). Riparian buffer zone policy for managing freshwater bodies in Ghana.

Mitchell, A. L., Rosenqvist, A., & Mora, B. (2017). Current remote sensing approaches to monitoring forest degradation in support of countries measurement, reporting and verification (MRV) systems for REDD+. *Carbon balance and management, 12(1)*, 1-22.

MOFA. (2024, February 7). *Eastern Region*. Retrieved from Ministry of Food and Agriculture - Republic of Ghana: https://mofa.gov.gh/site/directorates/47-regional-directorates/eastern-region/83-eastern-region

Mollicone, D., Achard, F., Federici, S., Eva, H. D., Grassi, G., Belward, A., . . . Schulze, E. D. (2007). An incentive mechanism for reducing emissions from conversion of intact and non-intact forests. *Climatic change, 83, 477-493.*

Molnár, T., & Király, G. (2024). Forest Disturbance Monitoring Using Cloud-Based Sentinel-2 Satellite Imagery and Machine Learning. *Journal of Imaging, 10(1), 14*.

Mon, M. S., Mizoue, N., Htun, N. Z., Kajisa, T., & Yoshida, S. (2012). Factors affecting deforestation and forest degradation in selectively logged production forest: A case study in Myanmar. *Forest Ecology and Management, 267, 190-198*.

Moomen, A. W., Lacroix, P., Benvenuti, A., Planque, M., Piller, T., Davis, K., . . . Giuliani, G. (2022). Assessing the Applications of Earth Observation Data for Monitoring Artisanal and Small-Scale Gold Mining (ASGM) in Developing Countries. *Remote Sensing*, 14(13), 2971.

Motohka, T., Nasahara, K. N., Oguma, H., & Tsuchida, S. (2010). Applicability of green-red vegetation index for remote sensing of vegetation phenology. *Remote Sensing, 2(10), 2369-2387.*

Mufungizi, I. (2024). Remote sensing for environmental monitoring and remediation of areas degraded by mining activities in the Democratic Republic of Congo: Call for action.

Muhe, S., & Argaw, M. (2022). Estimation of above-ground biomass in tropical afro-montane forest using Sentinel-2 derived indices. *Environmental Systems Research, 11(1), 5.*

Mullu, D. (2016). A review on the effect of habitat fragmentation on ecosystem. *Journal of Natural Sciences Research, 6(15), 1-15.*, 1-15.

Murdiyarso, D., Hergoualc'h, K., & Verchot, L. V. (2010). Opportunities for reducing greenhouse gas emissions in tropical peatlands. *Proceedings of the National Academy of Sciences, 107(46), 19655-19660.*

Muruganandam, M., Rajamanickam, S., Sivarethinamohan, S., Gaddam, M. K., Velusamy, P., Gomathi, R., . . . Muniasamy, S. K. (2023). Impact of climate change and anthropogenic activities on aquatic ecosystem–A review. *Environmental Research, 238, 117233*.

Mutanga, O., & Skidmore, A. K. (2004). Narrow band vegetation indices overcome the saturation problem in biomass estimation. *nternational journal of remote sensing, 25(19), 3999-4014*.

Nagel, T. A., Mikac, S., Dolinar, M., Klopcic, M., Keren, S., Svoboda, M., . . . Paulic, V. (2017). The natural disturbance regime in forests of the Dinaric Mountains: A synthesis of evidence. *Forest Ecology and Management, 388, 29-42*.

Nascimento, F. S., Gastauer, M., Souza-Filho, P. W., Nascimento Jr, W. R., Santos, D. C., & Costa, M. F. (2020). and cover changes in open-cast mining complexes based on high-resolution remote sensing data. *Remote Sensing*, 12(4), 611.

National Geographic. (2024, April 4). *Earth's Changing Climate*. Retrieved from National Geographic: https://education.nationalgeographic.org/resource/earths-changing-climate/

National REDD+ Secretariat, & Forestry Commission. (2017). Ghana's National Forest Reference Level.

Nogueira Jr, L. R., de Moraes Gonçalves, J. L., Engel, V. L., & Parrotta, J. (2011). Soil dynamics and carbon stocks 10 years after restoration of degraded land using Atlantic Forest tree species. *Forest systems, 20(3), 536-545*.

Nunes, M., Vaz, M., Camargo, J., et al. (2023). Edge effects on tree architecture exacerbate biomass loss of fragmented Amazonian forests. *Nat Commun 14, 8129 (2023)*.

Nyamekye, C., Ghansah, B., Agyapong, E., & Kwofie, S. (2021). Mapping changes in artisanal and small-scale mining (asm) landscape using machine and deep learning algorithms.-a proxy evaluation of the 2017 ban on asm in ghana. *Environmental Challenges*, 3, 100053.

Okyere, M., Ayitey, J. Z., & Ajabuin, B. A. (2021). Large scale mining in Ghana: a review of the implications on the host communities. *Journal of Degraded and Mining Lands Management, 9(1)*, 3193.

Orleans-Boham, H., Sakyi-Addo, G. B., Tahiru, A., & Amankwah, R. K. (2020). Women in artisanal mining: Reflections on the impacts of a ban on operations in Ghana. *The Extractive Industries and Society, 7(2), 583-586.*

Owusu-Prempeh, N., Awuah, K. O., Abebrese, I. K., & Amaning, E. N. (2022). Analysis of the status and ecological risks of heavy metals contamination in artisanal and small-scale gold mine-spoils at the Atewa Forest Landscape, Ghana. *Scientific African, 16, e01235*.

Pacheco-Angulo, C., Plata-Rocha, W., Serrano, J., Vilanova, E., Monjardin-Armenta, S., González, A., & Camargo, C. (2021). A low-cost and robust landsat-based approach to study forest degradation and carbon emissions from selective logging in the Venezuelan Amazon. *Remote Sensing, 13(8), 1435*.

Pacheco-Pascagaza, A. M., Gou, Y., Louis, V., Roberts, J. F., Rodríguez-Veiga, P., da Conceição Bispo, P., . . . Balzter, H. (2022). Near real-time change detection system using Sentinel-

2 and machine learning: A test for Mexican and Colombian forests. *Remote Sensing, 14(3), 707*.

Paine, C. T., Marthews, T. R., Vogt, D. R., Purves, D., Rees, M., Hector, A., & Turnbull, L. A. (2012). How to fit nonlinear plant growth models and calculate growth rates: an update for ecologists. *Methods in Ecology and Evolution, 3(2), 245-256*.

Pan, Y., Birdsey, R. A., Fang, J., Houghton, R., Kauppi, P. E., Kurz, W. A., . . . Hayes, D. (2011). A large and persistent carbon sink in the world's forests. *science, 333(6045), 988-993.*

Pandey, S., Kumari, N., & Al Nawajish, S. (2023). Land use land cover (LULC) and surface water quality assessment in and around selected dams of Jharkhand using water quality index (WQI) and Geographic Information System (GIS). *ournal of the Geological Society of India, 99(2), 205-218.*

Pandit, S., Tsuyuki, S., & Dube, T. (2018). Estimating above-ground biomass in sub-tropical buffer zone community forests, Nepal, using Sentinel 2 data. *Remote Sensing, 10(4), 601.*

Park, S. E. (2015). The effect of topography on target decomposition of polarimetric SAR data. *Remote Sensing, 7(5), 4997-5011*.

Patel, N. R., Saha, S. K., & Dadhwal, V. K. (2007). nvestigating the vegetation and agricultural responses to El Nino/Southern Oscillation using AVHRR data. *Geocarto International, 22(4),*

Penman, J., Gytarsky, M., Hiraishi, T., Krug, T., Kruger, D., Pipatti, R., . . . Wagner, F. (2003). Definitions and methodological options to inventory emissions from direct human-induced degradation of forests and devegetation of other vegetation types. *Hayama Kanagawa: IPCC National Greenhouse Gas Inventories Programme-Technical Support Unit*, http://www. ipcc-nggip. iges. or. jp, 32.

Peterson, G. D., & Heemskerk, M. (2001). Deforestation and forest regeneration following small-scale gold mining in the Amazon: the case of Suriname. *Environmental Conservation, 28(2), 117-126.*

Pfeifer, M., Lefebvre, V., Peres, C. A., Banks-Leite, C., Wearn, O. R., Marsh, C. J., … Ewers, R. M. (2017). Creation of forest edges has a global impact on forest vertebrates. *Nature, 551(7679), 187-191*.

Planet. (2023, January 4). Retrieved from https://www.planet.com/explorer

Poorter, L., van der Sande, M. T., Arets, E. J., Ascarrunz, N., Enquist, B. J., Finegan, B., . . . Peña-Claros, M. (2017). Biodiversity and climate determine the functioning of Neotropical forests. *Global ecology and biogeography, 26(12), 1423-1434*.

Poorter, L., van der Sande, M. T., Thompson, J., Arets, E. J., Alarcón, A., Álvarez-Sánchez, J., . . . Peña-Claros, M. (2015). Diversity enhances carbon storage in tropical forests. *Global Ecology and Biogeography, 24(11), 1314-1328*.

Potapov, P. V., Turubanova, S. A., Hansen, M. C., Adusei, B., Broich, M., Altstatt, A.,… Justice, C. O. (2012). Quantifying forest cover loss in Democratic Republic of the Congo, 2000–2010, with Landsat ETM+ data. *Remote Sensing of Environment, 122, 106-116*.

Purwins, S. (2022). Bauxite mining at Atewa Forest Reserve, Ghana: a political ecology of a conservation-exploitation conflict. *GeoJournal, 87(2), 1085-1097*.

Quash, Y., Kross, A., & Jaeger, J. A. (2024). Assessing the impact of gold mining on forest cover in the Surinamese Amazon from 1997 to 2019: A semi-automated satellite-based approach. *Ecological Informatics, 80, 102442*.

Radoux, J., & Bogaert, P. (2017). Good practices for object-based accuracy assessment. *Remote Sensing, 9(7)*, 646.

Radwan, T. M., Blackburn, G. A., Whyatt, J. D., & Atkinson, P. M. (2021). Global land cover trajectories and transitions. *Scientific Reports 11, no. 1*, 12814.

Rajora, O. P., & Mosseler, A. (2001). Challenges and opportunities for conservation of forest genetic resources. *Euphytica, 118, 197-212*.

Reiche, J., Lucas, R., Mitchell, A. L., Verbesselt, J., Hoekman, D. H., Haarpaintner, J., . . . Herold, M. (2016). Combining satellite data for better tropical forest monitoring. *Nature Climate Change, 6(2), 120-122*.

Ripley, B. D. (1977). Modelling spatial patterns. *Journal of the Royal Statistical Society: Series B (Methodological), 39(2)*, 172-192.

Roach, K. A., Jacobsen, N. F., Fiorello, C. V., Stronza, A., & Winemiller, K. O. (2013). Gold mining and mercury bioaccumulation in a floodplain lake and main channel of the Tambopata River, Peru.

Ruppen, D., Runnalls, J., Tshimanga, R. M., Wehrli, B., & Odermatt, D. (2023). Optical remote sensing of large-scale water pollution in Angola and DR Congo caused by the Catoca mine tailings spill. *International Journal of Applied Earth Observation and Geoinformation, 118, 103237*.

Sakyi, E., & Ameko, S. (2025). Adverse Effects of Human Activities on Forest Reserves in Ghana: Lessons of Experience from the Yenku Forest Reserve in the Central Region. *American Journal of Environment and Climate, 4(1), 52–63*.

Sano, E. E., Rizzoli, P., Koyama, C. N., Watanabe, M., Adami, M., Shimabukuro, Y. E., . . . Freitas, D. M. (2021). Comparative analysis of the global forest/non-forest maps derived from SAR and optical sensors. Case studies from Brazilian Amazon and Cerrado biomes. *Remote Sensing, 13(3), 367*.

Schröder, T., & Fleig, F. D. (2017). Spatial patterns and edge effects on soil organic matter and nutrients in a forest fragment of southern Brazil. *Soil research, 55(7), 649-656*.

Schulze, R. E., & McGee, O. S. (1978). Climatic indices and classifications in relation to the biogeography of southern Africa. *In Biogeography and ecology of southern Africa (pp. 19-52). Dordrecht: Springer Netherlands*.

Schwartz, F. W., Lee, S., & Darrah, T. H. (2021). A review of the scope of artisanal and small-scale mining worldwide, poverty, and the associated health impacts. *GeoHealth, 5(1), e2020GH000325*.

Shen, W., Li, M., Huang, C., & Wei, A. (2016). Quantifying live aboveground biomass and forest disturbance of mountainous natural and plantation forests in Northern Guangdong, China, based on multi-temporal Landsat, PALSAR and field plot data. *Remote sensing, 8(7), 595*.

Shimabukuro, Y. E., Arai, E., Duarte, V., Jorge, A., Santos, E. G., Gasparini, K. A., & Dutra, A. C. (2019). Monitoring deforestation and forest degradation using multi-temporal fraction images derived from Landsat sensor data in the Brazilian Amazon. *International Journal of Remote Sensing, 40(14), 5475-5496*.

Shimizu, K., Ota, T., Mizoue, N., & Yoshida, S. (2019). A comprehensive evaluation of disturbance agent classification approaches: Strengths of ensemble classification, multiple indices, spatio-temporal variables, and direct prediction. *ISPRS Journal of Photogrammetry and Remote Sensing, 158, 99-112.*

Simionato, J., Bertani, G., & Osako, L. S. (2021). Identification of artisanal mining sites in the Amazon rainforest using geographic object-based image analysis (GEOBIA) and data mining techniques. *Remote Sensing Applications: Society and Environment*, 24, 100633.

Simula, M., & Mansur, E. (2011). A global challenge needing local response. *Unasylva, 62(238), 3-7*.

Singh, S. H. (2018). Understanding the role of slope aspect in shaping the vegetation attributes and soil properties in Montane ecosystems. *Tropical Ecology, 59(3), 417-430*.

Siqueira-Gay, J., Sonter, L. J., & Sánchez, L. E. (2020). Exploring potential impacts of mining on forest loss and fragmentation within a biodiverse region of Brazil's northeastern Amazon. *Resources Policy, 67, 101662*.

Skeie, R. B., Fuglestvedt, J., Berntsen, T., Peters, G. P., Andrew, R., Allen, M., & Kallbekken, S. (2017). Perspective has a strong effect on the calculation of historical contributions to global warming. *Environmental Research Letters, 12(2), 024022.*

Slagter, B., Reiche, J., Marcos, D., Mullissa, A., Lossou, E., Peña-Claros, & M., H. M. (2023). Monitoring direct drivers of small-scale tropical forest disturbance in near real-time with Sentinel-1 and-2 data. *Remote Sensing of Environment, 295, 113655.*

Song, C. (2005). Spectral mixture analysis for subpixel vegetation fractions in the urban environment: How to incorporate endmember variability? *Remote sensing of environment, 95(2), 248-263*.

Song, J., Tong, G., Chao, J., Chung, J., Zhang, M., Lin, W., . . . Zhu, W. (2023). Data driven pathway analysis and forecast of global warming and sea level rise. *Scientific Reports, 13(1), 5536.*

Sonter, L. J., Herrera, D., Barrett, D. J., Galford, G. L., Moran, C. J., & Soares-Filho, B. S. (2017). Mining drives extensive deforestation in the Brazilian Amazon. *Nature communications, 8(1), 1013*.

Souza Jr, C. (2013). Monitoring of forest degradation: a review of methods in the Amazon Basin. *Global Forest Monitoring from Earth Observation; Archard, F., Hansen, MC, Eds, 171-194*.

Souza Jr, C. M., Roberts, D. A., & Cochrane, M. A. (2005). Combining spectral and spatial information to map canopy damage from selective logging and forest fires. *Remote Sensing of Environment, 98(2-3), 329-343.*

Stips, A., Macias, D., Coughlan, C., Garcia-Gorriz, E., & Liang, X. S. (2016). On the causal structure between CO2 and global temperature. *Scientific reports, 6(1), 21691*.

Stratford, J. A., & Stouffer, P. C. (2015). Forest fragmentation alters microhabitat availability for Neotropical terrestrial insectivorous birds. *Biological Conservation, 188, 109-115*.

Streck, N. A., Rundquist, D., & Connot, J. (2002). Estimating residual wheat dry matter from remote sensing measurements. *Photogrammetric Engineering and Remote Sensing, 68(11), 1193-1202*.

Stritih, A., Senf, C., Seidl, R., Grêt-Regamey, A., & Bebi, P. (2021). The impact of land-use legacies and recent management on natural disturbance susceptibility in mountain forests. *Forest Ecology and Management, 484, 118950*.

Suardana, A. M., Anggraini, N., Nandika, M. R., Aziz, K., As-Syakur, A. R., Ulfa, A., . . . Dewanti, R. (2023). Estimation and mapping above-ground mangrove carbon stock using sentinel-2 data derived vegetation indices in Benoa Bay of Bali Province, Indonesia. *Forest and Society, 7(1), 116-134.*

Tadese, S., Soromessa, T., Bekele, T., Bereta, A., & Temesgen, F. (2019). Above Ground Biomass Estimation Methods and Challenges: A Review. *measurement, 9(8)*.

Tenkorang, E. Y. (2021). Illegal Small-Scale Mining in Asutifi North District, Ghana: Traditional Authority's Tacit Support for an Illegality. . *African Social Science Review, 11(1),7*.

Tetteh, E. (2010). Evaluation of land Reclamation practices at AngloGold Ashanti; Iduapriem Mines Ltd, Tarkwa. *MSc Thesis. Kwame Nkrumah University of Science and*.

The Ghana Chamber of Mines. (2019). Performance of The Mining Industry In 2019. *Ghana Chamber of Mines*.

The World Bank, & PROFOR, (. o. (2020, September 6). *Extractive Industries in Forest Landscapes: Balancing the Trade-offs and maximizing the benefits*. Retrieved from PROFOR: https://www.profor.info/knowledge/extractive-industries-forest-landscapes-balancing-trade-offs-and-maximizing-benefits

Tian, N., Poudyal, N. C., Hodges, D. G., Young, T. M., & Hoyt, K. P. (2015). Understanding the factors influencing nonindustrial private forest landowner interest in supplying ecosystem services in Cumberland Plateau, Tennessee. *Forests, 6(11)*, 3985-4000.

Tonyaloğlu, E. E., Erdogan, N., Çavdar, B., Kurtşan, K., & Nurlu, E. (2021). Comparison of Pixel and Object Based Classification Methods on Rapideye Satellite Image. *Turkish Journal of Forest Science, 5(1)*, 1-11.

Tsai, Y. H., Stow, D. A., López-Carr, D., Weeks, J. R., Clarke, K. C., & Mensah, F. (2019). Monitoring forest cover change within different reserve types in southern Ghana. *Environmental Monitoring and Assessment, 191, 1-15*.

Veiga, M. M., Silva, A. R., & Hinton, J. J. (2002). O garimpo de ouro na Amazônia: aspectos tecnológicos, ambientais e sociais. *CETEM/MCT*.

Verrelst, J., Schaepman, M. E., Koetz, B., & Kneubühler, M. (2008). Angular sensitivity analysis of vegetation indices derived from CHRIS/PROBA data. *Remote Sensing of Environment, 112(5), 2341-2353.*

Wahlang, R., & Chaturvedi, S. S. (2020). Relationship Between Above-Ground Biomass and Different Vegetation Indices of Forests of Ri-Bhoi District, Meghalaya, India. *Int. J. Eng. Tech. Res, 9.*

Wang, J., Xiao, X., Bajgain, R., Starks, P., Steiner, J., Doughty, R. B., & Chang, Q. (2019). Estimating leaf area index and aboveground biomass of grazing pastures using Sentinel-1, Sentinel-2 and Landsat images. *ISPRS Journal of Photogrammetry and Remote Sensing, 154, 189-201*.

Watrin, O. D., & da ROCHA, A. M. (1992). Levantamento da vegetação natural e do uso da terra no município de Paragominas (PA) utilizando imagens TM/LANDSA.

Whitcraft, A. K., Vermote, E. F., Becker-Reshef, I., & Justice, C. O. (2015). Cloud cover throughout the agricultural growing season: Impacts on passive optical earth observations. *Remote sensing of Environment, 156, 438-447*.

Whitehead, D. (2011). Forests as carbon sinks—benefits and consequences. *Tree physiology, 31(9), 893-902*.

Whiteside, T. G., Boggs, G. S., & Maier, S. W. (2011). Comparing object-based and pixel-based classifications for mapping savannas. *International Journal of Applied Earth Observation and Geoinformation*, 13(6), 884-893.

WHO. (2004). Guidelines for drinking-water quality. *WHO chronicle, 38(4), 104-8*.

Xu, H. J., Zhao, C. Y., & Wang, X. P. (2020). Elevational differences in the net primary productivity response to climate constraints in a dryland mountain ecosystem of northwestern China. *Land Degradation & Development, 31(15), 2087-2103*.

Yiridoe, E. K., & Nanang, D. M. (2001). An econometric analysis of the causes of tropical deforestation: Ghana.

Zanne, A., Lopez-Gonzalez, G., Coomes, D., Ilic, J., Jansen, S., Lewis, S., . . . Chave, J. (2009). *Global wood density database*. Retrieved from http://hdl.handle.net/10255/dryad.235

Zheng, X., Cao, H., Liu, B., Zhang, M., Zhang, C., Chen, P., & Yang, B. (2022). Effects of mercury contamination on microbial diversity of different kinds of soil. *Microorganisms, 10(5), 977*.

List of abbreviations

AGB: Above-ground biomass

ARFR: Atewa Range Forest Reserve

ASM: Artisanal and Small-scale miners

ATM: Airborne Thematic Mapper

BEF: Biomass expansion factor

BOA: bottom-of-atmosphere

CAc: Carbon accumulation

CF: Conversion Factor

CO_2: Carbon dioxide

DBH: Diameter at breast height

DEM: Digital Elevation Model

EPA: Environmental Protection Agency

ESA: European Space Agency

FAO: Food and Agriculture Organization

FAPAR: Fraction of Absorbed Photosynthetically Active Radiation

FCOVER: Fraction of vegetation cover

FCPF: Forest Carbon Partnership Facility

GEDI: Global Ecosystem Dynamics Investigation

GEOBIA: Geographic Object-Based Image Analysis

GFC: Ghana Forestry Commission

GHG: Greenhouse gases

GIS: Geographic Information Science

GLCM: Gray Level Co-occurrence Matrix

GNSS: Global Navigation Satellite System

GRVI: Green-Red Vegetation Index

GWP: Global Warming Potential

HFZ: High Forest Zone

IRECI: Inverted Red-Edge Chlorophyll Index

JAXA: Japan Aerospace Exploration Agency

KDE: Kernel Density Estimation

LAI: Leaf Area Index

LAI_CAB: Canopy chlorophyll content

LAI_Cw: Canopy water content

LSMA: Linear Spectral Mixture Analysis

LULC: Land Use and Land Cover

MOLI: Multi-sensing Observation Lidar and Imager Demonstration

MRV: Measurement, reporting, and verification

MSI: Multispectral Imager

NDVI: Normalized Difference Vegetation Index

NDVI45: Normalized Difference Vegetation Index with bands 4 and 5

NFI: National Forest Inventory

NIR: Near-infrared

NPP: Net Primary Productivity

NTU: Nephelometric Turbidity Units

OA: Overall Accuracy

PA: Producer’s Accuracy

PALSAR: Phased Array L-band Synthetic Aperture

REDD+: Reduced Emissions from Deforestation and Forest Degradation

RGB: Red, Green, and Blue

RMSE: Root Mean Square Error

RSE: Residual Standard Error

SAR: Synthetic Aperture Radar

SAVI: Soil Adjusted Vegetation Index

SMA: Spectral Mixture Analysis

SNAP: Sentinel Application Platform

SRTM: Shuttle Radar Topography Mission Digital Elevation Model

SWIR: shortwave infrared

TNDVI: Transformed Normalized Difference Vegetation Index

TOA: top-of-atmosphere

UA: User's Accuracy

UNFCCC: United Nations Framework Convention on Climate Change

USGS: United States Geological Survey

VIF: Variance inflation factor